Report
R-19-09
August 2019

Input data report for near-field and geosphere radionuclide transport modelling

Report for the safety evaluation SE-SFL

Pirouz Shahkarami

SVENSK KÄRNBRÄNSLEHANTERING AB

SWEDISH NUCLEAR FUEL
AND WASTE MANAGEMENT CO

Box 3091, SE-169 03 Solna
Phone +46 8 459 84 00
skb.se

SVENSK KÄRNBRÄNSLEHANTERING

ISSN 1402-3091
SKB R-19-09
ID 1718271
August 2019

Input data report for near-field and geosphere radionuclide transport modelling

Report for the safety evaluation SE-SFL

Pirouz Shahkarami, Kemakta Konsult AB

Keywords: Input data, Transport calculation, SFL repository, Safety evaluation, SE-SFL.

Abstract

The present report describes the input data required for the near-field and geosphere radionuclide transport calculations within the post-closure safety evaluation SE-SFL. This includes data used in the complete set of evaluation cases. This report also serves as the main document for the quality assurance of the input data used in the SE-SFL near-field and geosphere transport models. The report is structured such that each data set is presented in a dedicated section, where a short description of the data and their applications in the models are provided. The input data used in the calculations and their references are also listed and linked to a version-controlled repository, commonly referred to as SVN. Furthermore, limitations and uncertainties in the input data are briefly discussed.

Sammanfattning

I denna rapport redovisas de indata som behövs för radionuklidtransportberäkningarna i närzon och geosfär inom säkerhetsvärderingen SE-SFL. Detta omfattar indata som använts i samtliga utvärderingsfall. Denna rapport fungerar också som huvuddokument för kvalitetssäkring av de indata som används i närzons- och geosfärstransport-modellerna inom säkerhetsvärderingen SE-SFL. Rapporten är strukturerad så att varje dataset presenteras i ett eget avsnitt med en kort beskrivning av indata och tillämpningen av dessa i modellerna. De indata som används i beräkningarna, och referenser till dessa, är också listade med länkar till ett versionskontrollerat lagringsutrymme, vanligen kallat SVN. Vidare diskuteras också begränsningar och osäkerheter i indata.

Contents

1 Introduction

This report constitutes one of the additional references supporting the evaluation of post-closure safety for a proposed repository concept for the repository for long-lived waste (SFL) in Sweden. The purpose of the SFL safety evaluation (SE-SFL) is to provide input to the subsequent, consecutive steps in the development of SFL. These consecutive steps include further development of the design of the engineered barriers and the site-selection process for SFL. Further, the outcomes of SE-SFL can be used to prioritize areas in which the level of knowledge must be improved in order to perform a subsequent, full safety assessment for SFL. This chapter gives the background to the project and an overview of the safety evaluation. Moreover, the role of this report is described in the context of the evaluation.

1.1 Background

The Swedish power industry has been generating electricity by means of nuclear power for more than 40 years. The Swedish system for managing and disposal of the waste from operation of the reactors has been developed over that period. When finalised, this system will comprise three repositories: the repository for short-lived low- and intermediate-level radioactive waste (SFR), the repository for long-lived low- and intermediate-level waste (SFL), and the Spent Fuel Repository.

The system for managing radioactive waste is schematically depicted in Figure 1-1. SKB currently operates SFR at Forsmark in Östhammar municipality to dispose of low- and intermediate-level waste produced during operation of the various nuclear power plants, as well as to dispose waste generated during applications of radioisotopes in medicine, industry, and research. Further, SFR is planned to be extended to permit the disposal of waste from decommissioning of nuclear facilities in Sweden. The spent nuclear fuel is presently stored in the interim storage facility for spent nuclear fuel (Clab) in Oskarshamn municipality. Clab will be complemented by the Encapsulation Plant, together forming Clink. SKB has also applied to construct, possess and operate the Spent Fuel Repository at Forsmark in Östhammar municipality. The current Swedish radioactive waste management system also includes a ship and different types of casks for transport of spent nuclear fuel and other radioactive waste.

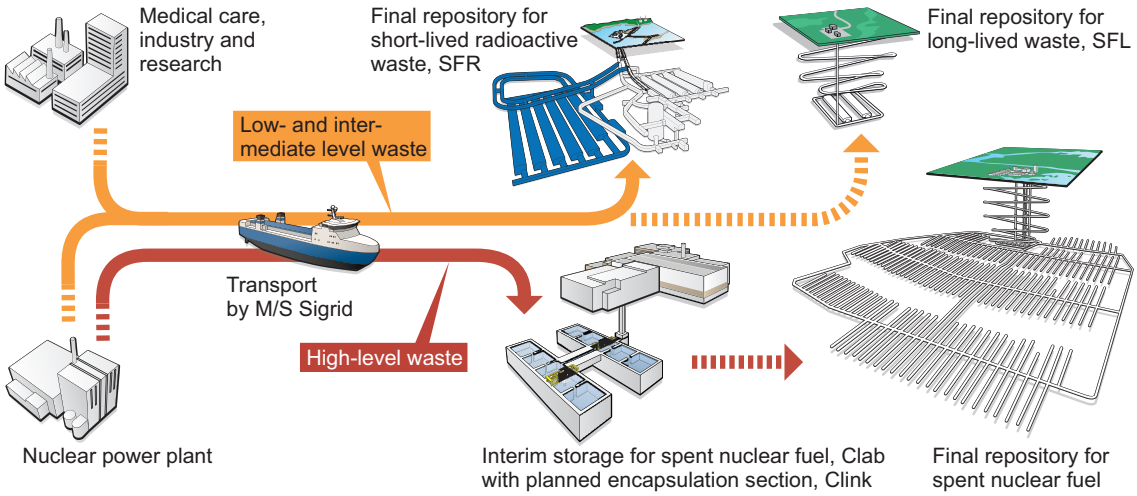

Figure 1-1. *The Swedish system for radioactive-waste management. Dashed arrows indicate future waste streams to facilities planned for construction.*

SFL will be used for disposal of the Swedish long-lived low- and intermediate-level waste. This comprises long-lived waste from the operation and decommissioning of the Swedish nuclear power plants, from early research in the Swedish nuclear programmes (legacy waste), from medicine, industry, and from research which includes the European Spallation Source (ESS) research facility. The long-lived low- and intermediate-level waste from the nuclear power plants consists of neutron-activated components and control rods and constitutes about one third of the waste planned for SFL. The rest originates mainly from the Studsvik site, where Studsvik Nuclear AB and Cyclife Sweden AB both produce and manage radioactive waste from medicine, industry and research. The legacy waste to be disposed of in SFL is currently managed by the company AB SVAFO.

A first preliminary repository concept for SFL was presented in the context of cost calculations for radioactive waste management (Plan 93 (SKB 1993)). Since the purpose of Plan 93 was to give cost estimations no safety related analyses were discussed. The first quantification related to safety was presented in a pre-study of final disposal of long-lived low and intermediate level waste. The objective was to make a first preliminary and simplified assessment of the near-field as a barrier to radionuclide dispersion (Wiborgh 1995). In 1999, a preliminary safety assessment was presented that focussed on a quantitative analysis of the environmental impact for a reference scenario (SKB 1999). The objective was to investigate the capacity of the facility to act as a barrier to the release of radionuclides and the importance of the repository location. The assessment was reviewed by the authorities (SKI/SSI 2001). One of the main comments was a lack of a clear account of the basis for the selection of the design and that no design alternatives had been considered.

Reflecting the comments from the authorities possible solutions for management and disposal of the Swedish long-lived low- and intermediate-level waste were examined in the SFL concept study (Elfwing et al. 2013). Among the considered alternatives a system was proposed as a basis for further assessment of post-closure safety. According to this concept, SFL is designed as a deep geological repository with two different sections:

- one waste vault, designed with a concrete barrier, BHK, for metallic waste from the nuclear power plants, and
- one waste vault, designed with a bentonite barrier, BHA, for the waste from Studsvik Nuclear AB, Cyclife Sweden AB and AB SVAFO.

A schematic illustration of SFL is displayed in Figure 1-2. In SE-SFL, it is assumed that the waste vaults are located at 500 m depth. BHK is approximately 135 m long and BHA is approximately 170 m long. Both vaults have a cross sectional area of approximately 20×20 m^2 (see further details in the **Initial state report**).

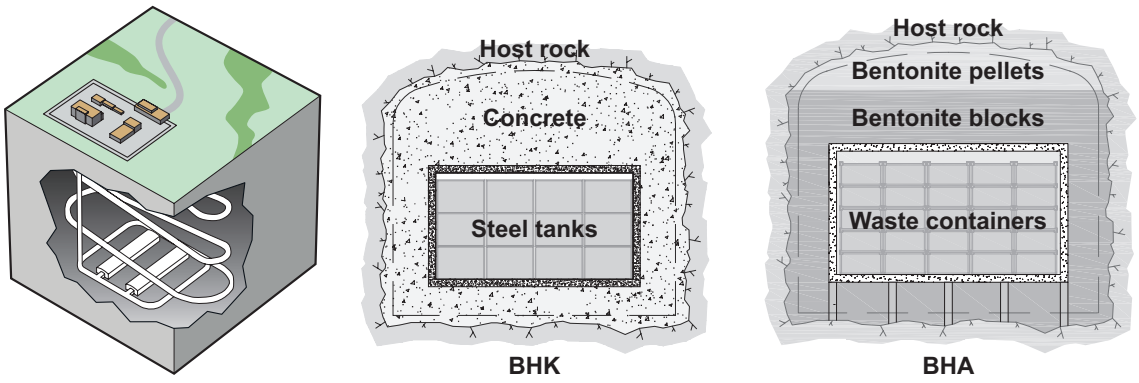

Figure 1-2. *Preliminary facility layout and the proposed repository concept for SFL (left), one waste vault for metallic waste from the nuclear power plants (BHK, centre) and one waste vault for waste from Studsvik Nuclear AB, Cyclife Sweden AB and AB SVAFO (BHA, right).*

1.2 The SE-SFL safety evaluation

There are two main objectives for SE-SFL. The first is to evaluate conditions in the waste, the barriers, and the repository environs under which the repository concept has the potential to fulfil the regulatory requirements for post-closure safety. The second is to provide SKB with a basis for prioritizing areas in which the level of knowledge and efficiency of methods must be improved in order to perform a full safety assessment for SFL. This is in line with the iterative safety analysis process that the SFL repository program follows, in which the results from post-closure safety analyses and related activities (e.g. information from a site selection process and development of numerical methods) are used to successively inform and improve the analysis. In accordance with the Nuclear Activities Act (1984:3), important research needs for the SFL programme that emerge as a result of SE-SFL will be reported in the research development and demonstration (RD&D) programme. An important aspect of this is to ensure that the industry has well founded information to support long-term planning.

The safety analysis methodology as applied in SE-SFL is a first evaluation of post-closure safety for the repository concept proposed by Elfwing et al. (2013) and is not part of a license application. As such, the methodology has been adapted to suit the needs of SE-SFL and thus differs from the methodology established by SKB for the most recent safety assessments for the extended SFR (SR-PSU; SKB 2015a) and for the Spent Nuclear Fuel repository (SR-Site; SKB 2011a). This also implies that the regulatory requirements on the methodology have not been applied rigorously, which would be needed for a safety analysis that is part of a license application. The evaluation is intentionally simplified as compared with SR-Site and SR-PSU, and more focus is given to aspects connected to the further development of the repository concept and related analyses. This is also reflected in using the term safety evaluation in comparison to safety assessment. The differences between SE-SFL and a full safety assessment are described in more detail in Section 2.1 in the **Main report**. The adaption of the methodology for the purposes of SE-SFL is described in Section 2.5 in the **Main report**.

To the extent applicable, SE-SFL builds on knowledge from SR-PSU and SR-Site. There are commonalities regarding the waste, engineered barriers, bedrock, surface ecosystems and external conditions relevant to post-closure safety. For instance, SE-SFL and SR-Site both address timescales of one million years (see Section 2.3 in the **Main report**). A further similarity is the proposed depth of 300–500 m. There are similarities between SFR and SFL regarding the waste and waste packaging and the proposed engineered barriers.

In SE-SFL, a first evaluation of a suitable repository design for disposal of the ESS waste is carried out. Since the information regarding the ESS inventory is not yet as well defined as for the other waste streams, the protective capability of the different waste vaults in relation to this waste is analysed separately.

No site has yet been selected for SFL and therefore data from SKB's site investigation programmes for the Spent Fuel Repository and for the extension of SFR have been utilized in SE-SFL. In order to have a realistic and consistent description of a site for geological disposal of radioactive waste, data from the Laxemar site in Oskarshamn municipality (see Figure 1-3), for which a detailed and coherent dataset exists, is used. Based on an initial hydrogeological analysis for SE-SFL, the example location for the SFL repository was selected to be a volume part of what was earlier found most suitable for a potential Spent Fuel Repository within the Laxemar site (SKB 2011b).

SE-SFL is further developed in comparison to the previous assessments, which were mentioned in Section 1.1. Important improvements are an updated inventory and more elaborate account of internal and external processes. Moreover, the biosphere was in the preliminary assessment handled in a simplified manner, whereas it is handled in an elaborate way in SE-SFL. The availability of data from the Spent Fuel Repository site investigations also allows for more detailed representations of the geosphere. In general, SKB's experiences with safety analysis work have led to many developments since the late 1990s.

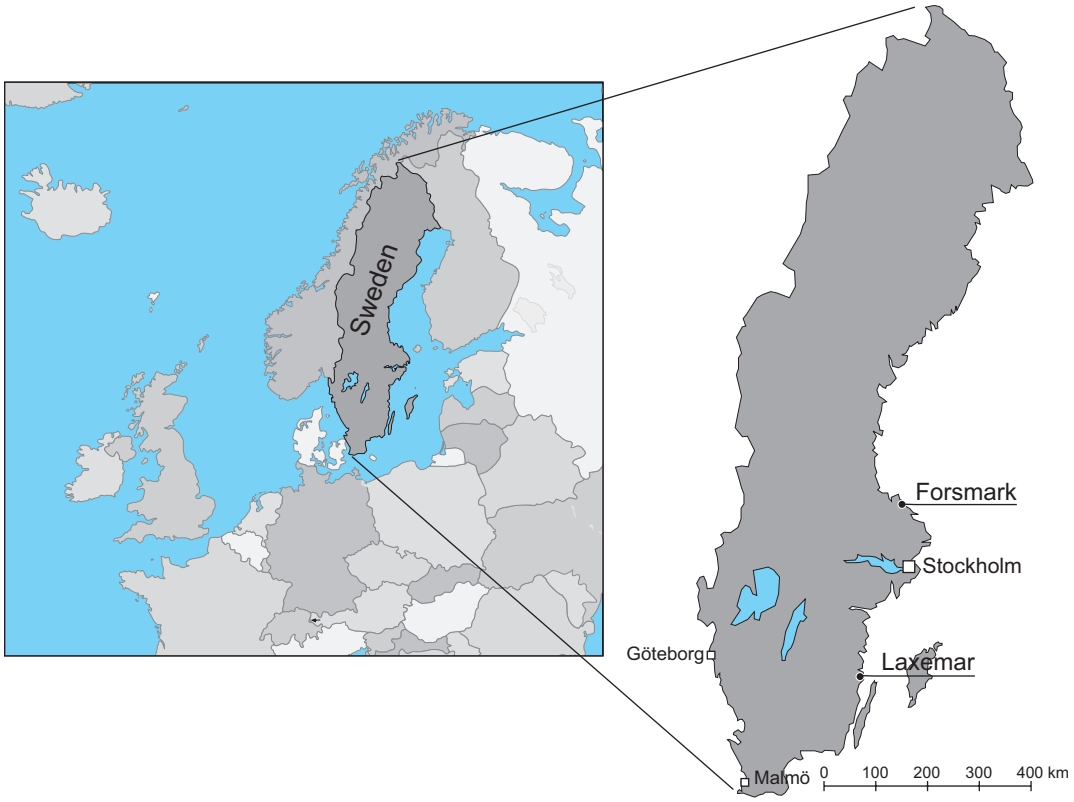

Figure 1-3. *Map showing the location of Laxemar and Forsmark. Data from the site investigations in Laxemar, along with the data from the SR-Site and SR-PSU assessments from Forsmark, are used in SE-SFL to obtain a coherent dataset of common conditions in Swedish crystalline bedrock and surface ecosystems.*

Post-closure safety for the proposed repository concept for SFL is evaluated in a set of *evaluation cases.* The base case for the radionuclide transport and dose calculations in SE-SFL, *present-day evaluation case*, is a hypothetical condition that assumes constant, present-day climatic and other external conditions throughout the full assessment period. In other words, the repository and its environs remain unchanged with conditions similar to the initial state described in Chapter 4 in the **Main report**. This case assumes that the repository is constructed at the example location in Laxemar, and, as in all evaluation cases in SE-SFL, that the repository is constructed according to the proposed design concept.

Further, a set of evaluation cases that assess the sensitivity of the resulting activity releases and doses to specific assumptions made regarding conditions in the repository and the repository environs are included in the analysis (see Figure 1-4). These cases were chosen to illustrate conditions in the repository and the repository environs that are likely to improve the repository performance in comparison with the base case. Further, cases that illustrate the effects of uncertainties in bedrock properties, discharge area and the effect of a drilled well, as well as uncertainties relating to the future climate evolution, are included in the evaluation. Descriptions of each of the sensitivity evaluation cases are given in Chapters 5–7 of the **Radionuclide transport report**. The sensitivity evaluation cases inherit a great majority of prerequisites and input data from the *present-day evaluation case*, while a limited set of data is modified.

1.3 The SE-SFL report hierarchy

The **Main report** and main references in SE-SFL are listed in Table 1-1, also including the abbreviations by which they are identified in the text (abbreviated names in bold text). It can be noted that there are no dedicated process reports for SE-SFL. The SFR and SFL waste and repository concepts have many similarities, for instance the use of similar barrier materials and thus similar process interactions with the surrounding bedrock environment (see Section 2.5.4 in the **Main report**). Therefore, the descriptions of internal processes for the waste (SKB 2014c) and the barriers (SKB 2014d) in SR-PSU are used in SE-SFL.

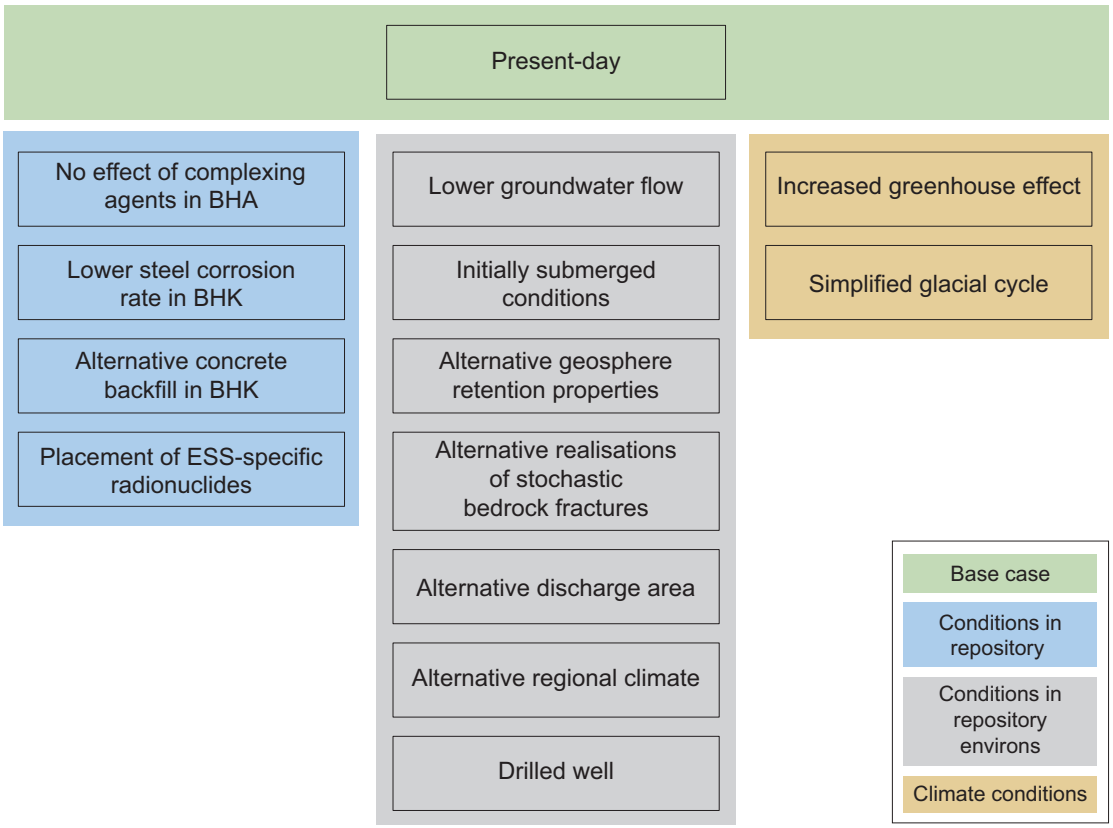

Figure 1-4. *Evaluation cases included in the evaluation of the potential for the proposed repository concept to meet applicable criteria on the maximum annual effective dose to humans after closure, grouped and colour-coded according to repository component that they address.*

For the bedrock system, the descriptions of internal processes for the geosphere in SR-Site (SKB 2010d) and SR-PSU (SKB 2014d) are used. There are also several additional references, which include documents compiled within SE-SFL, for instance input data reports for the radionuclide transport (i.e. the present report) and dose calculations (Grolander and Jaeschke 2019). But there are also references to documents that have been compiled outside of the project, either by SKB or other similar organisations, or are available in the scientific literature. In Figure 1-5, the hierarchy of the **Main report**, main references and additional references within SE-SFL is shown.

Table 1-1. Main references in SE-SFL and their abbreviations used in this report (in bold).

Abbreviation used when referenced in this report	Text in reference list
Main report	Main report, 2019. Post-closure safety for a proposed repository concept for SFL. Main report for the safety evaluation SE-SFL. SKB TR-19-01, Svensk Kärnbränslehantering AB.
Biosphere synthesis report	Biosphere synthesis, 2019. Biosphere synthesis for the safety evaluation SE-SFL. SKB TR-19-05, Svensk Kärnbränslehantering AB.
Climate report	Climate report, 2019. Climate and climate-related issues for the safety evaluation SE-SFL. SKB TR-19-04, Svensk Kärnbränslehantering AB.
FEP report	FEP report, 2019. Features, events and processes for the safety evaluation SE-SFL. SKB TR-19-02, Svensk Kärnbränslehantering AB.
Initial state report	Initial state report, 2019. Initial state for the repository for the safety evaluation SE-SFL. SKB TR-19-03, Svensk Kärnbränslehantering AB.
Radionuclide transport report	Radionuclide transport report, 2019. Radionuclide transport and dose calculations for the safety evaluation SE-SFL. SKB TR-19-06, Svensk Kärnbränslehantering AB.

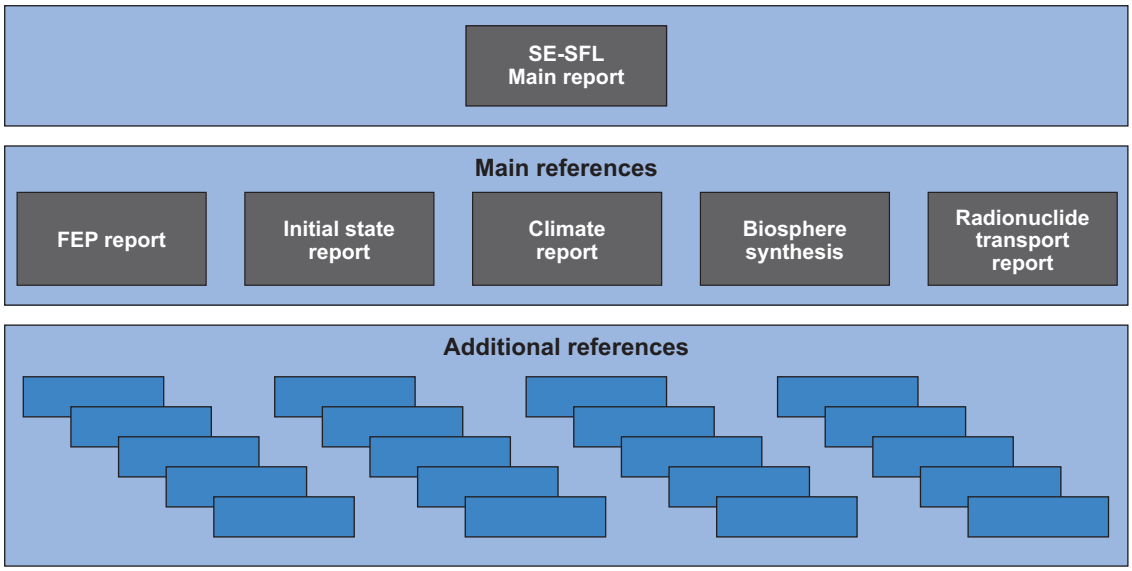

Figure 1-5. *The hierarchy of the Main report, main references and additional references in the safety evaluation of post-closure safety SE-SFL. The additional references either support the Main report or one or more of the main references.*

1.4 The role of this report in SE-SFL

The primary aim of this report is to provide the non-trivial input data used in the near-field and geosphere radionuclide transport modelling within the safety evaluation SE-SFL. This includes input data used in the complete set of evaluation cases. This report serves as the main document for the quality assurance (QA) of the input data used in the near-field and geosphere models in SE-SFL.

Figure 1-6 presents a schematic diagram of the flow of data within the SE-SFL radionuclide transport modelling chain. The chain consists of the near-field model that describes the release of radionuclides from the waste domain to the surrounding engineered barriers and bedrock, the geosphere model that describes the subsequent transport and retention of radionuclides in the host rock, and the biosphere model that consists of sub-models describing radionuclide transport in the surface ecosystems (natural and cultivated) and determines the dose to humans.

As part of SE-SFL, a hydrogeological modelling is performed that provides input data for the near-field and geosphere models. The importance of the SE-SFL hydrogeological modelling is evident from the fact that all long-range transport of radionuclides is modelled to occur by advection. The present report provides the hydrogeological data used in the near-field and geosphere models.

Furthermore, dedicated concrete degradation modelling is performed to evaluate the performance of the concrete backfill in the BHK vault. This report provides also the concrete related data that are used in the near-field RNT model.

There are also many data concerning the initial state of the SFL repository, which are used, directly or indirectly, in the near-field model. The data include the radionuclide inventory, amounts of materials, material properties, dimensions of the waste domain and engineered barriers, etc. These data are discussed in detail in the **Initial state report** and are briefly described in the present report.

It should also be emphasized that many of input data used in the near-field and geosphere models are adopted from the previously conducted safety assessments for other SKB repositories, e.g. information on radionuclide retardation in the engineered barriers and host rock. The present report provides references to all such non-trivial input data and briefly discusses their relevance to the SFL repository.

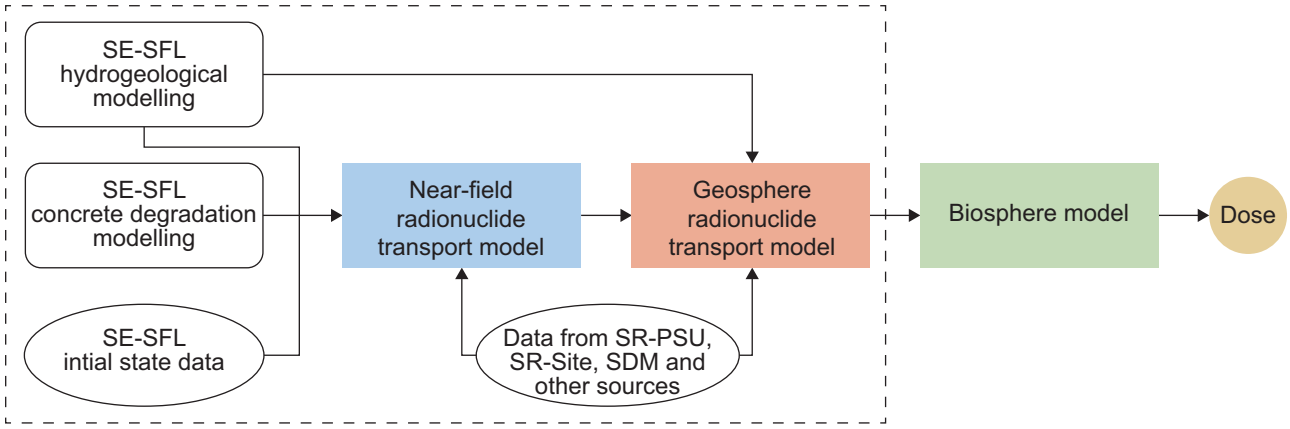

Figure 1-6. *Schematic representation of the SE-SFL radionuclide transport model chain and main sources of input for the respective models. The dashed line marks the scope of the present report.*

The geosphere model provides a radionuclide release term to the biosphere model. Input data to the biosphere model are provided in Grolander and Jaeschke (2019) and **Biosphere synthesis report**. Therefore, the present report will not further discuss the coupling information between the geosphere and biosphere models.

A more detailed diagram of the radionuclide transport modelling chain is provided in Section 1.7 in the so-called assessment model flowchart (AMF).

1.5 Structure of this report

This report gives an overview of the SFL repository design and briefly describes the near-field and geosphere transport models. The following is a brief description of the contents and structure of the report.

Chapter 1 – Introduction: This chapter describes the proposed repository concept for the SFL repository and provides background information on its post-closure safety evaluation. This chapter also highlights the main objectives of the present report, which is the main quality assurance document for the input data used in the SE-SFL near-field and geosphere models.

Chapter 2 – Data used in the near-field model: This chapter starts by identifying the required input data for the near-field model. This is followed by presenting the input data used in the SE-SFL *present-day evaluation case* also called the base case. This chapter explores the following categories:

- Identification of parameters used in the near-field model.
- Geometrical data used to set up the near-field models.
- Radionuclide inventory at initial state in waste compartments.
- Radionuclide decay data.
- Data for partitioning of radionuclides in waste compartments.
- Data for diffusive and advective transport in waste compartments.
- Data for partitioning of radionuclides in backfill compartments.
- Data for diffusive and advective transport in backfill compartments.
- Data for diffusion and advective transport at the vault-rock interfaces.
- Distribution of radionuclide release on host rock trajectories.

Chapter 3 – Data used in the geosphere model: This chapter gives an overview of the geosphere model and its required input parameters. This is followed by presenting the input data used in the SE-SFL base case. This chapter explores the following categories:

- Identification of parameters used in the geosphere model.
- Transport properties in geosphere.
- Retention properties in geosphere.

Chapter 4 – Sensitivity evaluation cases: This chapter presents the input data used in the sensitivity evaluation cases and, which deviate from the *present-day evaluation case*.

1.6 Management of input data and data quality assurance

The radionuclide transport calculations in the SFL repository and its host bedrock are carried out by using the SE-SFL near-field and geosphere radionuclide transport models (**Radionuclide transport report**, Sections 4.3 and 4.4). The present report is the main document for the quality assurance of the input data used in the computational tools. The goal is to ensure, in a verifiable manner, that the applied input data are appropriately chosen for the computational tools and their underlying models. As an additional part of the quality assurance procedure, the actual input data files used in the computational tools are stored on a version-controlled repository, commonly referred to as SVN. SVN also contains all the required scripts and files to run the evaluation cases.

It should be noted that the present report does not deal with the quality assurance of the modelling concepts. Furthermore, the quality assurance of the computational tools and their general implementations are beyond the scope of this document and are reported elsewhere (SKB 2014b, Wessely and Shahkarami 2019).

1.7 Assessment model flow chart

An assessment model flow chart (AMF) is a graphical illustration of the information exchange between the various activities within a performance assessment.

This section provides the AMF to describe the flow of data within the near-field and geosphere part of the modelling for the SE-SFL base case (see Figure 1-7).

The following convention is adopted to construct the AMF for SE-SFL: Each modelling or evaluation activity is represented by a rectangle outlined by a solid line. Supporting modelling or evaluation activities that supply data to the radionuclide transport modelling chain, are represented by rounded rectangles. It should be emphasized that some of the input data are adopted from the **Initial state report** or activities outside of the SE-SFL project. In the AMF, such input data are represented by ovals.

The background colours of the objects reflect the repository components, i.e. near-field, geosphere, and biosphere, for which they apply:

- Yellow – Near-field, i.e. waste and engineered barriers.
- Red – Geosphere.
- Green – Biosphere.
- Grey – Independent of the repository component.

The flow of data and information are indicated by arrows. In the AMF, input data enters an activity from above or left-hand side. Resulting data that are propagated to other part of the safety evaluation leaves the activities from below or right-hand side. For practical purposes, the AMF also contains small diamonds where streams of data can merge or split. Data streams, plotted as lines with no arrow head, may enter such “merge and split” diamonds from any direction. Data streams that exit such diamonds and enter an activity are provided with an arrow head, and therefore following the flow of data should be trivial.

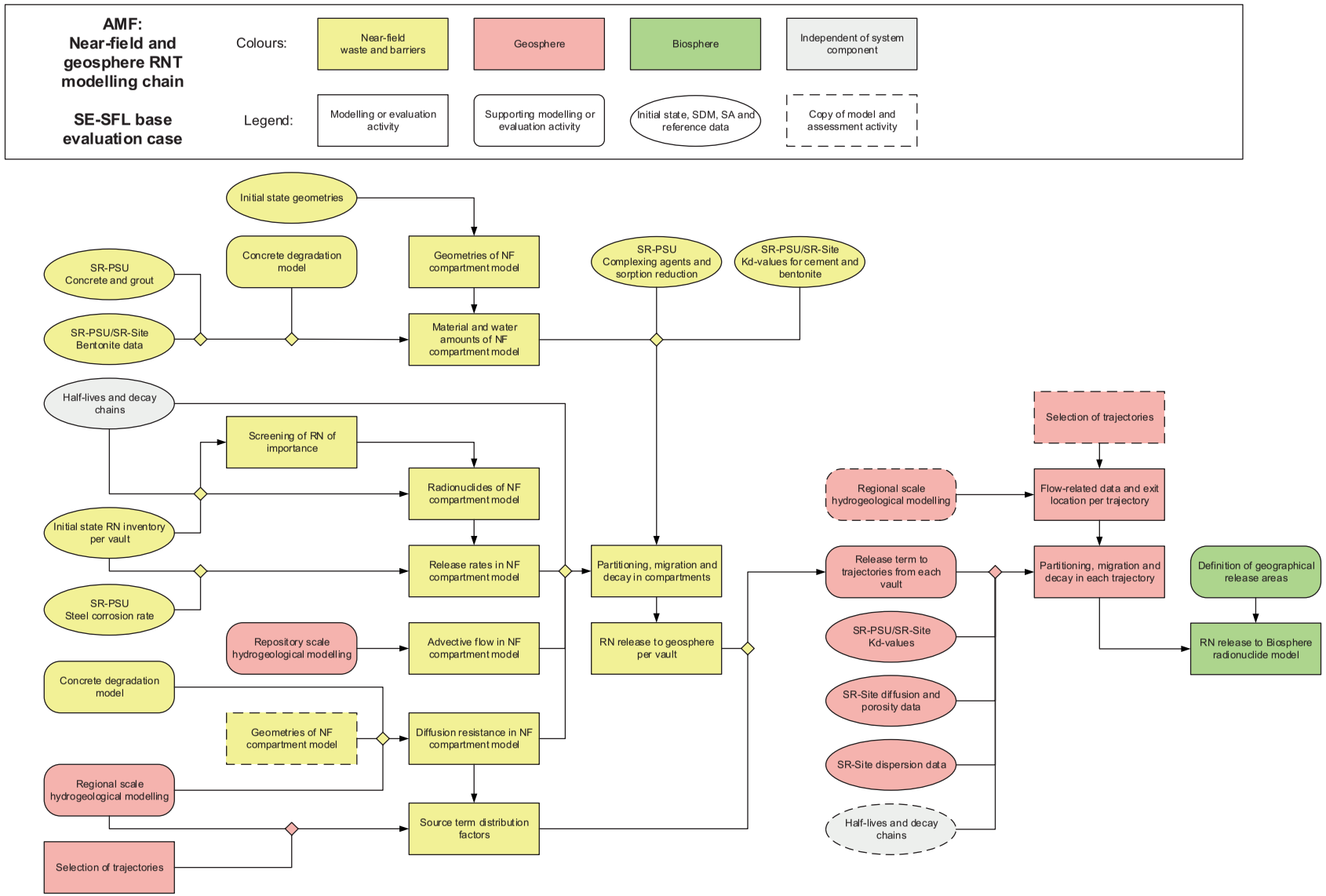

Figure 1-7. *Assessment model flowchart (AMF) of the SE-SFL base case, focusing on the near-field (NF) and geosphere part of the radionuclide transport (RNT) modelling chain.*

Finally, for practical purposes, it may be useful to make a copy of an activity. Such a copied object is encircled by dashed lines in the AMF and may only have data streams leaving the activity. All data streams must enter the original object.

In the AMF shown in Figure 1-7, there is no data that flows into the supporting modelling or evaluation activities, which are carried out within the SE-SFL project but are outside of the radionuclide transport modelling chain. This is because the quality assurance of such data is not handled in the present report.

Table 1-2 lists the objects displayed in the AMF. The objects are read column-wise from Figure 1-7, i.e. first downwards in a column and then shifting to a column on the right. The cell colours in the table reflect the objects background colours in the AMF. For each object, a short description of the data or activity is provided. Furthermore, a link (or links) is provided between the object and section (or sections) in this report. As such, the AMF can function as a reader's guide to this report.

Table 1-2. Short description of the objects in the AMF and links to the relevant sections in this report.

Object in AMF	Description of data/activity	Sections in report
SR-PSU concrete and grout	Fraction of cement and pore water.	2.5.1, 2.5.2, 2.7.1, 2.7.3
SR-PSU/SR-Site bentonite data	Fraction of bentonite and pore water.	2.7.2
Half-lives and decay chains	Simplified decay chains and half-lives of included nuclides.	2.4.1, 2.4.2
Initial state RN inventory per vault	RN inventory in different components of different release modes.	2.3.1, 2.3.2
SR-PSU steel corrosion rate	Corrosion rates under alkaline anoxic conditions	2.5.4
Concrete degradation model	Time varying porosity and sorption data for concrete due to degradation.	2.5.1, 2.5.2, 2.7.1, 2.7.3
Regional scale hydrogeology modelling	Equivalent flow rates used when calculating the diffusion resistance in the backfill.	2.9.1, 2.9.5
Selection of trajectories	Trajectories for which equivalent flow rates are used	3.2.1
Initial state geometries	Geometries used when setting up simplified dimensions of NF compartmental models.	2.2.1, 2.2.2
Concrete degradation model	Evolving porosity used when calculating pore water and cement quantities in compartments.	2.5.1, 2.5.2, 2.7.1, 2.7.3
Screening of RN of importance	A list of nuclides that are part of the modelling.	2.1.1
Repository scale hydrogeological modelling	Ground water flows running through the compartments.	2.6.3, 2.6.4, 2.8.3, 2.8.4
Geometries of NF compartmental model	Dimension of the compartmental model used when evaluating the diffusion transport resistance.	2.2.1, 2.2.2
Geometries of NF compartmental model	Dimension of the compartmental model used when calculating the quantities of pore water, cement and bentonite.	2.2.1, 2.2.2
Materials and water amount in NF compartmental model	Calculation of quantities of cement, pore water, and bentonite used for partitioning calculations.	2.5.1, 2.5.2, 2.7.1, 2.7.3
Radionuclides of NF compartmental model	Inventory of radionuclides screened as relevant for SE-SFL.	2.1.1
Release rates of NF compartmental model	Calculation of annual source term from the waste matrix.	2.3.2, 2.5.3, 2.5.4
Advective flow in NF compartmental model	Evaluation of the groundwater flow through NF compartments.	2.6.3, 2.6.4, 2.8.3, 2.8.4
Diffusion resistance in NF compartmental model	Evaluation of the diffusion resistance in NF compartments.	2.6.1, 2.6.2, 2.8.1, 2.8.2

Object in AMF	Description of data/activity	Sections in report
Source term distribution factors	Evaluation of what part of the total release term from the NF should be attributed to each trajectory leaving the vaults.	2.10.1, 2.10.2
SR-PSU complexing agents and sorption reduction	Evaluation of the amounts of complexing agents (and colloids if present) and the factor by which this reduces the K_d-values in BHA.	2.10.22.5.6
Partitioning, migration and decay in compartments	Calculation of what radionuclide activity in a compartment decays, remains immobilised by sorption, or migrates in or out of the compartment by diffusion or advection.	2.12.1.4
RN release to geosphere per vault	Radionuclide release from the NF interface compartment to the geosphere.	2.9.4, 2.9.7
SR-PSU/SR-Site speciation	Speciation of radionuclides, to the degree available.	3.3.1
SR-PSU/SR-Site K_d-values for cement and bentonite	Sorption coefficients in bentonite and cement.	2.5.5, 2.7.4, 2.7.5
Regional scale hydrogeology modelling	Flow related data used to calculate radionuclide transport in segments of selected trajectories.	3.2.1, 3.2.3
SR-Site dispersion data	Peclet number and longitudinal dispersivity in trajectories.	3.2.2
Release term to trajectories from each vault	The NF release term allocated to the first segment of individual trajectories.	2.10.1, 2.10.2,
SR-PSU/SE-Site K_d-values	Element specific K_d-values in the rock matrix.	3.3.5
SR-Site diffusion and porosity data	Charge specific diffusivities and porosities of the rock matrix.	3.3.2, 3.3.3, 3.3.4
Radionuclide speciation in geosphere	Assigning oxidation number and charge to each element.	3.3.1
Selection of trajectories	Selection of trajectories that leaves the vaults and exits at the biosphere.	3.2.1
Flow-related data and exit location per trajectory	Modification of trajectories' flow related data, including disregarding the advective travel time of some segments.	3.2.1
Partitioning, migration and decay in each trajectory	Calculation of what radionuclide activity in a segment decays, remains immobilised by sorption or matrix diffusion, or migrates in or out of the segment by advection.	3.1
Definition of geographical release areas	Setting up boundaries for different release areas (e.g. discharge areas). The SE-SFL base case only includes one release area.	–
RN release to Biosphere radionuclide model	The combined radionuclide specific release rates to the biosphere from all trajectories emanating from each vault.	–

2 Data used in the near-field model

In SE-SFL, radionuclide transport within the repository near-field components, i.e. the waste and engineered barriers, is modelled using the near-field computational tool and its dedicated model called the SE-SFL near-field radionuclide transport model (**Radionuclide transport report**, Section 4.3). This chapter aims to identify and present the input data used in the near-field model for the SE-SFL base case, i.e. *present-day evaluation case*. In the validation step, the data are checked for consistency with corresponding values reported in the reference documents. It should be noted that some particular features, events, and processes are handled differently in the sensitivity evaluation cases. These evaluation cases are discussed in Chapter 4. For a comprehensive description of the near-field radionuclide transport model, the reader is referred to Wessely and Shahkarami (2019).

2.1 Identification of parameters used in the near-field model

To evaluate radionuclide release from the near-field, the near-field components are discretised into an appropriate number of compartments so that radionuclides can be assumed to be well mixed in each compartment. In all the evaluation cases, the model includes one waste compartment and three groups of backfill compartments representing the main engineered barriers in the repository, namely inflow backfill compartment, outflow backfill compartment and side backfill compartment. In the near-field model, each backfill compartment further consists of five homogeneous and evenly-sized sub-compartments with identical properties.

In the near-field model, the complexities of the waste packages and engineered barriers are greatly simplified (see Section 2.1.2), which reduces the number of model parameters. Nevertheless, it may require some input data to be pre-processed before they can be used within the model framework. This applies to both primitive and complex data that are closely tied to the adopted modelling approach. The primitive class of data can be exemplified by the dimensions of the vaults where simplified geometries are used in the near-field model. This simplification creates some deviations from the dimensions provided in the **Initial state report**. These deviations are further explained and clarified in Section 2.2.

The complex class of data can be exemplified by the equivalent flowrates, Q_{eq}, which are provided for fractures in the host rock that intersect the repository vaults (Joyce et al. 2019, Abarca et al. 2019). The equivalent flow rate concept is incorporated in the near-field model to represent the radionuclide diffusive transport from the backfill boundary sub-compartments to the seeping water in the fractures in the host rock. Therefore, the provided Q_{eq} should be processed before they can be used as input data in the near-field model. This is discussed in Sections 2.9.3 and 2.9.7.

2.1.1 Nuclides included in the modelling

In SE-SFL, 67 radionuclides are identified to be of interest for the safety evaluation (Crawford 2018). These radionuclides are tabulated in Table 2-1. The radionuclide inventory can also be found in the SVN database at:

svn://svn.skb.se/SFL/SFLSAK/Arbetsmaterial/RadionuclideTransport/GemensammaIndata/Radionuclides/Radionuclides.xlsx.

Sorption properties of carbon depends strongly on the form in which it is present. Therefore, C-14 activity is given a special treatment, where it is divided into the following three categories:

- C-14-ind: Induced activity in BHK.
- C-14-org: Organic compounds in BHA.
- C-14-inorg: Inorganic compounds.

Table 2-1. Radionuclides identified as being of interest for SE-SFL (Crawford 2018).

Radionuclides			
Ac-227	Cm-245	Ni-63	Sr-90
Ag-108m	Co-60	Pa-231	Tb-158
Am-241	Cs-135	Pb-210	Tc-99
Am-242m	Cs-137	Pd-107	Th-228
Am-243	Eu-150	Po-210	Th-229
Ba-133	Eu-152	Pu-238	Th-230
Be-10	Gd-148	Pu-239	Th-232
C-14-ind	H-3	Pu-240	Ti-44
C-14-inorg	Ho-166m	Pu-241	U-232
C-14-org	I-129	Pu-242	U-233
Ca-41	K-40	Ra-226	U-234
Cd-113m	La-137	Ra-228	U-235
Cl-36	Mo-93	Re-186m	U-236
Cm-242	Nb-93m	Se-79	U-238
Cm-243	Nb-94	Si-32	Zr-93
Cm-244	Ni-59	Sm-151	
Cm-246	Np-237	Tb-157	

2.1.2 Compartments of the near-field model

In this section, a brief description of the near-field model is presented. A comprehensive description of the modelling approach can be found in Wessely and Shahkarami (2019). In the near-field model, the BHK vault is assumed to be a cuboid with one waste compartment and three concrete backfill compartments, as schematically shown in Figure 2-1. By definition, each compartment is a homogeneous entity of the near-field components. Therefore, it can be described with averaged properties and shape.

The waste compartment represents the waste domain (wastes, waste packages and grout) and concrete structures (caissons). The waste compartment is assumed homogeneous in terms of materials and radionuclide inventory. This assumption holds during the entire simulation period.

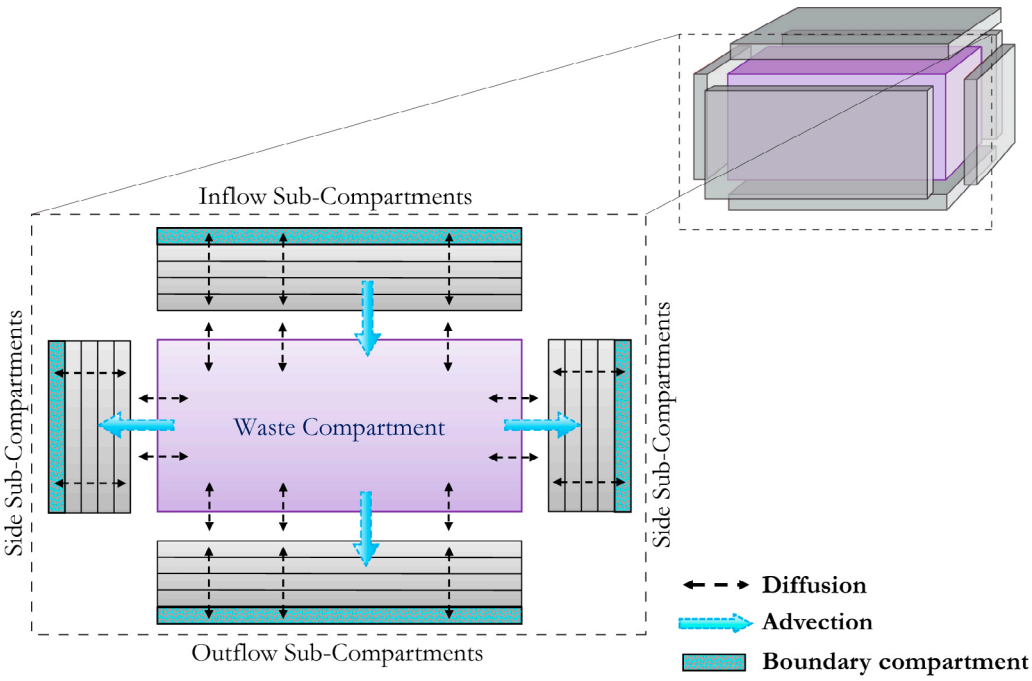

Figure 2-1. Schematic of the compartment discretization in the BHK waste package and the concrete backfill around it.

The waste that is planned to be stored in the BHK vault contains metallic components with neutron-induced activity. In the near-field model, the metallic components are categorized into different groups with increasing thickness (see Section 2.5.3). It should also be noted that in the near-field model, each group of the metallic components is represented by a compartment.

The near-field model assumes that the waste compartment in BHK is surrounded by three groups of backfill compartments, where each consists of five evenly-sized sub-compartments. The compartments include:

- Groundwater inflow compartment representing the backfill above the caissons.
- Groundwater outflow compartment representing the backfill below the caissons.
- Side compartment representing the backfill surrounding the sides of the caissons, i.e. the long-side and short-side walls of the vault.

The outermost sub-compartments, i.e. the boundary sub-compartments, connect to the geosphere at the vault-rock interface. The inflow and outflow sub-compartments have the same cross-section areas, which are approximated as the average of the top surface area of the waste compartment cuboid and the top surface area of the vault cuboid. The side sub-compartments are assumed cuboidal to represent the vault walls. Each sub-compartment has the same cross-section area, which is approximated as the average of the sum of the four side-walls of the waste compartment and the four side-walls of the vault. Numerical data on these cross-section areas are given in Section 2.2.2.

Given the hydrogeological condition at the Laxemar area (Abarca et al. 2019), it is presumed that the groundwater flow is directed downward through the BHK vault. Therefore, most of the radionuclide advective outflow to the host rock occurs through the outflow compartment, while none occurs over the inflow compartment. It should be noted that the near-field model also assumes a subordinate groundwater flow along and across the vault, allowing for an advective outflow through the side compartments.

Furthermore, radionuclides can spread into the backfill materials by molecular diffusion and migrate toward the water-bearing fractures in the surrounding rock. In each sub-compartment, diffusion is assumed one-dimensional in the direction normal to the cross-section areas of the compartments.

The near-field model for BHA has many similarities with that of BHK, especially in terms of the model formulation. Similar to BHK, the BHA vault is assumed to be a cuboid with one waste compartment and three backfill compartments, which each is divided to five sub-compartments of equal thickness and cross-section area. This is illustrated in Figure 2-2. The waste compartment includes the waste domain and concrete structure. The waste compartment is assumed homogeneous in terms of materials and radionuclide inventory, both initially and throughout the entire simulation time. The waste compartment is assumed to be surrounded by the following three groups of bentonite backfill compartments, each having the same thickness:

- Groundwater inflow compartment representing the backfill on one short side of the vault.
- Groundwater outflow compartment representing the backfill on the other short side of the vault.
- Side compartment representing the backfill above, below, and at the long sides of the waste compartment.

Despite the similarities with the BHK vault, the groundwater flow conditions are different in BHA. The groundwater flow rate through the BHA vault is very small and diffusion dominates the transport of radionuclides (Abarca et al. 2019). Furthermore, the main groundwater flow in BHA, if any, is directed along the vault, while the vertical component of the flow is subordinate. In this model, the side compartment is extended along the vault and holds the largest cross-section area between the bentonite and host rock, while the inflow and outflow compartments have relatively small cross-section areas. The cross-section areas play an important role in determining the diffusion transport resistances in the backfill compartments. It should also be noted that the effective diffusion transport resistance at the vault-rock interface is treated differently in the BHA model. This is further discussed in Section 2.8.

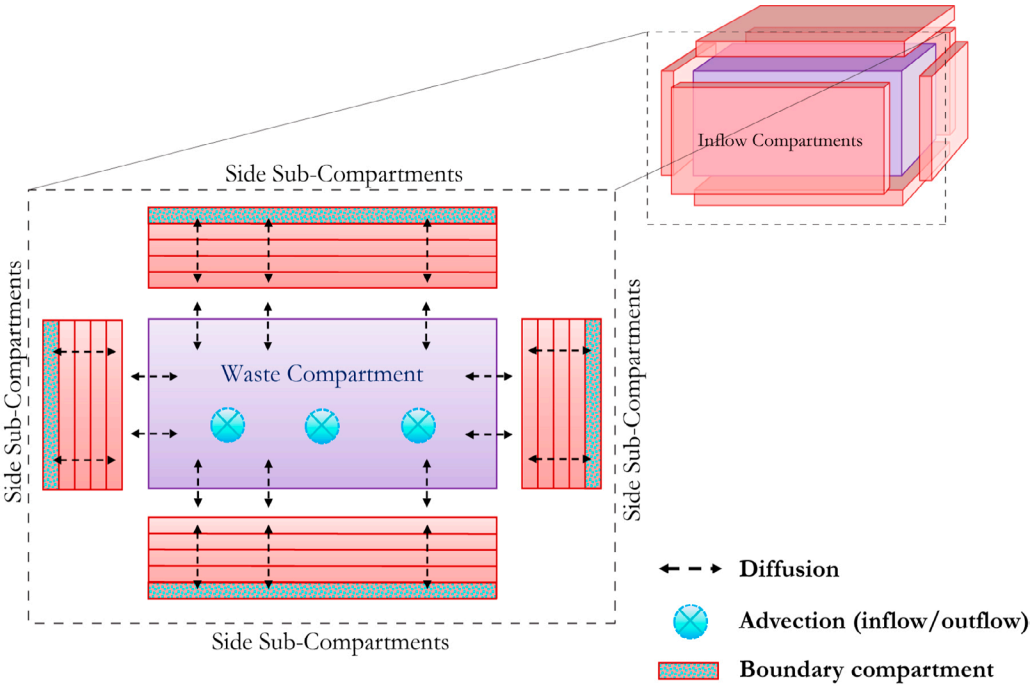

Figure 2-2. *Schematic of the compartment discretization in the BHA waste package and the bentonite backfill around it.*

2.1.3 Treatment of source terms in the waste domains

The near-field model assumes that the radionuclide inventories in BHA and BHK are initially tied to the waste matrices.

After the repository closure in the year 2075, the vaults are assumed to become instantly saturated with water. At this time, the entire radionuclide inventory in BHA is assumed to be released instantly from the waste matrix. Each radionuclide is then partitioned as being dissolved in the pore water in the waste compartment or as being sorbed to the cement particles contained in the concrete and grout.

However, the radionuclide release in BHK behaves differently because the BHK waste mainly contains metallic components with neutron-induced activity. Therefore, in the near-field model, one part of the radionuclide inventory in BHK is assumed to exist as surface contamination on metallic wastes and adjacent cementitious materials. Another part of the inventory is assumed to exist as induced activity incorporated in very thin metallic components, which corrode very rapidly. The radionuclides within the above waste categories are assumed to be released instantly upon water saturation in the year 2075. The third and fourth parts of the radionuclide inventory are assumed to exist as induced activity incorporated in thick and very thick metallic components, which require longer time to be fully corroded. In the near-field model, it is assumed that radionuclides within these metallic components are released gradually together with the corrosion products. Therefore, the activity release rates of the metallic components are calculated according to their thicknesses and the corrosion rate. This is further discussed in Sections 2.5.3 and 2.5.4. Each radionuclide is then partitioned as being dissolved in the pore water of the waste compartment or as being sorbed to the cement particles contained in concrete and grout.

It should be emphasized that, in the near-field model, each of the above metallic waste groups is represented by a compartment. Furthermore, whether the radionuclides are incorporated in the waste matrix, released to the pore water of the waste compartment or sorbed on cement particles, they are assumed to decay according to simplified decay chains, as described in Section 2.4.

2.1.4 Transport equations and parameters in the near-field model

In the near-field model, change in a compartment's inventory is governed by the continuity equation as follows:

$$\left(\frac{\partial}{\partial t}+\lambda^{i}\right)\left(V_j\left(\varepsilon_j^{i}+K_d^{i}\rho_{bulk}\right)c_j^{i}\right)-\sum_{m}V_j\left(\varepsilon_j^{m}+K_d^{m}\rho_{bulk}\right)Br_m^{i}\lambda^{i}c_j^{m} = \sum_{k}\left(N_{kj}^{i}-N_{jk}^{i}\right)+R_c^{i} \quad (2\text{-}1)$$

The superscripts *i* and *m* denote the daughter and parent nuclides, respectively, and the subscript *j* denotes the compartment index. The other terms in Equation 2-1 are defined below:

t = Time [s].

λ^{i} = Decay constant of radionuclide *i* [1/s].

V_j = Volume of compartment *j* [m^3].

ε^{i} = Diffusion available porosity for radionuclide *i* in compartment *j* [–].

K_d^{i} = Sorption coefficient for radionuclide *i* [m^3/kg].

ρ_{bulk} = Bulk density of the sorbing material i.e. concrete or bentonite [kg/m^3].

c_j^{i} = Activity concentration of species *i* in the pore water in compartment *j* [Bq/m^3].

Br_m^{i} = Branching ratio from parent radionuclide *m* to radionuclide *i* [–].

N_{kj}^{i} = Activity release of radionuclide *i* from compartment *k* to *j* [Bq/s].

R_c^{i} = Rate of release of species *i* by corrosion of metallic waste [Bq/s].

$V_j\left(\varepsilon_j^{i}+K_d^{i}\rho_{bulk}\right)$ = Capacity of compartment *j* for radionuclide *i* [m^3].

$\left(\varepsilon_m+K_d^{m}\rho_{bulk}\right)Br_m^{i}\lambda^{i}c^{m}$ = Rate of ingrowth of species *i* per unit volume by parent radionuclide *m* [Bq s^{-1} m^{-3}].

The equation accounts for advection, diffusion, sorption, radioactive decay, ingrowth and release from an internal source term, i.e. the release due to the corrosion of metallic waste components. It should be noted that dispersion is not explicitly considered in the compartmental approach formulation. However, when the compartmental approach is applied, the spatial discretization of the system introduces a numerical dispersive effect with respect to radionuclide transport. In the near-field model, this results in a dispersion, corresponding to Pe = 10, given the five-compartmental model assumed (Wessely and Shahkarami 2019). In the near-field model, the total transfer rate from compartment *k* to a neighbouring compartment *j*, N_{kj}^{i} [Bq/s], can be described by:

$$N_{kj}^{i}=\frac{\left(c_k^{i}-c_j^{i}\right)}{R_{kj}^{i}+R_{jk}^{i}}+Q_{kj}c_k^{i} \quad (2\text{-}2)$$

Where c_k^{i} [Bq/m^3] is the pore water activity concentration of radionuclide *i* in compartment *k*, Q_{kj} [m^3/s] is the water flow rate from compartment *k* to compartment *j*, and R_{kj}^{i} [s/m^3] is the diffusion resistance against the transport of radionuclide *i* from compartment *k* toward compartment *j*, given by:

$$R_{kj}^{i}=\frac{l_{kj}/2}{A_{kj}.D_{e,k}^{i}} \quad (2\text{-}3)$$

where A_{kj} is the contact area between the compartments *k* and *j*, l_{kj} is the diffusion length of compartment *k* in the direction of compartment *j*, and $D_{e,k}^{i}$ is the effective diffusivity of radionuclide *i* in the compartment *k*.

At the vault-rock interface, where the vault is intersected by high-permeable fractures, the water flowing in the fractures will take up solutes from the low permeable backfill interface by diffusion (Wessely and Shahkarami 2019). The diffusive transport rate from a boundary compartment *b* to the

seeping water in fractures is obtained by introducing the concept of equivalent flow rate, Q_{eq} and its corresponding diffusion resistance, $R_{eq} = {}^{1}/_{Q_{eq}}$ (Neretnieks et al. 2010). Hence, the total transfer rate of radionuclide i from the boundary compartment b, N_{bw}^{i} [Bq/s], can be obtained by:

$$N_{bw}^{i} = \frac{\left(c_b^i - c_w^i\right)}{R_{plug}^{i} + \frac{1}{Q_{eq}^{i}}} + Q_b c_b^i \qquad (2\text{-}4)$$

where R^{i}_{plug} [s/ m^3] is the geometrical transport resistance at the fracture opening connected to the boundary compartment (Neretnieks 1986). Q_{eq}^{i} [m^3/s] is the equivalent flow rate; Q_b [m^3/s] is the water flow rate from the boundary compartment to the fracture in the rock; c_b^i is the activity concentration of radionuclide i in the boundary compartment; c_w^i is the activity concentration of radionuclide i in the flowing water in the fracture. The first term in Equation 2-4 denotes the diffusive transport from the boundary compartment and the second term denotes the advective transport.

In the waste compartments, radionuclides can sorb onto the cement embedded in the grout and concrete structures. However, in BHA, dissolved complexing agents including Isosaccharinic Acid (ISA) can react with radionuclides and reduce their tendency to sorb on the cement particles embedded in the grout and concrete structure. It should also be noted that no sorption is assumed to occur on the waste and corrosion products. Furthermore, no sorption is assumed to occur on the concrete ballast.

2.1.5 Identified input data categories

In light of the above discussion, the required input data for the near-field model are listed in Table 2-2 that also points the reader to the sections where the data are provided.

Table 2-2. Categories of input data needed for the near-field model.

Category	Section
Geometries used when setting up the compartmental model:	
• Geometry of BHA.	2.2.1
• Geometry of BHK.	2.2.2
Radionuclide inventory at initial state in waste domain:	
• BHA radionuclide inventory.	2.3.1
• BHK radionuclide inventory.	2.3.2
Radionuclide decay data.	2.4
Data for partitioning of radionuclides in the waste compartments:	
• Pore volume in the BHA waste compartment.	2.5.1
• Pore volume in the BHK waste compartment.	2.5.1
• Amount of cement in the BHA waste compartment.	2.5.2
• Amount of cement in the BHK waste compartment.	2.5.2
• Amounts and thickness of metallic waste components in BHK.	2.5.3
• Corrosion rate of metallic waste components in BHK.	2.5.4
• Sorption coefficients in cement.	2.5.5
• Sorption reduction factors due to complexing agents.	2.5.6
Data for diffusive and advective transport out of waste compartments:	
• Diffusion transport resistance in the BHA waste compartment.	2.6.1
• Diffusion transport resistance in the BHK waste compartment.	2.6.2
• Advective flow in the BHA waste compartment.	2.6.3
• Advective flow in the BHK waste compartment.	2.6.4
Data for partitioning of radionuclides in backfill compartments:	
• Pore volume in the BHA backfill compartments.	2.7.1
• Pore volume in the BHK backfill compartments.	2.7.1
• Amount of bentonite in the BHA backfill compartments.	2.7.2
• Amount of cement in the BHK backfill compartments.	2.7.3

Category	Section
• Sorption coefficients in cement.	2.7.4
• Sorption coefficients in bentonite.	2.7.5
• Sorption reduction factors due to complexing agents.	2.7.6
Data for diffusive and advective transport out of backfill compartments:	
• Diffusion transport resistance in the BHA backfill compartments.	2.8.1
• Diffusion transport resistance in the BHK backfill compartments.	2.8.2
• Advective flow in the BHA backfill compartments.	2.8.3
• Advective flow in the BHK backfill compartments.	2.8.4
Data for diffusion and advective transport at the vault-rock interfaces:	
• Transport properties of the intersecting fractures at the BHA vault-rock interface.	2.9.1
• Effective diffusion transport resistance to the intersecting fractures at the BHA vault-rock interface.	2.9.2
• Effective diffusion transport resistance between the BHA backfill boundary sub-compartments and the host rock.	2.9.3
• Transport from the BHA backfill to the water seeping in the host rock.	2.9.4
• Transport properties of the intersecting fractures at the BHK vault-rock interface.	2.9.5
• Total equivalent flow rate at the BHK vault-rock interface.	2.9.6
• Transport from the BHK backfill to the water seeping in the host rock.	2.9.7
Distribution of radionuclide release on host rock trajectories:	
• Source term distribution factors in BHA.	2.10.1
• Source term distribution factors in BHK.	2.10.2

2.2 Geometrical data used to set up the near-field models

2.2.1 Geometry of the BHA vault

Short description of data

This set of data describes the applied geometries in the compartmental representation of the BHA vault, in the near-field model. The model includes one waste compartment and the three groups of bentonite backfill compartments as depicted in Figure 2-2. The geometrical data used in the model are derived from the vault dimensions, which are detailed in the **Initial state report**.

Use in model or evaluation activity

For the modelling, the geometrical data of the near-field components are required to characterise the backfill and waste compartments. These data are used to setup the compartmental representation of the near-field, given the following simplifications. The model assumes that the waste compartment is a cuboid of width W, length L, and height H. The inflow and outflow compartments are also assumed to be cuboids of thickness D that represent the backfill between the waste domain and the short-side walls of the BHA vault. The side compartment represents the backfill volumes that are located between the waste domain and the vault floor, vault roof, and the two long-side walls of the vault. For mathematical convenience, these four volumes are straightened out into a single cuboid with the assumed width, length, and thickness.

The thicknesses and cross-section areas of the waste and bentonite backfill compartments are required to determine the diffusion transport resistance in each compartment. In addition, the volumes of the compartments are required to determine the pore water volume and the dissolved radionuclide activity concentrations in the compartments.

Input data used in near-field model

The applied dimensions are listed in Table 2-3, together with their respective indicators in Figure 2-3 and parameters in the SE-SFL near-field radionuclide transport model (**Initial state report**).

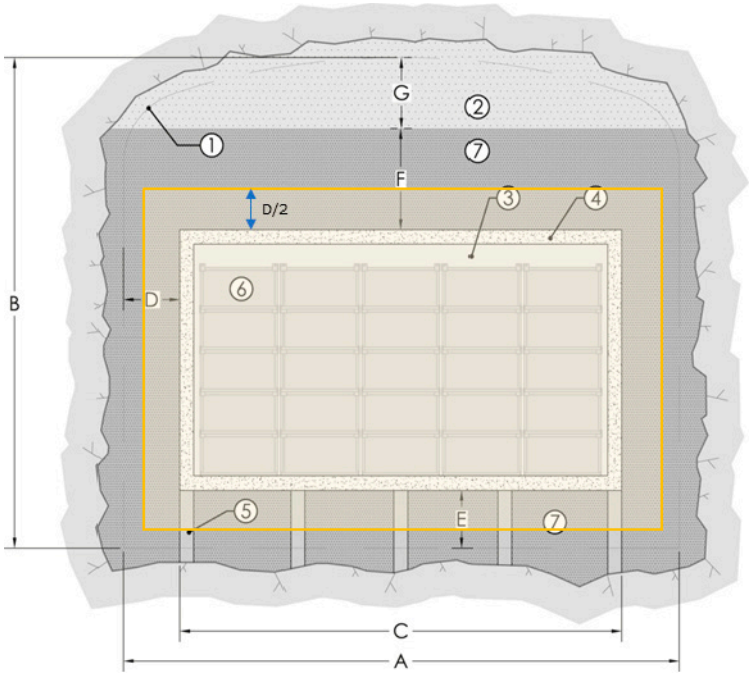

Figure 2-3. *Schematic cross-sectional layout of BHA with (1) Theoretical tunnel contour, (2) Bentonite pellets, (3) Grout, (4) Concrete structure (0.5 m), (5) Granite pillars, (6) Waste packages, (7) Bentonite blocks. Approximate dimensions: A = 20.6 m, B = 18.4 m, C = 16 m, D = 2.3 m, E = 2.4 m, F = 4 m, G = 3.7 m. After Elfwing et al. (2013).*

Table 2-3. Dimensions of the BHA vault and concrete structure.

Description	Value [m]	Parameter in the model
Excavated rock cavity		
Total length	169.3	tunnel_length
Width (A)	20.6	tunnel_width
Height (B)	18.4	tunnel_height
Concrete structure		
Length outer	140	cs_length
Width outer (C)	16	cs_width
Height outer (B-(E+F+G))	8.4	cs_height
Thickness of concrete lid	0.5	lid_thickness
Thickness of concrete floor	0.5	floor_thickness
Thickness of outer walls	0.5	iz_wall_thickness rz_wall_thickness side_wall_thickness
Bentonite thickness		
Bottom bentonite thickness	2.4	bottom_bf_height
Top bentonite thickness	7.6	top_bf_height

From these data, the BHA waste compartment is considered to have the following dimensions:

- BHA waste compartment: L_{wc} = 140 m, W_{wc} = 16 m, H_{wc} = 8.4 m, V_{wc} = 18 816 m^3.

where the subscripts *wc* denotes the waste compartment. Hence, the cross-section area normal to the flow direction, A_{nf}, can be obtained by:

$$A_{nf}^{wc} = H_{wc} \cdot W_{wc} = 134.4 \text{ m}^2 \quad (2\text{-}5)$$

In a similar manner, the cross-section area normal to the side direction, A_{ns}, can be calculated by:

$$A_{ns}^{wc} = L_{wc} \cdot (2 \cdot W_{wc} + 2 \cdot H_{wc}) = 6\,832 \text{ m}^2 \quad (2\text{-}6)$$

It should be emphasized that the waste compartment consists of the waste domain and concrete structure. Since the thicknesses of the structure outer walls, floor, and lid are 0.5 m, it can be inferred that the dimensions of the waste domain are:

- BHA waste domain: $L_{wd} = 139$ m, $W_{wd} = 15$ m, $H_{wd} = 7.4$ m, $V_{wd} = 15\,429$ m^3.

where the subscript *wd* denotes the waste domain. Hence, the volume of the BHA concrete structure, indexed *cs*, becomes:

- BHA concrete structure: $V_{cs} = V_{wc} - V_{wd} = 3\,387$ m^3.

According to the proposed design for BHA, Figure 2-3, the actual thickness of the bentonite backfill varies around the concrete structure. However, in the near-field model, it is assumed that the backfill can be represented by compartments with a fixed thickness of D. Given the parameter names in Table 2-3, the compartment thickness D can be pessimistically estimated as:

$$D = \frac{(tunnel\_width) - (cs\_width)}{2} = 2.3\ m \quad (2\text{-}7)$$

Hence, given the corresponding values in the waste compartment, the width and height of the inflow and outflow compartments can be determined as:

- BHA inflow backfill compartment:

$$W_{ic} = W_{wc} + 2D = 20.6 \text{ m} \quad (2\text{-}8)$$

$$H_{ic} = H_{wc} + 2D = 13 \text{ m} \quad (2\text{-}9)$$

- BHA outflow backfill compartment:

$$W_{oc} = W_{wc} + 2D = 20.6 \text{ m} \quad (2\text{-}10)$$

$$H_{oc} = H_{wc} + 2\text{D} = 13 \text{ m} \quad (2\text{-}11)$$

The subscripts *ic* and *oc* denote the inflow compartment and outflow compartment, respectively. Given this information, the available diffusion area in BHA, i.e. the cross-section area normal to the inflow direction, can be calculated as (the shaded region in Figure 2-3):

$$A_{nf}^{bA} = (W_{wc} + D) \cdot (H_{wc} + D) = 195.8 \text{ m}^2 \quad (2\text{-}12)$$

In the near-field model, the length of the side compartments, L_{sc} [m] is assumed to be identical to the length of the waste compartment, i.e. 140 m. Therefore, the total cross-section area along the flow direction in BHA is calculated, for the four side compartments, as:

$$A_{ns}^{bA} = (2 \cdot W_{wc} + 4 \cdot D + 2 \cdot H_{wc}) \cdot L_{sc} = 8\,120 \text{ m}^2 \quad (2\text{-}13)$$

The volumes of the backfill compartments are also calculated and listed in Table 2-4 together with the compartment cross-section areas calculated above.

Table 2-4. Volumes and cross-section areas of the waste and backfill compartments in BHA.

Compartment/domain	Cross-section area [m^2]	Volume [m^3]
BHA – Waste domain		15 429
BHA – Concrete structure		3 387
BHA – Waste compartment		18 816
BHA – Waste compartment inflow/outflow*	134.4	
BHA – Waste compartment side**	6 832	
BHA – Inflow backfill compartment	195.8	616
BHA – Outflow backfill compartment	195.8	616
BHA – Side backfill compartment	8 120	18 676

* Cross-section area normal to the inflow/outflow direction.

** Cross-section area normal to the side direction.

Source of data and justifications

The primary source for the BHA geometrical data is the **Initial state report**. The geometry data are also justified in the SE-SFL Initial state report.

In general, two sets of data are required to set up the BHA near-field model.

– The length, width, and height of the concrete structure, which are viewed as length, width, and height of the waste compartment.

– The differences between the length, width, and height of the concrete structure and the vault, which are evaluated as:

  (tunnel_length − cs_length)/2 = 14.7 m
  (tunnel_height − cs_height)/2 = 5 m
  (tunnel_width − cs_width)/2 = 2.3 m

For the modelling, a relatively small value, i.e. 2.3 m, is used to assign the backfill thickness for all the compartments. Therefore, the backfill thickness is underestimated.

Known limitations in data

Geometries of the waste and backfill components are simplified in the near-field model. Furthermore, since the selected backfill thickness lies in the lower range of the actual thickness, the backfill thickness is underestimated. Note that this is a pessimistic assumption, as it neglects part of the backfill that can contribute to the diffusion transport resistance.

2.2.2 Geometry of the BHK vault

Short description of data

This set of data concern the applied geometries in the compartmental representation of the BHK vault, in the near-field model. The model includes one waste compartment and the three groups of concrete backfill compartments depicted in Figure 2-1. The data are selected from the geometry data provided in the **Initial state report** for the proposed design of the BHK vault, Figure 2-4.

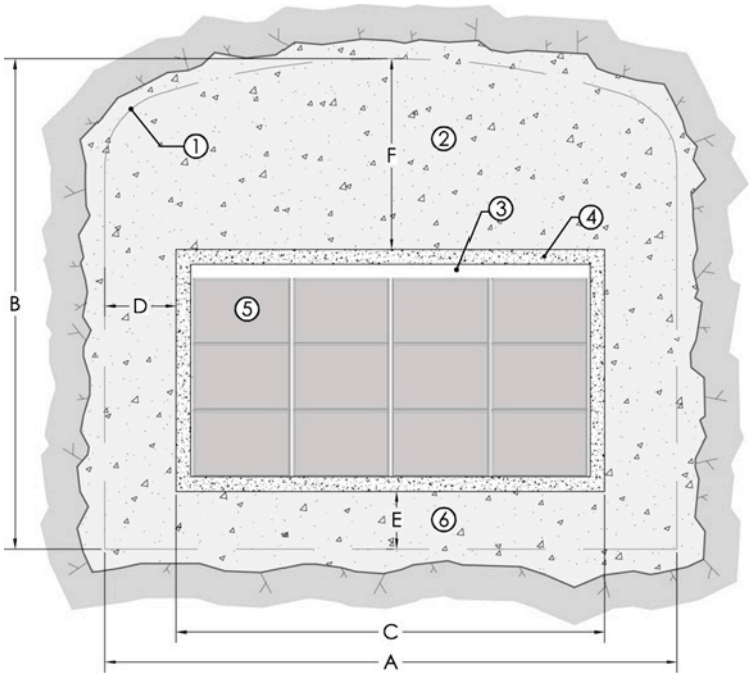

Figure 2-4. *Schematic cross-sectional layout of BHK with (1) Theoretical tunnel contour, (2) Concrete backfill, (3) Grout, (4) Concrete structure (0.5 m), (5) Steel tanks, (6) Concrete. Approximate dimensions: A = 20.6 m, B = 19.6 m, C = 15 m, D = 2.8 m, E = 2.4 m, F = 8.8 m. After Elfwing et al. (2013).*

Use in model or evaluation activity

For the modelling, the geometrical data of the near-field components are required to characterise the backfill and waste compartments. These data are used to set up the compartmental representation of the system, given the following simplifications. The model assumes that the waste compartment is a cuboid of width W, length L, and height H. The inflow and outflow compartments are also cuboids of thickness D that represent the backfill between the waste domain and the vault floor and the vault roof. The side compartment represents backfill volumes, which are located between the waste domain and the two short-side walls and two long-side walls of the vault. For mathematical convenience, these four volumes are straightened out into a single cuboid of the assumed height, length, and thickness.

Similar to BHA, the thicknesses and cross-section areas of the waste and concrete backfill compartments are required to determine the diffusion transport resistance in each compartment. In addition, the volumes of the compartments are required to determine the pore water volume and the dissolved radionuclide activity concentrations in the compartments.

Input data used in near-field model

The applied dimensions are listed in Table 2-5, together with their respective indicators in Figure 2-4 and parameters in the SE-SFL near-field radionuclide transport model.

Table 2-5. Dimensions of the BHK vault and concrete structure.

Description	Value [m]	Parameter in model
Excavated rock cavity		
Total length	134.1	tunnel_length
Width (A)	20.6	tunnel_width
Height (B)	19.6	tunnel_height
Concrete structure		
Length outer	90	
Width outer (C)	15	cs_width_outer
Height outer (B−(F+E))	8.4	cs_height_outer
Thickness of concrete lid	0.5	cs_lid_thickness
Thickness of outer wall	0.5	cs_wall_thickness
Thickness of concrete floor	0.5	cs_floor_thickness

When setting up the compartmental model, the six caissons are combined into a single waste compartment where the distances between the caissons are assumed negligible. Hence, given the data provided in Table 2-5, the BHK waste compartment is considered to have the following dimensions:

- BHK waste compartment: $L_{wc} = 90$ m, $W_{wc} = 15$ m, $H_{wc} = 8.4$ m, $V_{wc} = 11\,340$ m^3.

Accordingly, the cross-section area normal to the flow direction, is calculated by

$$A_{nf}^{wc} = L_{wc} \cdot W_{wc} = 1\,350 \text{ m}^2 \quad (2\text{-}14)$$

In a similar manner, the cross-section area normal to the side direction, is calculated by

$$A_{ns}^{wc} = H_{wc} \cdot (2 \cdot W_{wc} + 2 \cdot L_{wc}) = 1\,764 \text{ m}^2 \quad (2\text{-}15)$$

It should be noted that, since the waste compartment consists of the waste domain and concrete structure, the total volume should be decomposed into the volumes of the waste domain and the concrete structure. As can be seen in Table 2-5, the thickness of the walls, floor, and lid of the six concrete caissons is 0.5 m. Hence, the dimensions of the waste domain become:

- BHK waste domain: $L_{wd} = 89$ m, $W_{wd} = 14$ m, $H_{wd} = 7.4$ m, $V_{wd} = 9\,220.4$ m^3.

and the volume of the BHK concrete structure becomes:

- BHK concrete structure: $V_{cs} = V_{wc} - V_{wd} = 2\,119.6$ m^3.

According to the proposed design for BHK, the actual thickness of the concrete backfill surrounding the concrete structure varies. However, in the compartmental model, it is assumed that the backfill can be represented by compartments with a fixed thickness. Given the parameters in Table 2-5, the thickness is pessimistically estimated as:

$$D = \frac{(tunnel\_width)-(cs\_width\_outer)}{2} = 2.8\ m \quad (2\text{-}16)$$

Thus, given the corresponding values in the waste compartment, the width and length of the inflow and outflow backfill compartments, indexed *ic* and *oc*, are obtained by:

- BHK inflow compartment:

$$W_{ic} = W_{wc} + 2D = 20.6 \text{ m} \quad (2\text{-}17)$$

$$L_{ic} = L_{wc} + 2D = 95.6 \text{ m} \quad (2\text{-}18)$$

- BHK outflow compartment:

$$W_{oc} = W_{wc} + 2D = 20.6 \text{ m} \quad (2\text{-}19)$$

$$L_{oc} = L_{wc} + 2D = 95.6 \text{ m} \quad (2\text{-}20)$$

Hence, the available diffusion area in BHK, i.e. the cross-section area normal to the inflow direction, is calculated as:

$$A_{nf}^{bK} = (W_{wc} + D) \cdot (L_{wc} + D) = 1\,652 \text{ m}^2 \quad (2\text{-}21)$$

The height of the side compartments, H_{sc} [m], is assumed identical to the height of the waste compartment, i.e. 8.4 m. Hence, the total cross-section area along the inflow direction, is calculated, for the four sides, as:

$$A_{ns}^{bK} = (2 \cdot W_{wc} + 4 \cdot D + 2 \cdot L_{wc}) \cdot H_{wc} = 1\,858 \text{ m}^2 \quad (2\text{-}22)$$

The volumes of the backfill compartment are also calculated and listed in Table 2-6 together with the compartment cross-section areas calculated above.

Table 2-6. Volumes and cross-section areas of the waste and backfill compartments in BHK.

Compartment	Cross-section area [m^2]	Volume [m^3]
BHK – Waste domain		9 220
BHK – Concrete structure		2 120
BHK – Waste compartment		11 340
BHK – Waste compartment inflow/outflow*	1 350	
BHK – Waste compartment side**	1 764	
BHK – Inflow backfill compartment	1 652	5 514
BHK – Outflow backfill compartment	1 652	5 514
BHK – Side backfill compartment	1 858	5 203

* Cross-section area normal to the inflow/outflow direction.

** Cross-section area normal to the side direction.

Source of data and justification

The primary source for the BHK geometry data is the **Initial state report**. The geometry data are also justified in the SE-SFL Initial state report.

Two sets of data are required to set up the BHK compartmental model.

– The width and height of the concrete structures, which are viewed as width and height of the waste compartment. The waste compartment contains the six concrete structures in the vault. Therefore, the length of the waste compartment is set to be six times of that of the concrete structure length. This approach neglects the concrete filled space between the caissons.
– The differences between the width, height and outer length of the concrete structure and the rock cavity, which are evaluated as:

  (tunnel_length – Total length outer)/2 = 14.7 m
  (tunnel_height – cs_height_outer)/2 = 5.5 m
  (tunnel_width – cs_width_outer)/2 = 2.8 m

For the modelling, a relatively small value, i.e. 2.8 m, is used to assign the backfill thickness for all compartments. Therefore, the backfill thickness is underestimated.

Known limitations in data

Geometries of the near-field components are greatly simplified in the compartmental model. Furthermore, since the selected backfill thickness lies in the lower range of the actual thickness, the backfill thickness is underestimated. Note that this is a pessimistic assumption, as it neglects part of the backfill that can contribute to the diffusion transport resistance. It should also be noted that the assigned cross-section areas of the backfill compartments, A_{ns}^{bK}, can underestimate the true effect of cross-section areas.

2.3 Radionuclide inventory at initial state in waste compartments

In total, 67 different radionuclides are included in the radionuclide transport modelling in SE-SFL, as listed in Table 2-1. A special treatment is given to C-14, where the total C-14 inventory is separated on three components, namely, induced C-14, inorganic C-14, and organic C-14. It should be noted that the ESS-specific radionuclides, i.e. radionuclides deriving from the planned European Spallation Source (ESS), are not included in the SE-SFL base case.

2.3.1 BHA radionuclide inventory

Short description of data

The data concern the radionuclide inventory in the BHA vault upon the repository closure in the year 2075. Since radionuclides with low activity levels or short half-lives do not contribute to radiological risk, the provided data does not include such radionuclides. This is discussed in Crawford (2018).

Use in model or evaluation activity

In the near-field model, the radionuclide inventory in BHA is assumed to be instantly released from the waste matrix to the pore water in the waste domain upon the repository closure (**Radionuclide transport report**). Furthermore, the model assumes that the initial state activity is uniformly distributed over the waste compartment.

Input data used in near-field model

The inventory data in BHA are provided in Table 2-7, where radionuclides with zero initial activities are also listed. However, the data excludes the ESS radionuclide inventory and nuclides that exclusively exist in the BHK vault. The data are stored in the SVN database at:

svn://svn.skb.se/SFL/SFLSAK/Arbetsmaterial/RadionuclideTransport/CalculationCases/CC1/Nearfield/CC_specific_indata/TotalInitialAmount.xlsx.

Table 2-7. Total activity of radionuclides in the BHA vault at initial state in 2075 [a].

Radionuclide	Activity [Bq]	Radionuclide	Activity [Bq]	Radionuclide	Activity [Bq]
Ac-227	0	Cs-137	2.18E+13	Pu-242	1.41E+10
Ag-108m	2.57E+12	Eu-152	9.26E+11	Ra-226	3.30E+12
Am-241	7.84E+12	H-3	4.13E+13	Ra-228	0.00E+00
Am-242m	5.69E+08	Ho-166m	0.00E+00	Se-79	2.28E+07
Am-243	2.34E+09	I-129	1.64E+07	Sm-151	9.81E+09
Ba-133	1.87E+05	K-40	5.53E+09	Sr-90	2.52E+13
Be-10	2.67E+10	Mo-93	6.46E+12	Tc-99	1.85E+15
C-14-ind	0.00E+00	Nb-93m	1.13E+09	Th-228	1.08E+10
C-14-inorg	0.00E+00	Nb-94	3.86E+09	Th-229	0.00E+00
C-14-org	5.88E+13	Ni-59	4.03E+12	Th-230	0.00E+00
Ca-41	0.00E+00	Ni-63	1.80E+15	Th-232	4.82E+09
Cd-113m	0.00E+00	Np-237	3.65E+10	U-232	1.23E+06
Cl-36	2.95E+13	Pa-231	0.00E+00	U-233	4.16E+02
Cm-242	0.00E+00	Pb-210	0.00E+00	U-234	7.79E+10
Cm-243	3.65E+08	Pd-107	5.46E+06	U-235	1.35E+10
Cm-244	3.71E+10	Po-210	0.00E+00	U-236	1.19E+09
Cm-245	2.35E+07	Pu-238	2.74E+13	U-238	2.46E+11
Cm-246	6.23E+06	Pu-239	1.64E+12	Zr-93	0.00E+00
Co-60	4.34E+11	Pu-240	5.60E+12		
Cs-135	5.46E+07	Pu-241	3.95E+13		

Source of data and justification

The inventory is based on relatively sparse data from gamma spectroscopy and sampled surface contamination in combination with a correlation procedure[1] (**Initial state report**, Section 3.8.2). The non-zero inventory data in Table 2-7 can be found in a reference document[1]. The provided data include activities from historical waste, operation waste, and decommissioning waste that are planned to be disposed in the SFL repository. The data are justified in the same reference document[1].

Known limitations in data

There is a high degree of uncertainty in the estimated inventory of the radionuclides. This uncertainty is more pronounced when the estimated inventory relies on the activities of other radionuclides. The inventory is based on relatively sparse data from gamma spectroscopy and sampled surface contamination in combination with the correlation procedure[1]. The reader may refer to the reference document for detailed discussions.

2.3.2 BHK radionuclide inventory

Short description of data

The data concern the radionuclide inventory in the BHK vault at the initial state. The radionuclide inventory in BHK is divided into two fractions: an instant release fraction and a fraction where the radionuclides are released by corrosion. Since radionuclides with low activity levels or short half-lives do not contribute to radiological risk, the provided data does not include such radionuclides.

[1] Herschend B, 2015. Long-lived waste from AB SVAFO and Studsvik Nuclear AB. SKBdoc 1431282 ver 1.0, Svensk Kärnbränslehantering AB. Internal document.

Use in model or evaluation activity

In the near-field model, the BHK radionuclide inventory is categorized as:

1. Induced activity incorporated in very thin metal parts, which corrode very rapidly.
2. Surface contamination on metal parts and other unspecified activities.
3. Induced activity incorporated in metal parts with the thicknesses of 1 mm, 1 cm and 2 cm.

In the near-field model, it is assumed that the activities of the first two categories release instantly upon the repository closure, in the year 2075. The activity of the second category, however, is assumed to be released gradually together with the corrosion products as the metal parts start to corrode after the repository closure. The model also assumes that activities are homogenously distributed between the metal parts and that the metal parts corrode at a constant rate.

In the near-field model, it is assumed that the release from a metal part continues until the metal part is fully corroded and its entire inventory is released. This released activity in the waste compartment is then partitioned between the two phases, i.e. as dissolved species in the pore water and as sorbed species onto cement surfaces. Furthermore, the initial state activity, per category, is assumed to be uniformly distributed over the waste compartment.

Input data used in near-field model

The inventory data in BHK are provided in Table 2-8 to Table 2-12. The data can also be found in the SVN database at:

svn://svn.skb.se/SFL/SFLSAK/Arbetsmaterial/RadionuclideTransport/CalculationCases/CC1/Nearfield/CC_specific_indata/TotalInitialAmount.xlsx.

The inventory is based on data that has been corrected for some errors made in the previous calculations, resulting in a 0–13 % decrease in the total inventory of long-lived activation products[2].

The data for the SE-SFL base case are presented in different spreadsheets giving the inventory for the following inventory categories:

- BHKInduced00: Very thin metal parts, which are assumed to be instantly corroded.
- BHKInduced01: Metal parts with thickness of 1 mm.
- BHKInduced02: Metal parts with thickness of 1 cm.
- BHKInduced03: Metal parts with thickness of 2 cm.
- BHKSurface: Surface contamination and other activity.

This is further discussed in Section 2.5.3.

[2] Herschend B, 2016. Initial state SFL. SKBdoc 1441724 ver 1.0, Svensk Kärnbränslehantering AB. Internal document.

Table 2-8. Initial state activity in metal category including very thin metal parts in BHK.

Radionuclide	Activity [Bq]	Radionuclide	Activity [Bq]	Radionuclide	Activity [Bq]
Ac-227	0.00E+00	Gd-148	0.00E+00	Re-186m	0.00E+00
Ag-108m	5.40E+01	H-3	2.16E+07	Se-79	2.87E+04
Am-241	9.20E+07	Ho-166m	8.45E+01	Si-32	0.00E+00
Am-242m	8.34E+04	I-129	3.27E+04	Sm-151	1.08E+08
Am-243	1.06E+06	K-40	0.00E+00	Sr-90	2.58E+10
Ba-133	7.21E+02	La-137	0.00E+00	Tb-157	0.00E+00
Be-10	0.00E+00	Mo-93	1.78E+11	Tb-158	0.00E+00
C-14-ind	1.30E+12	Nb-93m	1.67E+12	Tc-99	2.27E+10
C-14-inorg	0.00E+00	Nb-94	2.14E+10	Th-228	0.00E+00
C-14-org	0.00E+00	Ni-59	7.98E+12	Th-229	0.00E+00
Ca-41	0.00E+00	Ni-63	8.06E+14	Th-230	0.00E+00
Cd-113m	9.63E+03	Np-237	6.29E+05	Th-232	0.00E+00
Cl-36	4.12E+08	Pa-231	0.00E+00	Ti-44	0.00E+00
Cm-242	0.00E+00	Pb-210	0.00E+00	U-232	1.39E+06
Cm-243	1.50E+05	Pd-107	1.97E+04	U-233	0.00E+00
Cm-244	1.93E+07	Po-210	0.00E+00	U-234	0.00E+00
Cm-245	2.35E+04	Pu-238	3.16E+09	U-235	4.32E-01
Cm-246	9.13E+03	Pu-239	7.08E+06	U-236	4.70E+05
Co-60	9.06E+12	Pu-240	6.81E+06	U-238	0.00E+00
Cs-135	3.87E+05	Pu-241	1.66E+08	Zr-93	2.37E+06
Cs-137	2.79E+10	Pu-242	8.14E+04		
Eu-150	0.00E+00	Ra-226	0.00E+00		
Eu-152	3.73E+04	Ra-228	0.00E+00		

Table 2-9. Initial state activity in metal category including 1 mm thick metal parts in BHK.

Radionuclide	Activity [Bq]	Radionuclide	Activity [Bq]	Radionuclide	Activity [Bq]
Ac-227	0.00	Gd-148	0.00	Re-186m	0.00
Ag-108m	2.94E+02	H-3	7.32E+14	Se-79	1.49E+05
Am-241	8.02E+08	Ho-166m	4.38E+02	Si-32	0.00
Am-242m	1.86E+06	I-129	1.70E+05	Sm-151	5.50E+08
Am-243	6.08E+06	K-40	0.00	Sr-90	1.44E+11
Ba-133	3.79E+03	La-137	0.00	Tb-157	0.00
Be-10	7.04E+02	Mo-93	9.27E+12	Tb-158	0.00
C-14-ind	5.06E+13	Nb-93m	5.84E+13	Tc-99	1.47E+12
C-14-inorg	0.00	Nb-94	7.88E+11	Th-228	0.00
C-14-org	0.00	Ni-59	3.68E+14	Th-229	0.00
Ca-41	8.80E-06	Ni-63	3.27E+16	Th-230	0.00
Cd-113m	1.03E+05	Np-237	3.22E+06	Th-232	0.00
Cl-36	2.32E+10	Pa-231	0.00	Ti-44	0.00
Cm-242	0.00	Pb-210	0.00	U-232	8.00E+06
Cm-243	1.03E+07	Pd-107	1.02E+05	U-233	0.00
Cm-244	8.11E+07	Po-210	0.00	U-234	0.00
Cm-245	7.19E+07	Pu-238	1.47E+10	U-235	6.59E+02
Cm-246	5.39E+04	Pu-239	8.40E+09	U-236	2.27E+06
Co-60	3.31E+14	Pu-240	6.21E+07	U-238	0.00
Cs-135	2.01E+06	Pu-241	9.38E+08	Zr-93	6.14E+11
Cs-137	1.57E+11	Pu-242	1.11E+09		
Eu-150	0.00	Ra-226	0.00		
Eu-152	1.86E+05	Ra-228	0.00		

Table 2-10. Initial state activity in metal category including 1 cm thick metal parts in BHK.

Radionuclide	Activity [Bq]	Radionuclide	Activity [Bq]	Radionuclide	Activity [Bq]
Ac-227	0.00	Gd-148	0.00	Re-186m	0.00
Ag-108m	8.34E+00	H-3	6.11E+09	Se-79	5.39E+03
Am-241	9.73E+06	Ho-166m	1.32E+01	Si-32	0.00
Am-242m	1.24E+04	I-129	5.15E+03	Sm-151	1.56E+07
Am-243	1.67E+05	K-40	0.00	Sr-90	2.98E+09
Ba-133	4.31E+01	La-137	0.00	Tb-157	0.00
Be-10	3.92E+03	Mo-93	6.65E+12	Tb-158	0.00
C-14-ind	1.35E+14	Nb-93m	4.99E+13	Tc-99	9.80E+11
C-14-inorg	0.00	Nb-94	8.70E+11	Th-228	0.00
C-14-org	0.00	Ni-59	5.53E+14	Th-229	0.00
Ca-41	0.00	Ni-63	5.41E+16	Th-230	0.00
Cd-113m	7.15E+03	Np-237	9.91E+04	Th-232	0.00
Cl-36	2.77E+10	Pa-231	0.00	Ti-44	0.00
Cm-242	0.00	Pb-210	0.00	U-232	1.93E+05
Cm-243	1.76E+04	Pd-107	3.10E+03	U-233	0.00
Cm-244	1.82E+06	Po-210	0.00	U-234	0.00
Cm-245	3.69E+03	Pu-238	4.52E+08	U-235	7.14E-02
Cm-246	1.44E+03	Pu-239	1.12E+06	U-236	7.40E+04
Co-60	5.08E+14	Pu-240	1.05E+06	U-238	0.00
Cs-135	6.10E+04	Pu-241	1.34E+07	Zr-93	7.02E+05
Cs-137	3.27E+09	Pu-242	1.28E+04		
Eu-150	0.00	Ra-226	0.00		
Eu-152	2.87E+03	Ra-228	0.00		

Table 2-11. Initial state activity in metal category including 2 cm thick metal parts in BHK.

Radionuclide	Activity [Bq]	Radionuclide	Activity [Bq]	Radionuclide	Activity [Bq]
Ac-227	0.00	Gd-148	0.00	Re-186m	0.00
Ag-108m	1.95E+12	H-3	5.77E+13	Se-79	7.00E+10
Am-241	1.51E+07	Ho-166m	1.56E+01	Si-32	0.00
Am-242m	1.74E+04	I-129	5.95E+03	Sm-151	2.43E+07
Am-243	1.94E+05	K-40	0.00	Sr-90	8.84E+09
Ba-133	6.57E+02	La-137	0.00	Tb-157	0.00
Be-10	0.00	Mo-93	6.36E+12	Tb-158	0.00
C-14-ind	1.71E+14	Nb-93m	7.46E+14	Tc-99	8.86E+11
C-14-inorg	0.00	Nb-94	1.19E+13	Th-228	0.00
C-14-org	0.00	Ni-59	8.15E+14	Th-229	0.00
Ca-41	3.79E+10	Ni-63	9.15E+16	Th-230	0.00
Cd-113m	1.43E+09	Np-237	1.14E+05	Th-232	0.00
Cl-36	5.32E+10	Pa-231	0.00	Ti-44	0.00
Cm-242	0.00	Pb-210	0.00	U-232	3.30E+05
Cm-243	5.02E+04	Pd-107	3.59E+03	U-233	0.00
Cm-244	9.45E+06	Po-210	0.00	U-234	0.00
Cm-245	4.28E+03	Pu-238	7.12E+08	U-235	4.42E-02
Cm-246	1.67E+03	Pu-239	1.29E+06	U-236	8.56E+04
Co-60	4.68E+15	Pu-240	1.23E+06	U-238	0.00
Cs-135	7.05E+04	Pu-241	1.03E+08	Zr-93	1.01E+08
Cs-137	9.33E+09	Pu-242	1.48E+04		
Eu-150	0.00	Ra-226	0.00		
Eu-152	2.46E+04	Ra-228	0.00		

Table 2-12. Surface contamination and other activities.

Radionuclide	Activity [Bq]	Radionuclide	Activity [Bq]	Radionuclide	Activity [Bq]
Ac-227	0.00	Eu-155	3.40E+09	Pu-241	1.53E+11
Ag-108m	5.37E+11	Fe-55	1.40E+11	Pu-242	1.10E+10
Am-241	5.25E+10	Gd-152	0.00	Ra-226	0.00
Am-242m	3.77E+08	H-3	4.10E+13	Ra-228	0.00
Am-243	1.08E+09	Ho-166m	4.21E+09	Ru-106	0.00
Ba-133	4.95E+09	I-129	1.69E+08	Sb-125	4.65E+08
Be-10	5.94E+04	In-115	0.00	Se-79	1.01E+09
C-14-ind	8.68E+10	Ir-192	0.00	Sm-147	0.00
C-14-inorg	0.00	K-40	0.00	Sm-151	4.51E+11
C-14-org	0.00	Mo-93	8.03E+09	Sn-126	1.92E+07
Ca-41	2.85E+11	Na-22	0.00	Sr-90	4.68E+11
Cd-113m	3.60E+07	Nb-93m	2.00E+13	Tc-99	5.19E+09
Cl-36	2.60E+09	Nb-94	1.93E+11	Th-228	0.00
Cm-242	0.00	Ni-59	3.07E+12	Th-229	0.00
Cm-243	1.37E+08	Ni-63	2.81E+14	Th-230	0.00
Cm-244	1.25E+10	Np-237	1.24E+07	Th-232	0.00
Cm-245	6.28E+08	Pa-231	0.00	U-232	1.61E+05
Cm-246	6.34E+06	Pb-210	0.00	U-233	0.00
Co-60	2.83E+12	Pd-107	4.05E+07	U-234	0.00
Cs-134	2.10E+07	Pm-147	2.79E+07	U-235	5.60E+02
Cs-135	0.00	Po-210	0.00	U-236	9.94E+06
Cs-137	7.81E+08	Pu-238	6.48E+10	U-238	
Eu-152	3.37E+12	Pu-239	1.14E+10	Zr-93	

Source of data and justification

The inventory data concerning the induced activity of the metal parts have been calculated[3]. However, it should be emphasized that due to some errors, corrections are made in the original calculations, resulting in a 0–13 % decrease in the total inventory of long-lived radionuclides compared to the original data[3]. Each of the four metal categories relies on a number of subcategories in the reference document. The surface contamination data are also taken from the same document[3].

Known limitations in data

There is a high degree of uncertainty in the estimated inventory of the radionuclides in BHK. The main uncertainty regards the conceptual uncertainties that lay in the radionuclide estimation methods. This is further investigated in a reference document[3]. Furthermore, thickness of the metal parts differs considerably in BHK. Therefore, uncertainties can also rise owing to the different distribution of the radionuclide activities over the metal parts with varying thickness.

The reader may refer to the reference documents for discussions on the uncertainties in the inventory data.

2.4 Radionuclide decay data

2.4.1 Decay constant

Short description of data

The following data concern the half-life information of the radionuclides included in SE-SFL.

Use in model or evaluation activity

In total, 67 radioactive nuclides are included in the transport modelling. In the near-field model, the radionuclide half-live $t_{½}$ [s] is correlated to the radionuclide decay constant l [s^{-1}] by:

$$t_{½} = \frac{\ln 2}{\lambda} \qquad (2\text{-}23)$$

[3] Herschend B, 2016. Initial state SFL. SKBdoc 1441724 ver 1.0, Svensk Kärnbränslehantering AB. Internal document.

Input data used in near-field model

Table 2-13 lists the half-life information of the radionuclides included in SE-SFL. The data, unless otherwise specified, are obtained from Firestone et al. (1998). It should be noted that the table also includes information of the radionuclides originating from the ESS inventory (ICRP 2008). However, the ESS-specific radionuclides are not included in the SE-SFL base case. The Half-life information can also be found in the SVN database at:

svn://svn.skb.se/SFL/SFLSAK/Arbetsmaterial/RadionuclideTransport/GemensammaIndata/Radionuclides/halfLife.xlsx.

Table 2-13. Half-life information of the radionuclides included in SE-SFL.

Radionuclide	Half-life [a]	Reference	Radionuclide	Half-life [a]	Reference
Ac-227	2.18E+01		Np-237	2.14E+06	
Ag-108m	4.38E+02	(Schrader 2004)	Pa-231	3.28E+04	
Am-241	4.32E+02		Pb-210	2.23E+01	
Am-242m	1.41E+02		Pd-107	6.50E+06	
Am-243	7.37E+03		Po-210	3.79E-01	
Ba-133	1.05E+01		Pu-238	8.77E+01	
Be-10	1.51E+06		Pu-239	2.41E+04	
C-14-ind	5.73E+03		Pu-240	6.56E+03	
C-14-inorg	5.73E+03		Pu-241	1.44E+01	
C-14-org	5.73E+03		Pu-242	3.73E+05	
Ca-41	1.03E+05		Ra-226	1.60E+03	
Cd-113m	1.41E+01		Ra-228	5.75E+00	
Cl-36	3.01E+05		Re-186m	2.00E+05	(ICRP 2008)
Cm-242	4.46E-01		Se-79	3.27E+05	(Jörg et al. 2010)
Cm-243	2.91E+01		Si-32	1.32E+02	(ICRP 2008)
Cm-244	1.81E+01		Sm-151	9.00E+01	
Cm-245	8.50E+03		Sr-90	2.88E+01	
Cm-246	4.73E+03		Tb-157	7.10E+01	(ICRP 2008)
Co-60	5.27E+00		Tb-158	1.80E+02	(ICRP 2008)
Cs-135	2.30E+06		Tc-99	2.11E+05	
Cs-137	3.01E+01		Th-228	1.91E+00	
Eu-150	3.69E+01	(ICRP 2008)	Th-229	7.34E+03	
Eu-152	1.35E+01		Th-230	7.54E+04	
Gd-148	7.46E+01	(ICRP 2008)	Th-232	1.40E+10	
H-3	1.23E+01		Ti-44	6.00E+01	(ICRP 2008)
Ho-166m	1.20E+03		U-232	6.89E+01	
I-129	1.57E+07		U-233	1.59E+05	
K-40	1.28E+09		U-234	2.46E+05	
La-137	6.00E+04	(ICRP 2008)	U-235	7.04E+08	
Mo-93	4.00E+03		U-236	2.34E+07	
Nb-93m	1.61E+01		U-238	4.47E+09	
Nb-94	2.03E+04		Zr-93	1.53E+06	
Ni-59	7.60E+04				
Ni-63	1.00E+02				

Source of data and justification

The half-life data are mostly taken from the work of Firestone et al. (1998). References are also made to Schrader (2004), Jörg et al. (2010), and ICRP (2008). The half-lives given in Table 2-13 are in many cases similar to those used in SR-PSU (SKB 2014a, Table 3-4).

Known limitations in data

The reader may refer to the reference documents for discussions on the uncertainties in the half-life data.

2.4.2 Decay chain and branching ratio

Short description of data

Many of the radionuclides are correlated through decay chains. The following data concern the decay chains and branching ratios incorporated in the near-field model. During a radionuclide chain decay process, a parent radionuclide decays and forms a daughter, which in turns decays. However, if the daughter is released to the biosphere, it can contribute to the radiological risk.

Use in model or evaluation activity

In SE-SFL, simplified radionuclide decay chains are assumed. That is, if the half-life of a daughter radionuclide is much shorter than the half-life of the parent radionuclide, the daughter radionuclide is not explicitly modelled. Instead, its contribution to the dose release is calculated assuming secular equilibrium. The model, therefore, assumes that the parent radionuclide directly produces the subsequent daughter in the chain (see Table 2-14 and Table 2-15). The simplified decay chains may, therefore, affect the modelling outcome, though to a very minor degree.

Table 2-14. Radionuclide decay chains considered in the SFL radionuclide transport calculations (black bold – explicitly modelled radionuclides of the initial inventory, black – explicitly modelled radionuclides that are not part of the initial inventory but where ingrowth is assumed, dark red – not explicitly modelled short-lived radionuclides accounted for in the dose calculations assuming secular equilibrium, green – stable isotope.

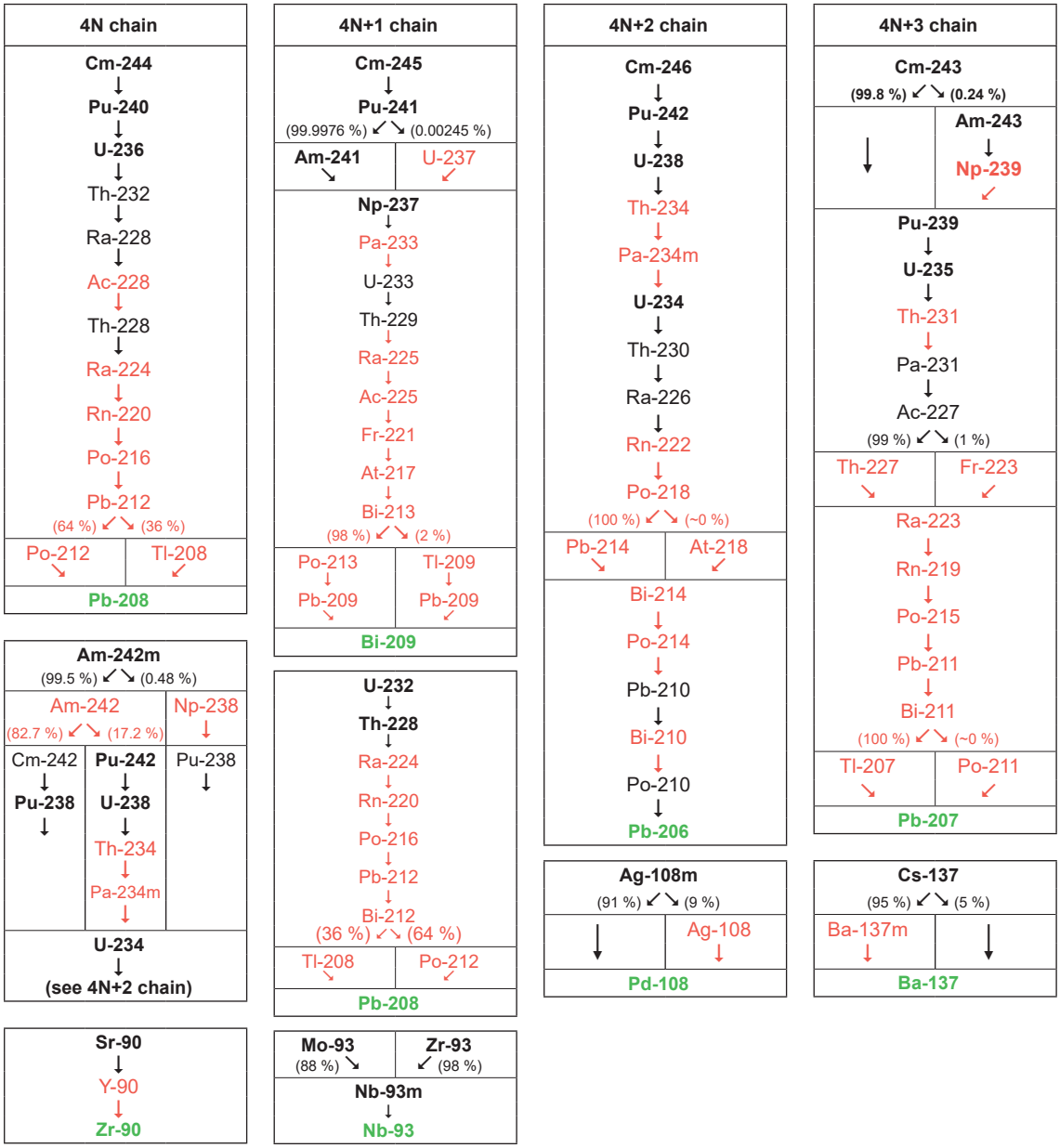

Input data used in near-field model

Table 2-15 provides the considered decay pairs, if any, for the near-field radionuclide transport modelling within SE-SFL.

Table 2-15. Decay chains and branching ratios included in SE-SFL.

Radionuclide	Daughter	Branching Ratio
Ac-227		
Ag-108m		
Am-241	Np-237	1.000
Am-242m	Cm-242	0.823
Am-242m	Pu-238	0.005
Am-242m	Pu-242	0.172
Am-243	Pu-239	1.000
Ba-133		
Be-10		
Ca-41		
Cd-113m		
C-ind-14		
C-inorg-14		
Cl-36		
Cm-242	Pu-238	1.000
Cm-243	Pu-239	0.998
Cm-243	Am-243	0.002
Cm-244	Pu-240	1.000
Cm-245	Pu-241	1.000
Cm-246	Pu-242	0.999
Co-60		
C-org-14		
Cs-135		
Cs-137		
Eu-150		
Eu-152		
Gd-148		
H-3		
Ho-166m		
I-129		
K-40		
La-137		
Mo-93	Nb-93m	0.880
Nb-93m		
Nb-94		
Ni-59		
Ni-63		
Np-237	U-233	1.000
Pa-231	Ac-227	1.000
Pb-210	Po-210	1.000
Pd-107		
Po-210		
Pu-238	U-234	1.000
Pu-239	U-235	1.000
Pu-240	U-236	1.000
Pu-241	Am-241	0.999
Pu-241	Np-237	2.45E-05
Pu-242	U-238	1.000
Ra-226	Pb-210	1.000
Ra-228	Th-228	1.000
Re-186m		
Se-79		
Si-32		
Sm-151		
Sr-90		
Tb-157		
Tb-158		
Tc-99		
Th-228		
Th-229		
Th-230	Ra-226	1.000
Th-232	Ra-228	1.000
Ti-44		
U-232	Th-228	1.000
U-233	Th-229	1.000
U-234	Th-230	1.000
U-235	Pa-231	1.000
U-236	Th-232	1.000
U-238	U-234	1.000
Zr-93	Nb-93m	0.975

Source of data and justification

The data are tabulated and justified in a reference document[4]. They can also be found in the SVN database at:

svn://svn.skb.se/SFL/SFLSAK/Arbetsmaterial/RadionuclideTransport/GemensammaIndata/Radionuclides/DecayPairs.xlsx.

Known limitations in data

The decay chains in SE-SFL are modelled under the assumption of secular equilibrium between the short-lived radionuclides, i.e. radionuclides with half-lives of less than 0.379 [a], and their parents. Therefore, the contributions of the short-lived radionuclides are not explicitly considered. This can affect the modelling outcome, though to a very minor degree. Such modelling approach was previously used in the radionuclide transport and dose calculations for the safety assessment SR-PSU (SKB 2015b).

[4] Herschend B, 2015. Long-lived waste from AB SVAFO and Studsvik Nuclear AB. SKBdoc 1431282 ver 1.0, Svensk Kärnbränslehantering AB. Internal document.

2.5 Data for partitioning of radionuclides in waste compartments

2.5.1 Porosity and pore volume in the waste compartments

Short description of data

The data concern the physical porosity and pore volume in the BHA and BHK waste compartments. In general, the pore volume of a system is defined as the physical porosity of the system times its volume. In the near-field model, both the waste domain and concrete structure contribute to the pore volume of the waste compartment. The volumes of the waste domains and concrete structures in BHA and BHK are estimated in Section 2.2.1 and Section 2.2.2, respectively. In this section, the values of physical porosity are presented from which the pore volumes are estimated. The data are used to model dissolved radionuclide activity concentrations in the waste compartments. This is further described in Wessely and Shahkarami (2019).

Use in model or evaluation activity

In the near-field model, radionuclides in a waste compartment are modelled as being dissolved in the pore water. The sorbing radionuclides can also sorb on the cement minerals in the concrete structure. To calculate the activity concentrations of radionuclides in the waste compartment, the pore volume of the compartment is needed. If a given radionuclide can sorb, the sorption information is also required (see Section 2.5.5). It should be emphasized that only dissolved radionuclides can migrate out of the waste compartment. Furthermore, since the entire waste compartment is assumed to be homogeneous, both the pore volumes of the waste domain and concrete structure contribute to the compartment pore volume.

Input data used in near-field model

The volumes of the BHA and BHK waste domains and concrete structures are given in Table 2-4 and Table 2-6, respectively. The initial state physical porosities of the waste domains and concrete structure are as follows (**Initial state report**, Section 7.1.1):

- Physical porosity of the BHA waste domain, ϵ_w^{BHA}: 31 %.
- Physical porosity of the BHK waste domain, ϵ_w^{BHK}: 28 %.
- Physical porosity of the concrete structure in BHA and BHK, ϵ_{cs}: 11 %.

It should be noted that, when degraded, the physical porosity of the concrete structure increases. Therefore, to take this effect into account, the near-field model assumes that the physical porosity of the concrete structure evolves similarly to that of BHK backfill outflow and side compartments, given in Table 2-16 (see Section 2.7.1). It should also be noted that the anions, Neutral species and cations are assumed to have access to all the physical porosities in the concrete structure. In other words, the effect of anion exclusion is neglected.

Table 2-16. Evolution of the concrete structure porosity.

Physical Porosity [%]	Timeframe [a]
11–11.3 %	2.08E+03 – 1.72E+05
11.3–19 %	1.72E+05 – 3.92E+05
19–20 %	3.92E+05 – 7.82E+05
20–24 %	7.82E+05 – 1.00E+06

Furthermore, to approximate the porosities in each time step, a linear interpolation is made between the values in Table 2-16. Figure 2-5 shows the increasing porosity of the concrete structure over time.

Hence, given the estimated volumes of the waste domains and concrete structures in BHA and BHK, the initial state pore volumes of the waste compartments can be obtained as:

- The initial state pore volume of the BHA waste compartment: 5 156 m^3.
- The initial state pore volume of the BHK waste compartment: 2 815 m^3.

The graphs showing the pore volume evolutions of the BHA and BHK waste compartments are plotted in Figure 2-6.

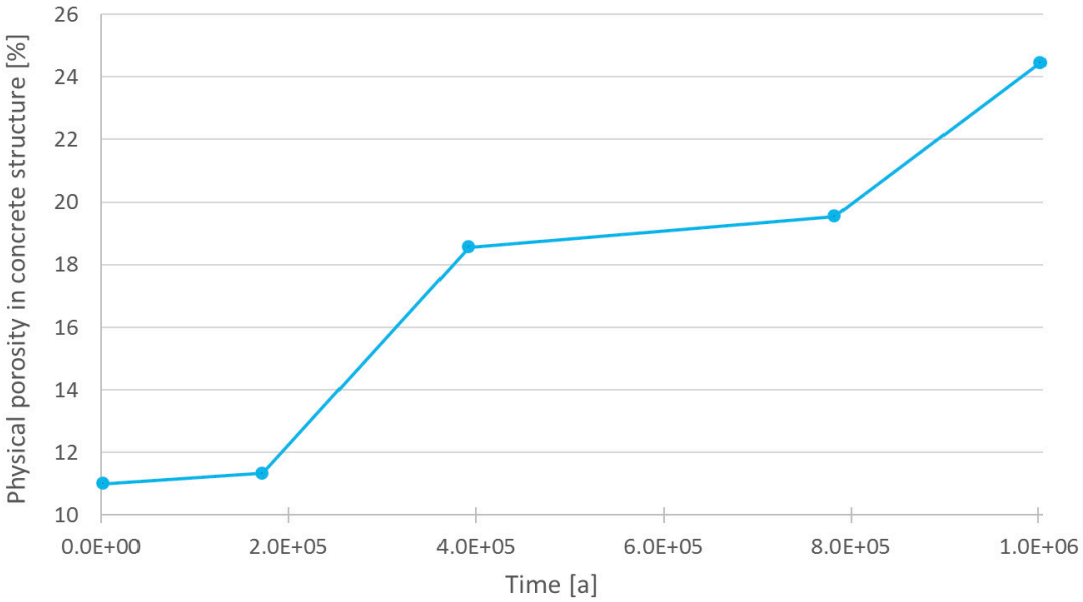

Figure 2-5. *Increasing porosity of the concrete structure in BHA and BHK due to the concrete degradation.*

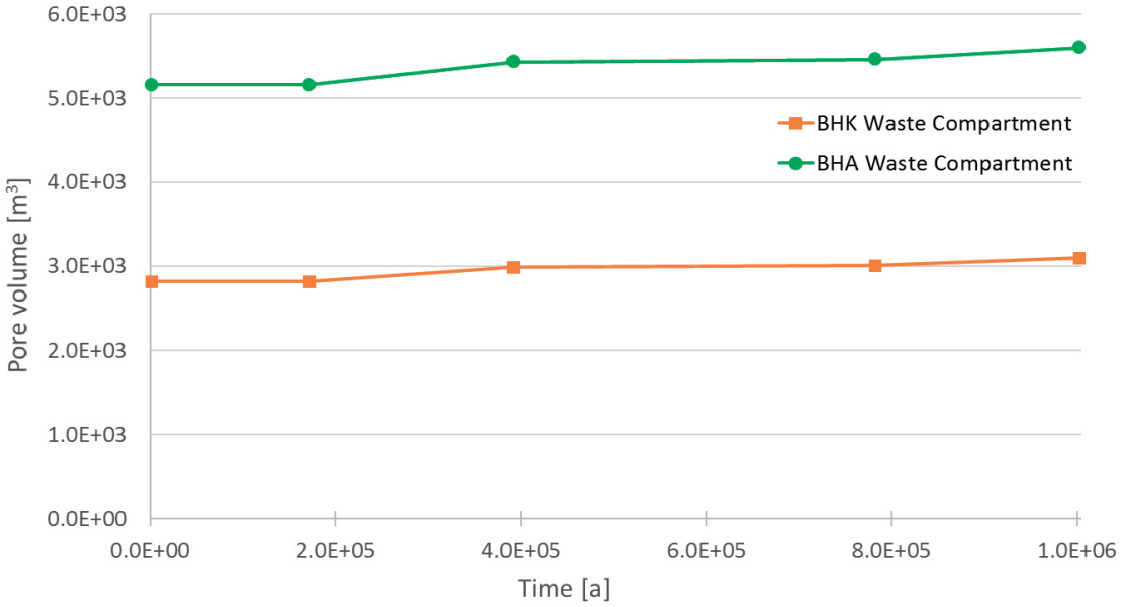

Figure 2-6. *Evolution of the pore volumes in the BHA and BHK waste compartments incorporated in the near-field model.*

Source of data and justification

The volumes of the waste domains and concrete structures in BHA and BHK are estimated in Sections 2.2.1 and 2.2.2, respectively. The initial state porosities of the waste domains in BHA and BHK are provided in the **Initial state report**, where the initial state porosity of the concrete structure is estimated as 11 %. For the modelling, it is assumed that the varying porosity of the concrete structure is comparable with the porosity of the outflow and side compartments in the BHK concrete backfill.

Known limitations in data

The estimated pore volumes are strongly dependent on the simplified geometries of the waste compartments defined in Section 2.2. Furthermore, since the porosity varies inside and between the waste domains, using a single-value porosity for the waste domain is an approximation. It should also be noted that in the **Initial state report**, the initial state porosity of construction concrete ranges between 9 % and 15 %, which is approximated to be 11 % in the near-field model.

2.5.2 Amount of cement in the BHA and BHK waste compartment

Short description of data

The waste compartments in BHA and BHK consist of the grouted waste domains and the concrete structures. The data presented in this section describe the amount of cement in the waste compartments that is embedded in the grout and concrete structures. It should be noted that cement, in this context, refers to the hydrated cement and not un-hydrated cement particles or cement powder. The procedure to estimate the amount of cement in the waste compartments, in terms of the compartment storage capacities, is detailed in Wessely and Shahkarami (2019).

Use in model or evaluation activity

Radionuclides in the waste compartments in BHA and BHK are assumed to sorb only onto the hydrated-cement embedded in the grout and concrete structure. That is, no nuclides are assumed to sorb on the ballast. Therefore, to calculate the amount of radionuclides that can be sorbed onto the cement, it is required to have information on the amount of cement in the BHA and BHK waste compartments. In the near-field model, it is assumed that the cement is evenly distributed in the waste compartment in each vault.

Input data used in the near-field model

The amount of unsaturated grout in the BHA waste domain is estimated to be 8.649×10^6 kg (**Initial state report**). However, only 0.3467 of this amount is made of cement. This cement fraction is estimated from the mixing proportions of the Silo grout in SKB (2014a, Table 7-1), which contains 325 kg cement powder/m^3, 366 kg water/m^3, and 1 302 kg ballast/m^3. In mathematical form, it can be expressed as:

- Fraction of cement in grout = (325 + 366) / (325 + 366 + 1 302) = 0.3467.

Hence, the amount of cement in the waste domain can be obtained by multiplying the cement fraction times the grout mass:

- Amount of cement in BHA waste domain: $0.3467 \times 8.649 \times 10^6 = 3.00 \times 10^6$ kg.

In the above formulation, it is assumed that no vapour loss or water leakage occurs during the curing. That is, all the water becomes part of the hydrated cement.

The estimated volume of the concrete structure in BHA is 3 387 m^3 (see Section 2.2.1), which is assumed to consist of solid particles, 89 %, and porosity, 11 % (**Initial state report**). Furthermore, the mixing proportions of the concrete structure is approximated to be 350 kg cement powder/m^3, 164.5 kg water/m^3, and 1 829 kg ballast/m^3 (SKB 2014a, Table 7-1). Hence, the density, solid particle density, and fraction of ballast in the concrete structure are calculated to be 2.34×10^3 kg/m^3, 2.63×10^3 kg/m^3, and 0.695, respectively.

- Density of concrete structure: (350 + 164.5 + 1 829) = 2 344 kg/m^3.
- Solid particle density of concrete structure: (350 + 164.5 + 1 829) / (1 − 0.11) = 2 633 kg/m^3.
- Fraction of ballast in the concrete structure: 1 829 × (1 − 0.11) / (350 + 164.5 + 1 829) = 0.6946.

Given the above values and the volume of concrete in the BHA concrete structure, i.e. 3 387 m^3 (see Section 2.2.2), the amount of cement in BHA concrete structure can be calculated as:

- Amount of cement in BHA concrete structure = 3 387 × (350 + 164.5) = 1.74 × 10^6 kg.

The total amount of cement in the BHA waste compartment can then be obtained by summing the cement mass in the BHA waste domain and concrete structure to give:

- Amount of cement in BHA waste compartment: 4.74 × 10^6 kg.

In the BHK waste domain, the amount of grout is estimated to be 5.415 × 10^6 kg (**Initial state report**). By multiplying this value by the fraction of cement in grout, i.e. 0.3467, the amount of cement in the BHK waste domain can be obtained as:

- Amount of cement in BHK waste domain: 0.3467 × 5.415 × 10^6 = 1.88 × 10^6 kg.

The volume of concrete in the BHK concrete structure is estimated to be 2 120 m^3 (Section 2.2.2). The amount of cement in the BHK concrete structure can then be calculated as:

- Amount of cement in BHK concrete structure: 2 120 × (350 + 164.5) = 1.09 × 10^6 kg.

The total amount of cement in the BHK waste compartment can then be obtained by summing the cement mass in the BHK waste domain and concrete structure to give:

- Amount of cement in BHK waste compartment: 2.97 × 10^6 kg.

In the near-field model, it is assumed that the amount of cement in the BHK and BHA concrete structures gradually decreases due to the concrete leaching. This results in an increased concrete porosity. To take this change into account, the varying amount of cement per volume of the concrete structure, i.e. density of cement in the concrete structure, p_c, is approximated as:

$$p_c = (1 - \epsilon_{cs} - \varphi) \cdot p_p \qquad (2\text{-}24)$$

where:

ϵ_{cs} = Porosity of concrete structure (Figure 2-5) [–].

φ = Fraction of ballast in the concrete structure [–].

p_p = Solid particle density of the concrete structure [kg/m^3].

Hence, with the help of Figure 2-5 the amount cement in the BHA and BHK waste compartments in each time step can be approximated. The estimated values are plotted in Figure 2-7.

Source of data and justification

Volumes of the waste domains and concrete structures are estimated in Sections 2.2.1 and 2.2.2. The amounts of grout in the BHA and BHK waste domains are taken from the **Initial state report**. The porosity of 11 % for the construction concrete is also taken from the initial state report. The solid particle density of concrete and cement fractions are calculated from the mixing proportions of the concrete structure and silo grout (SKB 2014a, Table 7-1).

Known limitations in data

Since the exact recipe of the concrete and grout are not known yet, the relevant information from the SFR repository has been used. There may also be uncertainties in the initial state amounts of concrete and grout. Furthermore, the simplified geometries of the models can result in an under-estimated amount of cement in the vaults.

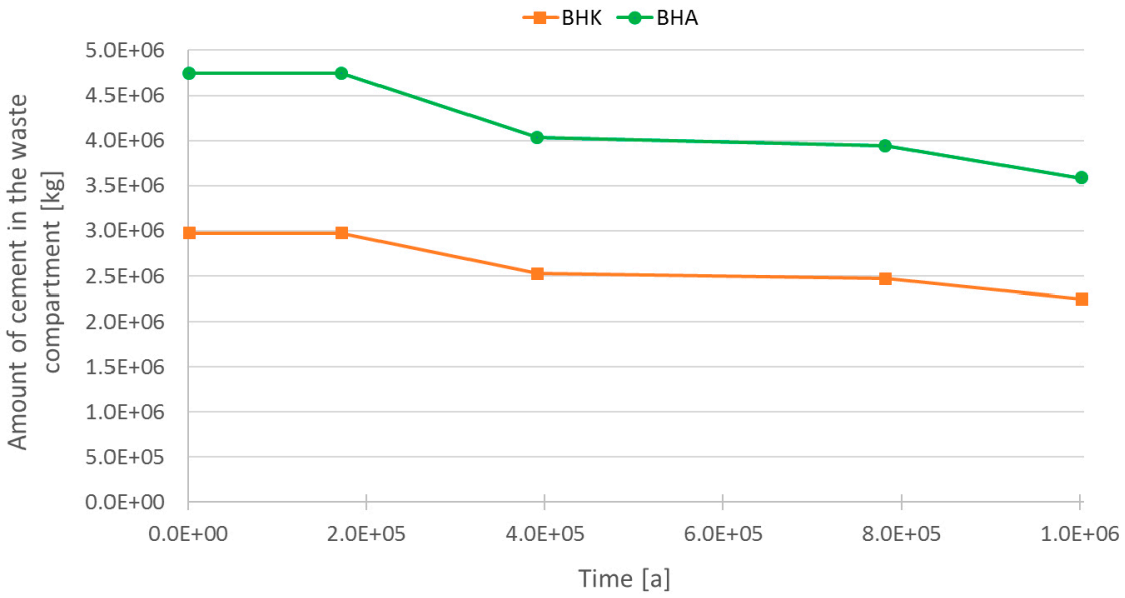

Figure 2-7. *Evolution of cement mass in the BHA and BHK waste compartments.*

In the near-field model, it is assumed that the concrete structure in BHA experiences similar degradation process as that in BHK, even though it is protected by very low-permeable bentonite. This is, therefore, a pessimistic assumption.

2.5.3 Thickness of metallic waste components in BHK

Short description of data

The metallic components in the BHK waste will corrode over time, resulting in radionuclide release from the vault. In this report, the term metallic components are used to describe a collection of metallic alloys and other types of non-cementitious materials in BHK. The time required for the metal components to be become fully corroded, strongly depends on their thickness. In BHK, thickness of the components differs considerably. Therefore, in the near-field model, the metallic components are grouped into four different categories based on their thickness, and each category is assigned a single-value thickness.

Use in model or evaluation activity

In the near-field model, each metallic category is represented by a compartment, where the induced activity of the contained metallic compartment can change by ingrowth, chain decay and the activity release due to the corrosion from the metallic waste components. In mathematical terms:

$$\left(\frac{\partial}{\partial t}+\lambda^i\right)A_l^i-\sum_m Br_m^i\lambda^i A_l^m=-R_{c,l}^i=-\sum_l H(T_l-t)\frac{A_l^i}{T_l-t} \qquad (2\text{-}25)$$

with

A_l^i = Induced activity of radionuclides i in waste fraction l [Bq] (see Section 2.3.2).

Br_m^i = Branching ratio from parent radionuclide m to radionuclide i [–] (see Section 2.4.2).

$Br_m^i\lambda^i A_l^m$ = Ingrowth by parent radionuclide m [Bq/s] (see Section 2.4.1).

$R_{c,l}^i$ = Release rate of radionuclides i due to corrosion of waste fraction l [Bq/s] (see Section 2.5.4).

T_l = The time it takes to corrode the metal components in waste fraction l [s].

$H(t)$ = The Heaviside step function.

The release rate of induced activity from the BHK vault strongly depends on the initial amount of the induced activity, the metal thickness, and the metal corrosion rate (see Section 2.5.4).

Input data used in near-field model

The data that describe the thickness of the metallic components in BHK are provided in Table 2-17. It should be emphasized that nine categories of metallic components are defined in a reference document[5]. However, in the near-field model, these categories are generally combined into four categories where in each category the lowest value of the underlying thickness range is assigned to the category thickness (see Table 2-17). In other words, while the total activity of the metallic components is maintained, the total activity is assigned to thinner components resulting in the faster release of induced activities. This is a pessimistic approach. The following categories are defined and corresponding times until complete corrosion are given:

Table 2-17. Categories of metal parts in BHK and their assumed thickness.

Category	Metal thickness	Underlying thickness range	Release time [a]
00	0 mm	0–1 mm	Instant release.
01	1 mm	1–5, 5–10 mm	5.0E+04
02	10 mm	10–11, 11–20 mm	5.0E+05
03	20 mm	20–60 mm, 109 mm, 216 mm, 300 mm	1.0E+06

Source of data and justification

The data are taken from a reference document[5].

Known limitations in data

Since the total induced activity is assigned to thin metallic components in the near-field model, the corrosion resistance is underestimated. This is, therefore, a pessimistic approach.

The reader may refer to the reference document[6] for discussions on the uncertainties in the data.

2.5.4 Corrosion rate of metallic waste components in BHK

Short description of data

Induced activities will be released from the metallic components due to corrosion. The data presented in this section concern the corrosion rate of the metallic components in BHK.

Use in model or evaluation activity

In the near-field model, the corrosion release is assumed to start immediately after the repository closure in the year 2075. The model also assumes that the metallic components corrode at a constant rate during the time of interest for SE-SFL. In other words, the corrosion rate of a metallic component remains constant until the component is completely corroded. Thereafter, no corrosion will occur and, therefore, no induced activity will be released.

It should be noted that in the near-field model, all the metallic components in the BHK waste matrix are assumed to corrode at the same constant rate.

Input data used in near-field model

Most of non-cementitious waste in BHK consists of carbon steel and stainless steel. In fact, steel constitutes about 96 % of the BHK waste, provided that the concrete parts of the waste are disregarded (Herschend 2014, Table 5-7). Out of this steel, over two-third consists of stainless steel.

[5] Herschend B, 2016. Initial state SFL. SKBdoc 1441724 ver 1.0, Svensk Kärnbränslehantering AB. Internal document.

[6] Herschend B, 2016. Initial state SFL. SKBdoc 1441724 ver 1.0, Svensk Kärnbränslehantering AB. Internal document.

Only waste from Ringhals contains carbon steel that constitutes the remaining ~32 % of the steel components (and 42 % of the total induced activity) in the BHK waste. In the SE-SFL base case, it is assumed that all the metallic components corrode at the same rate as stainless steel under alkaline and anoxic conditions. The corrosion rate is proposed after the preceding safety assessment SR-PSU (SKB 2014a, Tables 5-4) as follows:

- Corrosion rate of all metal parts: 10 [nm/a].

Source of data and justification

The proposed corrosion rate is the corrosion rate of stainless steel under alkaline anoxic conditions. The concrete in the BHK grout and backfill provides an alkaline environment, which can create a passivating layer on the surface of the steel components, reducing the corrosion rate of steel. Furthermore, after the initial period of aerobic corrosion, the oxygen will be depleted, and the anaerobic corrosion will take place, given the anoxic condition (SKB 2014a).

The proposed value is taken from and justified in the SR-PSU data report (SKB 2014a, Table 5-4). Nevertheless, it should be noted that since air will be initially present within the SFL repository, corrosion rates can be higher than 10 [nm/a]. Therefore, the assumed constant corrosion rate may underestimate the release of induced activity. This situation is, however, alleviated by assuming that the induced activity of the thinnest metal category releases instantly upon the repository closure in the year 2075.

Known limitations in data

All metallic components are assumed to corrode at the same corrosion rate as stainless steel under alkaline and anoxic conditions. However, it should be noted that part of the waste from Ringhals nuclear power plant consists of carbon steel. The corrosion rate of carbon steel in SR-PSU is proposed to be five times larger than that for stainless steel, under the same alkaline conditions (SKB 2014a, Table 5-3). This limitation is deemed to be acceptable, as the majority of the BHK waste consists of stainless steel.

2.5.5 Sorption coefficients of cement in the waste compartments

Short description of data

Radionuclides in the BHA and BHK waste compartments may sorb onto immobile solids in the compartments. The near-field model assumes that linear sorption occurs on the cement internal surface in the grout and concrete structure (Bodin et al. 2003). Therefore, the data in this section concern linear sorption coefficients K_d [m^3/kg] of the modelled radionuclides in cement.

Use in model or evaluation activity

In the near-field model, radionuclides in the BHA waste compartment are partitioned as dissolved in the pore water or as sorbed on the cement embedded in the grout or concrete structure. The partitioning may also be influenced by complexing agents, which is handled by reducing the K_d-value of certain radionuclides (see Section 2.5.6). Radionuclides that are sorbed on the cement are then considered immobile and cannot leave the waste compartment.

In the BHK waste compartment, the situation is very similar. However, the concentration of complexing agents is believed to be too small to impact the sorption coefficients. Furthermore, radionuclides can also sorb on the cement in the BHK concrete backfill compartments, i.e. inflow, outflow and side compartments, which experience different levels of degradation. This is included in the near-field model as explained in the following.

Input data used in near-field model

Table 2-18 provides the K_d-values used in the base case for different degradation states in the BHA waste and BHK waste and backfill compartments. The data are mostly taken from SKB (2014a,

Tables 7-7 to 7-10). As the concrete degrades, its sorption capacity changes due to the pH evolution associated with cement leaching.

Initially, all cementitious materials are in the chemical degradation state I (dissolution of sodium and potassium hydroxides and the pH is higher than 12.5. It follows by the degradation state II (dissolution of portlandite pH≈12.5), degradation state IIIa (incongruent dissolution of calcium silicate hydrate (CSH) phases, presence of Ca-aluminates pH≈12), and degradation state IIIb (incongruent dissolution of CSH phases, absence of Ca-aluminates pH≈10.5).

To account for these phenomena, different K_d-values are assigned in each time step. For this purpose, the K_d-values in different compartments are obtained by the linear interpolation of the K_d-values given in Table 2-18. It should be emphasized that in the near-field model, the K_d-values in the concrete structure are assumed to evolve similarly to the corresponding values in the BHK backfill outflow and side compartments.

The breakpoints of the linear interpolation are given in Table 2-19. The applied K_d-values in BHK and their associated timeframes in the base case are stored in the SVN database at:

svn://svn.skb.se/SFL/SFLSAK/Arbetsmaterial/RadionuclideTransport/CalculationCases/CC1/Nearfie d/CC_specific_indata/Kd.xlsx.

svn://svn.skb.se/SFL/SFLSAK/Arbetsmaterial/RadionuclideTransport/CalculationCases/CC1/Nearfield/CC_specific_indata/KdSelectorBHK.xlsx.

It should be emphasized that the BHK inflow compartment is subjected to more severe degradation than the outflow and side compartments. In the near-field model, this is represented by the assigned time periods for the different degradation states. For instance, in the model, going from the first state to the second is assumed to take 5 000 years in inflow compartment, while it takes 10 000 years in outflow and side compartments.

Source of data and justification

For most of the radionuclides, the sorption coefficients in cement are taken from SR-PSU (SKB 2014a, Table 7-7 to Table 7-10). Radionuclides that are considered non-sorbing in the near-field model are H and induced C-14. It should be noted that in practice, little is known of the speciation of the induced C-14 in BHK. Therefore, it is assumed to behave similar to the organic C-14 in this regard, which is a pessimistic assumption. Radionuclides for which K_d-values are assigned based on their analogue species are Be, Gd, K, La, Re, Si, Tb, and Ti. For a few radionuclides, the likelihood of certain oxidation states has been ruled out as compared to in SKB (2014a, Table 7-6). These are Np(VI), Pa(V), Pu(V), Pu(VI), Tc(VII), and U(VI). This is likely because reducing conditions are expected to hold at the SFL repository depth. Pu(III) is also ruled out when using the data on degradation states II, IIIa, and IIIb, since the K_d-value for the Pu(III) is lower than for Pu(IV) for these states in SKB (2014a, Table 7-8 to Table 7-10).

The breakpoints of the linear interpolation between different chemical degradation states are taken from Idiart and Laviña (2019). Initially, all cementitious materials are in the chemical degradation state I (dissolution of sodium and potassium hydroxides and the pH is higher than 12.5). It is followed by the degradation state II (dissolution of portlandite pH≈12.5), degradation state IIIa (incongruent dissolution of CSH phases, presence of Ca-aluminates pH≈12), and degradation state IIIb (incongruent dissolution of CSH phases, absence of Ca-aluminates pH≈10.5).

Known limitations in data

For a radionuclide for which there is a lack in observations, the supplied K_d-value is estimated from data obtained for one or more analogue species. Uncertainties can, therefore, occur with a lack of suitable analogues.

It should also be noted that the concrete backfill degrades inhomogeneously. The linear interpolation between different chemical degradation states represents a uniform leaching through the concrete.

Table 2-18. Sorption coefficients K_d [m^3/kg] in cement for different degradation states.

Element	Oxidation state/ Analogue	K_d (State I)	K_d (State II)	K_d (State IIIa)	K_d (State IIIb)	Reference/Note
Ac	Ac(III)	10	10	10	10	(SKB 2014a)
Ag	Ag(I)	0	0	0	0	(SKB 2014a)
Am	Am(III)	10	10	10	10	(SKB 2014a)
Ba	Ba(II)	0.1	0.03	0.01	0.1	(SKB 2014a)
Be	Be(II)/Ba(II)	0.1	0.03	0.01	0.1	Assumed analogue to Ba(II).
Ca	Ca(II)	3.54E-02	3.09E-03	3.09E-03	4.67E-02	(SKB 2014a)
Cd	Cd(II)	0.06	0.06	0.06	0.06	(SKB 2014a)
C-ind		0	0	0	0	Assumed non-sorbing.
C-inorg	^{14}C, carbonate species	2	5	2	0.7	(SKB 2014a)
Cl	Cl(-I)	0.001	0.001	0.001	0.001	(SKB 2014a)
Cm	Cm(III)	10	10	10	10	(SKB 2014a)
Co	Co(II)	0.006	0.04	0.04	0.04	(SKB 2014a)
C-org	^{14}C, CH_4, organic acids	0	0	0	0	(SKB 2014a)
Cs	Cs(I)	0.001	0.002	0.02	0.02	(SKB 2014a)
Eu	Eu(III)	10	10	10	10	(SKB 2014a)
Gd	Gd/(III)/Eu(III)	10	10	10	10	Assumed analogue to Eu(III).
H		0	0	0	0	(SKB 2014a) / Assumed non-sorbing.
Ho	Ho(III)	10	10	10	10	(SKB 2014a)
I	I(-I)	0.001	0.001	0.001	0.001	(SKB 2014a)
K	K(I)/Cs(I)	0.001	0.002	0.02	0.02	Assumed analogue to Cs(I).
La	La(III)/Eu(III)	10	10	10	10	Assumed analogue to Eu(III).
Mo	Mo(VI)	0.003	0.003	0.003	0	(SKB 2014a)
Nb	Nb(V)	50	50	50	5	(SKB 2014a)
Ni	Ni(II)	0.03	0.2	0.2	0.2	(SKB 2014a)
Np	Np(IV)	30	30	30	30	(SKB 2014a) / Np(V) ruled out.
Pa	Pa(IV)	30	30	30	30	(SKB 2014a) / Np(V) ruled out.
Pb	Pb(II)	0.3	3	30	30	(SKB 2014a)
Pd	Pd(II)	0.3	3	30	30	(SKB 2014a)
Po	Po(IV)	0.02	0.02	0.02	0.02	(SKB 2014a)
Pu	Pu(IV)	5	30	30	30	(SKB 2014a) / Pu(III), Pu(V), and Pu(VI) ruled out.
Ra	Ra(II)	0.3	0.1	0.8	0.8	(SKB 2014a)
Re	Re(IV)/Tc(IV)	3	3	3	3	Assumed analogue to Tc(IV).
Se	Se(-II)	0	0	0	0	(SKB 2014a) / Pessimistic choice.
Si	Si(IV)/U(IV)	30	30	30	30	Assumed analogue to U(IV).
Sm	Sm(III)	10	10	10	10	(SKB 2014a)
Sn	Sn(IV)	20	20	10	4	(SKB 2014a)
Sr	Sr(II)	0.1	0.03	0.01	0.1	(SKB 2014a)
Tb	Tb(III)/Eu(III)	10	10	10	10	Assumed analogue to Eu(III).
Tc	Tc(IV)	3	3	3	3	(SKB 2014a) / Tc(VII) ruled out.
Th	Th(IV)	30	30	30	30	(SKB 2014a)
Ti	Ti(IV)/Zr(IV)	5	10	100	100	Assumed analogue to Zr(IV).
U	U(IV)	30	30	30	30	(SKB 2014a)
Zr	Zr(IV)	5	10	100	100	(SKB 2014a)

Table 2-19. Time periods for different degradation states leading to different K_d values in concrete.

	Degradation state	State I	State II	State IIIa	State IIIb
Time [a]	BHK – Waste, outflow and side compartments	2.08E+03	1.21E+04	3.42E+05	4.02E+05
	BHK – Inflow compartments	2.08E+03	7.08E+03	1.72E+05	3.62E+05
	BHA – Waste compartment	2.08E+03	1.21E+04		

2.5.6 Sorption reduction factors due to complexing agents

Short description of data

Dissolved and mobile complexing agents may react with radionuclides in a way that they cannot, or at least have a lesser tendency to, sorb on immobile minerals of the cement and bentonite in the BHA backfill. In BHK, the waste exclusively consists of metallic parts. Therefore, no organic material that might form metal-organic complexes will be present in this waste vault.

Use in model or evaluation activity

Complexing agents reduce the tendency of radionuclides to sorb to cement and bentonite. In the near-field model, this process is formulated by introducing sorption reduction factors. Thus, to obtain a new K_d-value that is valid for certain concentrations of complexing agents, the K_d-value obtained in the absence of complexing agents is divided by the reduction factors.

Input data used in near-field model

The sorption reduction factor is dependent on the concentration of the complexing agent. In SE-SFL, iso-saccarinate (ISA) is viewed as the most important complexing agent and its concentration in BHA is assumed to quickly reach the saturation concentration, i.e. 20 mM (**Initial state report**). In SKB (2014a, Table 7-11a), a no-effect concentration level is provided for ISA, under which no sorption reduction occurs. Furthermore, a sorption reduction factor is provided for ISA concentrations just above the no-effect level.

It is also proposed that the reduction factors increase by a factor of 10 with each 10-fold increase in the ISA concentration above the no-effect level. The only exceptions are Pb and Pd. Therefore, with a no-effect of 1 mM and a reduction factor of 10, sorption values are expected to be reduced by a factor of 10 when 1 mM < ISA < 10 mM and by a factor of 100 when 10 mM < ISA < 100 mM, etc.

In the fourth column of Table 2-20, the assumed ISA saturation concentration, i.e. 20 mM, is divided by the no-effect level given in the third column (SKB 2014a, Table 7-11a). The sorption reduction factor just above the no-effect level is given in the fifth column. In the rightmost column, the assumed resulting sorption reduction factor for BHA is provided. It should be noted that the inverse of the sorption reduction factors is used in the near-field model. Where no data exist for the specific radionuclide, an analogue species is used instead as in Table 2-18. The sorption reduction factor is used in both the waste compartment, where the sorption occurs in cement, as well as in the backfill, where the sorption occurs on internal surface of bentonite.

Table 2-20. Sorption reduction factors in cement and bentonite in BHA.

Element	Oxidation state/ Analogue	no-effect ISA concentration level (mM)	ISA concentration/ no-effect level	Reduction factor just above no-effect level	Used reduction factor
Ac	Ac(III)	1	20	10	100
Ag	Ag(I)	NEX*	–	1	1
Am	Am(III)	1	20	10	100
Ba	Ba(II)	10	2	10	10
Be	Be(II)/Ba(II)	10	2	10	10
Ca	Ca(II)	NEX	–	1	1
Cd	Cd(II)	10	2	10	10
C-ind		NR	–	–	–
C-inorg	^{14}C, carbonate species	NEX	–	1	1
Cl	Cl(-I)	NEX	–	1	1
Cm	Cm(III)	1	20	10	100
Co	Co(II)	NEX	–	1	1
C-org	^{14}C, CH_4, organic acids	NR	–	–	–
Cs	Cs(I)	NEX	–	1	1
Eu	Eu(III)	1	20	10	100
Gd	Gd/(III)/Eu(III)	1	20	10	100
H		NR		–	–
Ho	Ho(III)	1	20	10	100
I	I(-I)	NEX	–	1	1
K	K(I)/Cs(I)	NEX	–	1	1
La	La(III)/Eu(III)	1	20	10	100
Mo	Mo(VI)	NEX	–	1	1
Nb	Nb(V)	NA**	–	–	1
Ni	Ni(II)	NEX	–	1	1
Np	Np(IV)	0.1	200	100	10 000
Pa	Pa(IV)	0.1	200	100	10 000
Pb	Pb(II)	0.02	1 000	100, constant.	100
Pd	Pd(II)	0.02	1 000	100, constant.	100
Po	Po(IV)	0.1	200	10	1 000
Pu	Pu(IV)	0.1	200	100	10 000
Ra	Ra(II)	10	2	10	10
Re	Re(IV)/Tc(IV)	0.1	200	100	10 000
Se	Se(-II)	NR	–	–	–
Si	Si(IV)/U(IV)	0.1	200	100	10 000
Sm	Sm(III)	1	20	10	100
Sn	Sn(IV)	0.1	200	100	10 000
Sr	Sr(II)	10	2	10	10
Tb	Tb(III)/Eu(III)	1	20	10	100
Tc	Tc(IV)	0.1	200	100	10 000
Th	Th(IV)	0.1	200	100	10 000
Ti	Ti(IV)/Zr(IV)	0.1	200	100	10 000
U	U(IV)	0.1	200	100	10 000
Zr	Zr(IV)	0.1	200	100	10 000

* No Effects Expected.

** Not Available.

The BHK waste mostly consists of metallic parts. Therefore, no organic material that might form metal-organic complexes is expected to be present in the BHK vault (**Initial state report**). Hence, the near-field model assumes that the ISA concentration is negligible so the sorption reduction due to complexation can be neglected.

Table 2-21. Sorption reduction factors for cement in BHK.

Radionuclide	ISA concentration/no-effect level	K_d-factor
All	Below no-effect level	1

Source of data and justification

The data are found and justified in SKB (2014a, Table 7-11a) in relation to sorption in bentonite and concrete in SR-PSU.

Known limitations in data

In SKB (2014a, Table 7-11a), no realistic no-effect level is provided for Nb(V). A conservative no-effect level is provided in SKB (2014a, Table 7-11c) as 0.1 mM, together with a conservative sorption reduction factor of 100. If adopting these conservative values for BHA, Nb(V) would experience no significant sorption in the near-field.

In Table 2-20, the same radionuclide analogues are used as in Table 2-18. There is uncertainty to what extent these analogues can be used in terms of sorption reduction factors.

2.6 Data for diffusive and advective transport in waste compartments

2.6.1 Diffusion transport resistance in the BHA waste compartment

Short description of data

In the near-field model, radionuclides are transported through the BHA waste compartment by advection and diffusion. The diffusive release of the dissolved radionuclides from the waste compartment to the backfill sub-compartment depends strongly on the diffusion transport resistance in the waste compartment as well as concentration gradient between the waste and the neighbouring sub-compartment, Equation 2-2. The data provided in this section concern the diffusion transport resistance in the BHA waste compartment.

Use in model or evaluation activity

In the near-field model, to calculate the diffusive release from the BHA waste compartment to a neighbouring backfill sub-compartment, the concentration gradient between the compartments is divided by the sum of the diffusion resistances in each compartment, Equation 2-2. It should be noted that since the compartments are assumed homogeneous, radionuclide concentration in the compartments are represented by an averaged concentration at any given time. Hence, the radionuclide specific activity that is transferred between the BHA waste and backfill sub-compartments by diffusion in each time step can be obtained by multiplying the diffusive release rate times the duration of the time step. The detailed mathematical formulations and methods to calculate the diffusion transport resistance in compartments are provided in Wessely and Shahkarami (2019).

Input data used in near-field model

The diffusion transport resistance in the BHA waste compartment can be determined by the dimensions of the compartment (see Section 2.2.1), and the effective diffusivity of radionuclides in the waste compartment, D_e^{wc}, Equations (2-26) and (2-27). In the near-field model, all the radionuclides are assumed to have a similar effective diffusivity in the BHA waste compartment, i.e. 2.0 E-9 m^2/s, which equals the diffusivity of radionuclides in water.

$$\boldsymbol{R_{nf}^{wc}} = \frac{\boldsymbol{l_{nf}^{wc}}}{\boldsymbol{A_{nf}^{wc} D_e^{wc}}} \tag{2-26}$$

$$R_{ns}^{wc} = \frac{l_{ns}^{wc}}{A_{ns}^{wc} D_e^{wc}} \quad (2\text{-}27)$$

Where A_{nf}^{wc} and A_{ns}^{wc} are the cross-section areas of the BHA waste compartment normal to the diffusive direction along and across the vault, respectively, Equations (2-5) and (2-6), and l_{nf}^{wc} and l_{ns}^{wc} are the diffusion lengths in the inflow/outflow and side directions, respectively.

In the near-field model, l_{nf}^{wc} is set to the concrete structure length divided by 2.5, i.e. 56 m, whereas l_{ns}^{wc} is set to the concrete structure height divided by 2.5, i.e. 3.36 m. Hence, since the cross-section areas and diffusion lengths are different for the inflow/outflow and side directions, radionuclides experience different diffusion transport resistances. The estimated diffusion transport resistances in the BHA waste compartment are provided in Table 2-22.

Table 2-22. Diffusion transport resistances in the BHA waste compartment.

Direction	Diffusion transport resistance [a/m^3]
Normal to the Inflow direction	6.602
Normal to the side direction	0.008
Normal to the outflow direction	6.602

Source of data and justification

The geometries of the BHA vault and waste compartment are provided in Section 2.2.1. The effective diffusivity of all radionuclides in the waste compartment is assumed to be equal to the diffusivity of radionuclide in water at room temperature.

Known limitations in data

As discussed in Section 2.2.1, the geometries of the BHA vault and waste compartment are simplified in the near-field model. The diffusion-length reduction factor 2.5 is tuned in the model to achieve a comparable release rate to the release obtained in an analytical solution for a system with zero concentration boundary condition. The chosen large effective diffusivity gives a pessimistic estimate of the diffusion resistance in the waste compartment.

2.6.2 Diffusion transport resistance in the BHK waste compartment

Short description of data

In the near-field model, radionuclides are transported through the BHK waste compartment by advection and diffusion. To calculate the diffusion rate from the BHK waste compartment to the backfill sub-compartment, it is required to have information on the diffusion transport resistance in the waste compartment and concentration gradient between the waste and the neighbouring sub-compartments, Equation 2-2. The data provided in this section concern the diffusion transport resistance in the BHK waste compartment.

Use in model or evaluation activity

In the near-field model, to calculate the diffusive release from the BHK waste compartment to a neighbouring backfill sub-compartment, the concentration gradient between the compartments is divided by the sum of the diffusion resistances in the compartments, Equation 2-2. It should be noted that since the waste compartment is assumed homogeneous, radionuclide concentration in the waste compartment is represented by an averaged concentration at any given time. Hence, the radionuclide specific activity transferred between the BHK waste and backfill sub-compartments by diffusion in each time step, can be obtained by multiplying the diffusive release rate times the duration of the time step. The detailed mathematical formulations to calculate the diffusion transport resistance in compartments are provided in Wessely and Shahkarami (2019).

Input data used in near-field model

The diffusion transport resistance in the waste compartment can be determined by the dimensions of the compartment, (see Section 2.2.2), and the effective diffusivity of radionuclides, D_e^{wc}, Equations (2-28) and (2-29). In the near-field model, all the radionuclides are assumed to have a similar effective diffusivity in the BHK waste compartment, i.e. 2.0 E-9 m^2/s, which equals the effective diffusivity of radionuclides in water.

$$\boldsymbol{R_{nf}^{wc}} = \frac{\boldsymbol{l^{wc}}}{\boldsymbol{A_{nf}^{wc} D_e^{wc}}} \tag{2-28}$$

$$\boldsymbol{R_{ns}^{wc}} = \frac{\boldsymbol{l^{wc}}}{\boldsymbol{A_{ns}^{wc} D_e^{wc}}} \tag{2-29}$$

Where A_{nf}^{wc} and A_{ns}^{wc} are the cross-section areas of the BHK waste compartment normal to the vertical and horizontal diffusive direction, respectively, and l^{wc} is the diffusion length within the compartment. Since cross-section areas and diffusions lengths are different for the inflow/outflow and side directions, radionuclides experience different diffusion transport resistances. In the near-field model, the diffusion length in the inflow/outflow direction is set to the concrete structure height divided by 2.5, whereas the diffusion length for the side compartment is set to the concrete structure width divided by 2.5. The diffusion transport resistances in the BHK waste compartment are compiled in Table 2-23.

Table 2-23. Diffusion transport resistances in the BHK waste compartment.

Direction	Diffusion transport resistance [a/m^3]
Normal to the Inflow direction	0.039
Normal to the side direction	0.054
Normal to the outflow direction	0.039

Source of data and justification

The dimensions of the BHK vault and waste compartment are provided in Section 2.2.2. The effective diffusivity of all radionuclides in the waste domain is assumed to be equal to the effective diffusivity of radionuclide in water at room temperature.

Known limitations in data

As discussed in Section 2.2.2, the geometries of the vaults are simplified in the near-field model. The factor 2.5 in the reduction of the diffusion length is introduced in order to achieve a release rate comparable to the release rate obtained in an analytical solution for a system with zero concentration boundary condition. The chosen large effective diffusivity gives a pessimistic estimate of the diffusion resistance in the waste compartment.

2.6.3 Advective flow in the BHA waste compartment

Short description of data

In the near-field model, radionuclides are transported through the BHA waste compartment by advection and diffusion. In order to calculate the advective release through the waste compartment, it is required to have information on the groundwater flow in the BHA vault. The flow information is provided by the repository scale model (Abarca et al. 2019). In the model, a stationary flow field is adopted in the near-field based upon a snap-shot of the regional hydrology simulation in the year 2000 (Joyce et al. 2019). Furthermore, in the repository scale model, it is assumed that the bentonite backfill retains its hydraulic properties during the safety evaluation period. Therefore, since the bentonite backfill is the central barrier limiting the groundwater flow through the BHA waste compartment, possible changes in the waste compartment hydraulic properties are neglected in the repository scale model (Abarca et al. 2019).

Use in model or evaluation activity

In the near-field model, to calculate the advective release from the BHA waste compartment to the neighbouring backfill outflow sub-compartment, the activity concentration of dissolved radionuclides is multiplied by the groundwater flow.

Input data used in near-field model

In the repository scale model (Abarca et al. 2019), the BHA vault is divided into 7 sections along its longitudinal axis. Five of these sections comprise a waste and four backfill control volumes to give a fair representation of flow through and around the waste control volume. The total groundwater flows through the waste control volumes in the *present-day evaluation case* are listed in Table 2-24 (Abarca et al. 2019). The selected names are in accordance with the convention described in Abarca et al. (2019).

Table 2-24. Groundwater flow through the BHA waste control volumes.

BHA flow control volume	Total flow [m^3/a]
BHA_1_Waste	3.33×10^{-4}
BHA_2_Waste	2.71×10^{-4}
BHA_3_Waste	5.11×10^{-4}
BHA_4_Waste	2.69×10^{-4}
BHA_5_Waste	1.66×10^{-4}
Sum of all five control volumes	1.55×10^{-3}

Contrary to the repository scale model, the near-field model contains a single BHA waste compartment. Therefore, the overall flow through this compartment is expressed as the sum of the total flows through the BHA waste control volumes given in Table 2-24, i.e. Q_{out} = 1.55 L/a. In the *present-day evaluation case*, the overall flow is assumed to be constant during the SFL safety evaluation period. Furthermore, the water is assumed to flow entirely horizontally towards the BHA backfill outflow sub-compartment.

Source of data and justification

The data are obtained from the modelling results in Abarca et al. (2019), where the data are also justified. As earlier discussed in Section 2.5.1, the near-field model assumes that the porosity of the concrete structure in BHA increases over time. However, the overall flow through the waste control volume is assumed invariant during the evaluation period. This can be justified because the resistance against the groundwater flow in BHA is mainly controlled by the bentonite backfill, which has very low hydraulic conductivity that persists over time.

Known limitations in data

The near-field model has a simplified representation of the flow through the waste and backfill, where the water is assumed to flow only in the direction along the vault. It should be noted that, when summing the flows through all the waste control volumes, the flow between the waste control volumes is counted twice. Therefore, the overall flow through the waste compartment is overestimated. However, since diffusion is expected to be the dominating transport mechanism in BHA, the estimated flow is believed to be sufficiently accurate for the safety evaluation.

2.6.4 Advective flow in the BHK waste compartment

Short description of data

In the near-field model, radionuclides are transported through the BHK waste compartment by advection and diffusion. In order to calculate the advective component, information on the groundwater flow rates and directions in the BHK vault is required. Similar to BHA, the groundwater flow information is provided in Abarca et al. (2019).

A stationary flow field is assumed in the repository scale model (Joyce et al. 2019). However, since the concrete backfill degrades over time, the local groundwater flow conditions will vary. To take this phenomenon into account, three states of degradation are considered in the repository scale and near-field models. These include:

- Intact Case (IC): The concrete backfill is intact and has initial state properties, 2075–87 083 [a].
- Degraded Zone Case (DZC): The outer half of the concrete backfill is degraded, 87 083–782 168 [a].
- Degraded Case (DC): The entire concrete backfill is degraded, 782 168–1 002 075 [a].

Use in model or evaluation activity

In the near-field model, the activity concentration of dissolved radionuclides is multiplied by the groundwater flow to calculate the advective release from the BHK waste compartment to the neighbouring backfill outflow and side sub-compartments. It is worth noting that, the majority of the advective flow in BHK is directed towards the outflow compartment and only a minor part is directed towards the side compartment.

Input data used in near-field model

Compared to BHA, a more detailed compartmentalisation is adopted for the BHK vault in the repository scale model. In the model, the BHK vault is divided into 8 sections along its axis, six of which comprise one waste and ten backfill control volumes to give a detailed representation of flow through the waste and backfill (Abarca et al. 2019, Appendix C).

For each control volume, the groundwater flow has been calculated with surface integrals over each of the six faces of the volume. The calculations are made for the three degradation states in the BHK backfill and the results are incorporated in the near-field model. The groundwater flow information taken from the repository scale model are tabulated in this report.

Table 2-25 provides the flows through the six faces of the BHK waste control volumes in the Intact Case (IC). The flow data are labelled BHK_X_Wa_Y, where X, Wa and Y denote index of vault section, waste control volume and index of the face, respectively.

This is in accordance with the convention described in Abarca et al. (2019). The headers in Table 2-25 represent the index of the face, Y.

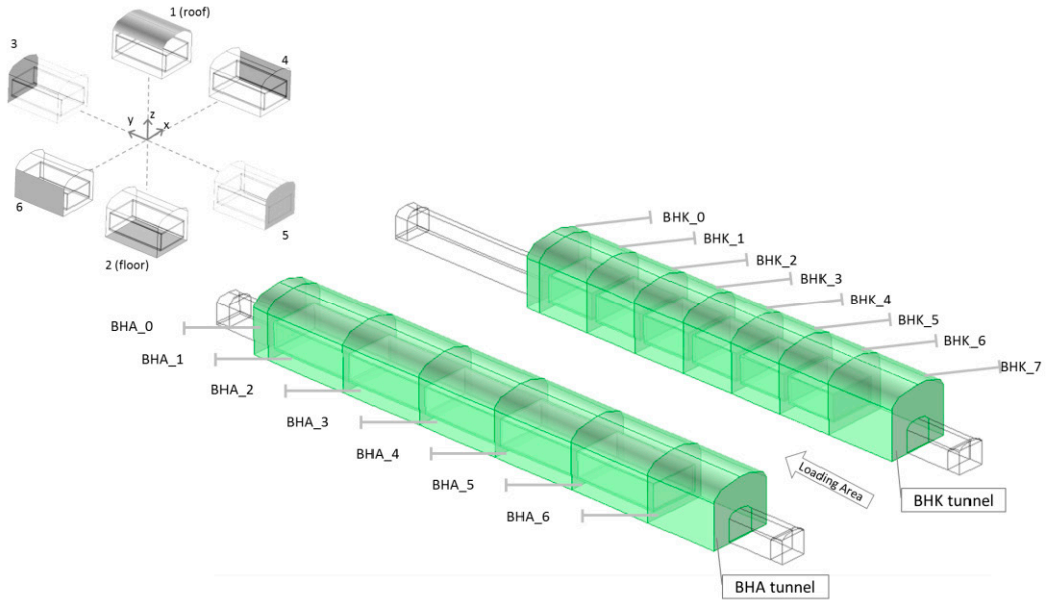

Figure 2-8. *Labelling of the sections along the BHA and BHK vaults and their surfaces.*

Table 2-25. Flow through the faces of the waste control volumes in the BHK vault in the Intact Case (IC).

Faces →	_1 [m³/a]	_2 [m³/a]	_3 [m³/a]	_4 [m³/a]	_5 [m³/a]	_6 [m³/a]
BHK_1_Wa	−0.04401	1.84E-02	8.71E-04	1.57E-02	9.74E-03	−3.29E-03
BHK_2_Wa	−3.92E-02	1.48E-02	−1.06E-02	−3.62E-03	3.99E-02	−1.32E-03
BHK_3_Wa	−1.80E-01	1.84E-01	−4.61E-02	2.13E-03	5.55E-02	−1.54E-02
BHK_4_Wa	−2.13E-01	1.71E-01	−5.45E-02	4.48E-02	8.79E-02	−3.55E-02
BHK_5_Wa	−8.67E-02	1.47E-01	−9.04E-02	−1.20E-04	3.24E-02	−1.95E-03
BHK_6_Wa	−4.95E-02	9.82E-02	−2.65E-02	−1.60E-03	−1.99E-02	−6.90E-04

The sign convention for the values is such that a positive value for a flow over a face of a control volume represents a flow out from that volume, and a negative value represents a flow into the control volume.

Therefore, to calculate the groundwater flow from the BHK waste compartment towards the backfill outflow sub-compartments in the near-field model, the positive values over the floor (face 2 = 0.633) and long-side walls (faces 4 and 6 (all negative) = 0.063) of each waste control volume are summed. This gives a total flow of 0.696 m^3/a from the waste compartment to the outflow sub-compartment.

The faces BHK_1_Wa_3 and BHK_6_Wa_5 compose the boundary surfaces of the vaults on the short-sides. The largest flow over these two faces is chosen to represent the groundwater flow out of the waste compartment towards the backfill side compartment. In doing this, the absolute value of the flows is used because the sign only indicates the direction of the flow. In the Intact Case (IC), this gives 1.99E-02 m^3/a.

Flow data in the Degraded Zone Case (DZC) and Degraded Case (DC) are also provided in Table 2-26 and Table 2-27, respectively. The flow rates from the waste compartment to the backfill outflow and side sub-compartments is estimated in a similar manner as done in the Intact Case (IC). The resulting flows in all the cases are provided in Table 2-28.

Table 2-26. Flows through the faces of the waste control volumes in the BHK vault in the Degraded Zone Case (DZC).

Faces →	_1 [m³/a]	_2 [m³/a]	_3 [m³/a]	_4 [m³/a]	_5 [m³/a]	_6 [m³/a]
BHK_1_Wa	−1.02E-02	1.08E-02	3.04E-03	5.85E-03	−1.63E-03	−8.14E-03
BHK_2_Wa	−1.88E-02	1.77E-02	4.69E-04	−6.13E-03	1.80E-02	−1.13E-02
BHK_3_Wa	−5.50E-02	8.23E-02	−2.06E-02	−5.23E-03	3.13E-02	−3.28E-02
BHK_4_Wa	−6.80E-02	9.03E-02	−3.22E-02	1.99E-03	4.85E-02	−4.05E-02
BHK_5_Wa	−4.14E-02	8.54E-02	−4.90E-02	−1.38E-02	2.92E-02	−1.04E-02
BHK_6_Wa	−2.38E-02	4.73E-02	−2.76E-02	−6.74E-03	1.10E-02	−1.10E-04

Table 2-27. Flows through the faces of the waste control volumes in the BHK vault in the Degraded Case (DC).

Faces →	_1 [m³/a]	_2 [m³/a]	_3 [m³/a]	_4 [m³/a]	_5 [m³/a]	_6 [m³/a]
BHK_1_Wa	−8.47E-02	3.17E-02	3.40E-02	3.56E-02	−1.36E-02	−9.08E-03
BHK_2_Wa	−9.79E-02	4.23E-02	1.02E-02	2.19E-03	4.82E-02	−4.94E-03
BHK_3_Wa	−4.20E-01	3.58E-01	−5.85E-02	2.88E-02	1.30E-01	−3.88E-02
BHK_4_Wa	−6.01E-01	3.14E-01	−1.44E-01	8.65E-02	3.91E-01	−4.66E-02
BHK_5_Wa	−2.46E-01	4.62E-01	−3.96E-01	−2.26E-02	2.03E-01	−1.08E-03
BHK_6_Wa	−1.30E-01	8.71E-02	−1.96E-01	−5.54E-03	2.40E-01	4.27E-03

Table 2-28. Groundwater flow leaving the BHK waste compartment toward the adjacent compartments, for the different states of concrete degradation.

Case	Flow towards outflow compartment [m³/a]	Flow towards side compartment [m³/a]
IC	0.696	0.020
DZC	0.342	0.011
DC	1.452	0.240

Degradation of the concrete backfill in BHK is also reflected by assigning the varying flow rates during the designated time periods for each degradation states, Figure 2-9.

Source of data and justification

The groundwater flow data are obtained from the numerical results of the dedicated SE-SFL repository scale modelling in Abarca et al. (2019, Appendix C). The data are also justified in the reference document.

The time periods used to represent the different instances associated with the concrete degradation states are set according to the leaching process of cement minerals (Idiart and Laviña 2019). In other words, in the near-field model, the DZC is assumed to start when half of the portlandite in the outer half of the backfill has been leached out, where the CD case is assumed to start when the CSH gel in the outer half of the backfill has been leached out.

Known limitations in data

The reader may refer to the reference document (Abarca et al. 2019) for discussions on the uncertainties in the flow data.

The near-field model has a very simple representation of the flow through the waste where the water is assumed to flow downwards and toward the side compartments.

Contrary to the other transient properties, for numerical reasons, a transition period of 100 years is used to interpolate between the flow magnitudes in the different states of concrete degradation.

There are several processes that can contribute to concrete degradation, leaching of cement minerals is the only process considered in the near-field model.

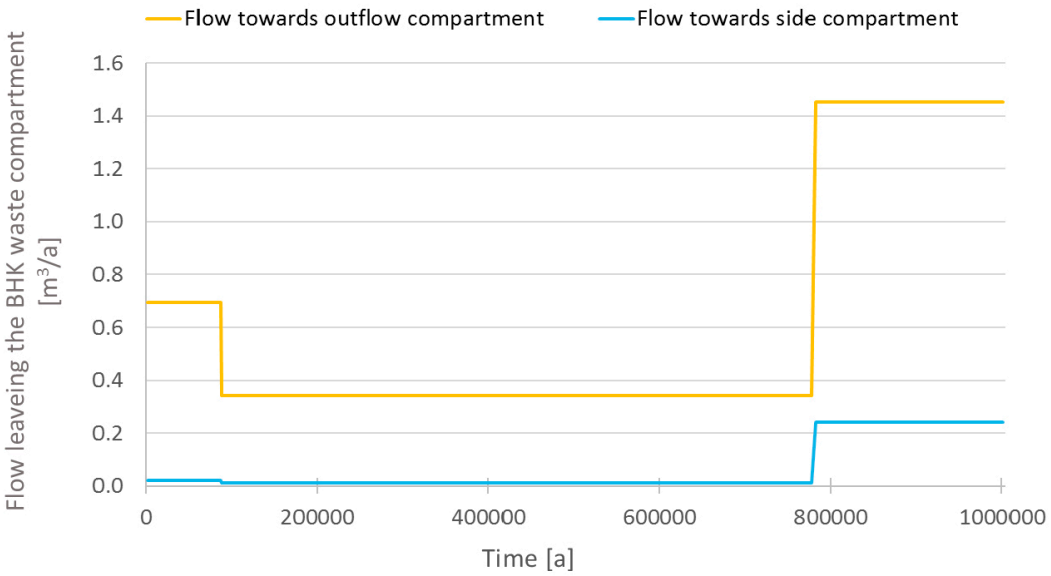

Figure 2-9. *Evolution of groundwater flow leaving the BHK waste compartment due to degradation.*

2.7 Data for partitioning of radionuclides in backfill compartments

2.7.1 Porosity and pore volume in BHA and BHK backfill compartments

Short description of data

The data provided in this section concern the porosity and pore volume in the BHA and BHK backfill sub-compartments. The near-field model assumes that each backfill compartment consists of five homogeneous and evenly-sized sub-compartments that hold one fifth of the compartment's total pore water volume. Therefore, in the near-field model, the total pore water volume in the backfill is calculated by multiplying the backfill volume (see Section 2.2) times the physical porosity of the backfill. Hence, the pore water volumes of the sub-compartments are obtained. It should be noted that the porosity of the concrete backfill evolves over time due to the concrete degradation and leaching of cement (Idiart and Laviña 2019). The provided data are used in the model to determine the pore water activity concentrations in the backfill compartments. This is further described in Wessely and Shahkarami (2019).

Use in model or evaluation activity

In the near-field model, radionuclides are released from the waste compartments and enter the backfill sub-compartments by advection and diffusion. In the sub-compartments, the radionuclides are then partitioned as dissolved in the pore water volume or as sorbed to bentonite or cement mineral surfaces. Therefore, it is required to have information on the pore volume of the backfill to calculate the activity concentrations of dissolved radionuclides in the backfill sub-compartments. It is worth emphasizing that, only the dissolved radionuclides can migrate through the backfill.

Input data used in the near-field model

To calculate the pore volume of a backfill compartment, the volume of the compartment is multiplied by the backfill physical porosity. The volumes of the BHA and BHK compartments are given in Table 2-4 and Table 2-5, respectively. The physical porosity of the bentonite in the BHA backfill compartments is assumed to remain constant throughout the entire SE-SFL timeframe. However, the physical porosity of the concrete in the BHK backfill compartment is assumed to experience a temporal change due to degradation. Physical porosity of the concrete backfill in different timeframes in the SE-SFL base case is tabulated in Table 2-29. It should be noted that for concrete, the whole physical porosity, ϵ_c, is available for transport of anions, cations and neutral species. For bentonite, however, the whole physical porosity ϵ_b is only available for transport of cations and neutral species, i.e. $\varepsilon_b^{cat} = 0.43$. For anions, the diffusion available porosity, ε_b, is less than the physical porosity, i.e. $\varepsilon_b^{an} = 0.17$. It should also be noted that in the near-field model, degradation of the inflow compartment is assumed to be more severe than that of the outflow and side compartments.

Table 2-29. Porosity of the backfill compartments during the repository evolution.

Compartment	Porosity [%]	Timeframe [a]
BHA – Bentonite backfill (Cations)	43 %	2.08E+03 – 1.00E+06
BHA – Bentonite backfill (Anions)	17 %	2.08E+03 – 1.00E+06
BHK – Intact concrete backfill	11 %	2.08E+03 – 1.72E+05
BHK – Inflow compartment	11–18 %	2.08E+03 – 1.72E+05
BHK – Inflow compartment	18–28 %	1.72E+05 – 7.82E+05
BHK – Inflow compartment	28–29 %	7.82E+05 – 1.00E+06
BHK – Outflow and side compartments	11–19 %	1.72E+05 – 3.92E+05
BHK – Outflow and side compartments	19–20 %	3.92E+05 – 7.82E+05
BHK – Outflow and side compartments	20–24 %	7.82E+05 – 1.00E+06

To approximate the varying physical porosity of the concrete backfill compartment in each time step, a linear interpolation is made between the values given in Table 2-29. The graphs showing the physical porosities of the BHA (constant) and BHK backfill compartments are plotted in Figure 2-10.

The resulting pore water volumes in the BHA and BHK backfill compartments are shown in Figure 2-11. It should be emphasized that the diffusion available porosity for anions in the BHA bentonite backfill is $\varepsilon_b = 0.17$. In the near-field model, the five sub-compartments that constitute each backfill compartment have identical volumes and porosities, and each holds one fifth of the backfill compartment's total pore volume.

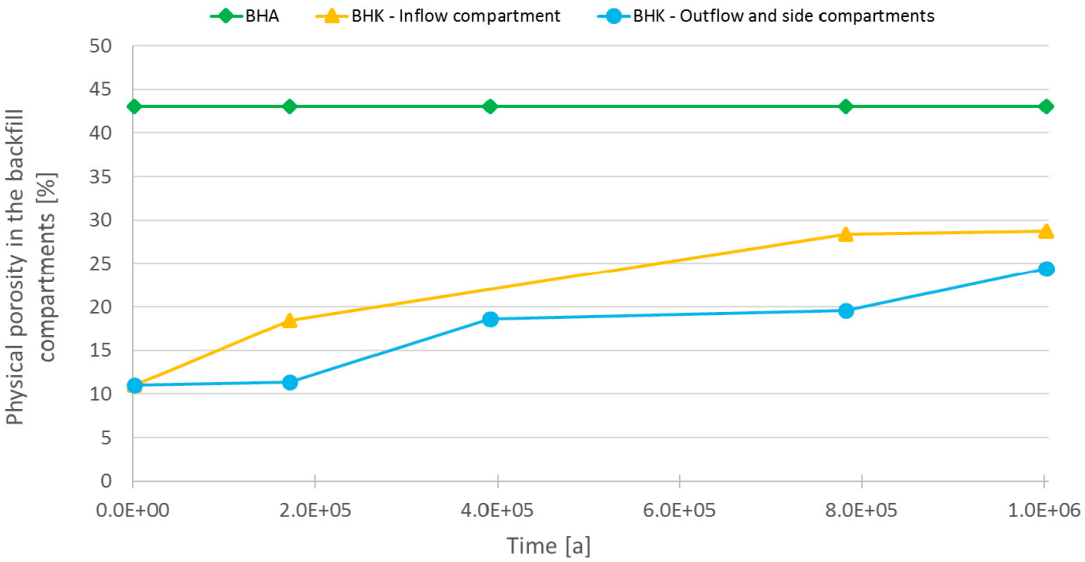

Figure 2-10. *Physical porosities of the BHA and BHK (inflow and side) backfill in the base case.*

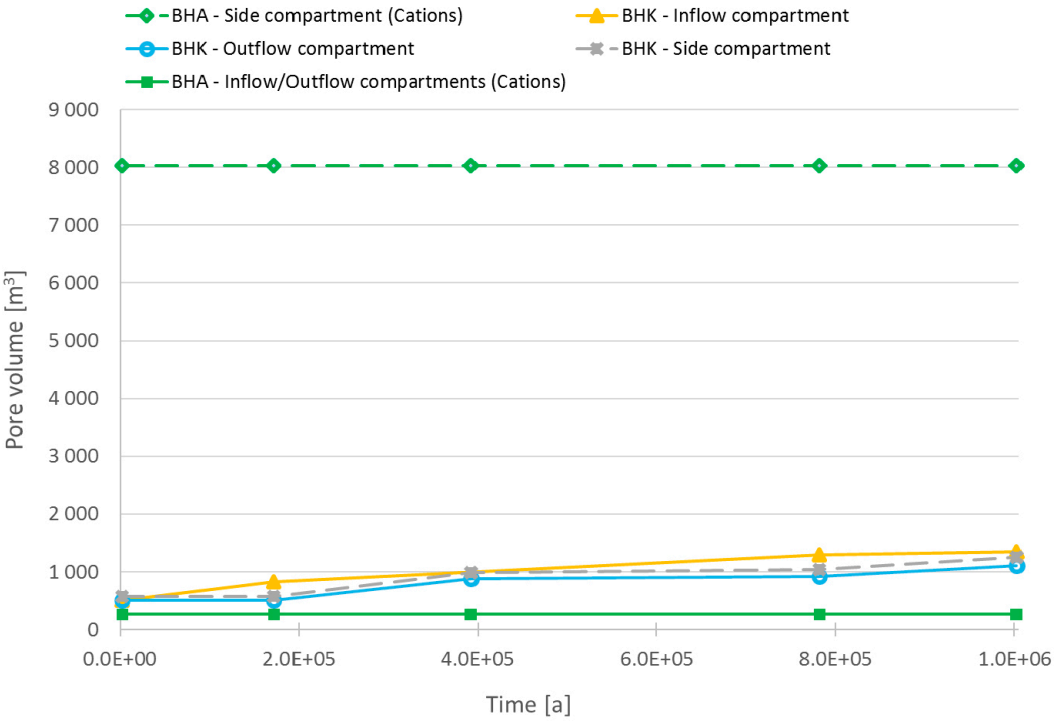

Figure 2-11. *Evolution of the pore volumes in the BHA and BHK backfill compartments incorporated in the near-field model.*

Source of data and justification

The volumes of the backfill compartments in BHA and BHK are estimated in Sections 2.2.1 and 2.2.2, respectively. The physical porosity and diffusion available porosity of bentonite for anions are rounded from the bentonite porosities adopted in SR-Site (SKB 2010a, Table 5-5, Table 5-15).

The initial state physical porosity of the concrete backfill is taken from the **Initial state report**, Section 7.3.1. The varying porosities of the degraded concrete backfill are obtained from Idiart and Laviña (2019, Figure 6-8), after some minor simplifications. In fact, the supporting data in Idiart and Laviña (2019) describe the degradation states of the inner and outer parts of the concrete backfill. This information is included in the near-field model, where the inflow compartment is represented by data from the outer part of the backfill (with a higher degradation rate), while the outflow and side compartments are represented by data from the inner part of the backfill (with a lower degradation rate).

Known limitations in data

In practice, the backfill porosity in BHK experiences temporal and spatial changes. However, the spatial variability within the backfill compartments cannot readily be introduced in the near-field model. Therefore, to incorporate the spatial variability suggested by Idiart and Laviña (2019) in the near-field model, it is assumed that the entire inflow compartment in BHK is subjected to more severe degradation than the outflow and side compartments.

In BHA, it is likely that bentonite degradation occurs at some rates at the vault-rock interface. Nevertheless, in the near-field model, no such degradation is assumed to occur in the bentonite backfill. This degradation effect is, however, addressed in the near-field model by assigning a relatively high porosity to bentonite, similar to that adopted in SR-Site (SKB 2010a).

Furthermore, as discussed in Section 2.2, the geometries of the SFL vaults are simplified in the near-field model. These simplifications cause the near-field model to underestimate the actual backfill volumes in the BHA and BHK vaults. Therefore, less pore volumes in the backfill compartments are available in the model, compared to the proposed volumes in the vault's designs.

2.7.2 Amount of bentonite in BHA backfill

Short description of data

The data in this section concern the amount of bentonite in the BHA backfill compartment.

Use in model or evaluation activity

In the near-field model, radionuclides in the BHA backfill compartments are assumed to sorb on bentonite. Therefore, to calculate the amount of radionuclides that can be sorbed onto the bentonite, it is required to have information on the mass of the solid phase in the bentonite.

Input data used in near-field model

In the near-field model, the volume fraction of solid phase in bentonite is $1 - 0.43 = 0.57$. Hence, the volume of the solid phase can be obtained by multiplying the BHA backfill compartment volumes, given in Table 2-4, times this fraction. It is then straightforward to obtain the amount of solid phase in the compartment by multiplying the solid volume times the density of the solid bentonite particle, 2 780 kg/m^3. The resulting amounts are listed in Table 2-30.

Table 2-30. Mass of bentonite in the BHA backfill compartments.

Compartment	Mass of solid bentonite particles [kg]
BHA – Inflow compartment	9.76E+05
BHA – Outflow compartment	9.76E+05
BHA – Side compartment	2.96E+07

Density of the solid bentonite particle is stored in the SVN database at:

svn://svn.skb.se/SFL/SFLSAK/Arbetsmaterial/RadionuclideTransport/CalculationCases/CC1/Nearfield/CC_specific_indata/rho.xlsx.

Source of data and justification

The volumes of the backfill compartments are taken from Table 2-4. The volume fraction of the solid, i.e. 57 % is approximated under the assumption that the physical porosities are connected. The density of the solid bentonite particle of 2 780 kg/m^3 is taken from SR-Site (SKB 2010f, Table A-1).

Known limitations in data

There are limitations in the data concerning the geometries of the model, and how it represents the real case, as well as some uncertainties in the used physical porosity and density of the solid particle. The simplified geometries used when setting up the models result in an underestimated amount of bentonite in the BHA vault.

2.7.3 Amount of cement in the BHK backfill

Short description of data

The data concern the amount of cement in the BHK backfill compartment in the near-field model. It should be emphasized that cement, in this context, refers to the hydrated cement and not un-hydrated cement particles (or cement powder). The procedure to estimate the amount of cement in the BHK backfill compartments, in terms of the compartment sorption capacities, is detailed in Wessely and Shahkarami (2019).

Use in model or evaluation activity

Radionuclides in the BHK backfill compartments are assumed to sorb only on the hydrated cement part of the concrete. In other words, no nuclides are assumed to sorb on the ballast. Therefore, to calculate the amount of radionuclides that can be sorbed onto the cement embedded in the concrete backfill, it is required to have information on the amount of cement in the BHK backfill compartments. In the near-field model, it is assumed that the cement is evenly distributed in the backfill compartments.

Input data used in near-field model

In the near-field model, it is assumed that the cement initial properties in the concrete backfill, are comparable to the properties of the concrete structure, derived in Section 2.5.2. Furthermore, the volumes of the BHK backfill compartments are given in Table 2-6. Hence, the initial state mass of cement in each compartment can be calculated as:

- BHK backfill side compartment: 5 203 · (350 + 164.5) = 2.67 × 10^6 kg.
- BHK backfill inflow compartment: 5 514 · (350 + 164.5) = 2.84 × 10^6 kg.
- BHK backfill outflow compartment: 5 514 · (350 + 164.5) = 2.84 × 10^6 kg.

However, the amount of cement in the concrete backfill decreases as the concrete porosity increases due to degradation. To take this change into account, the cement mass per cubic meter of concrete, i.e. the cement density, p_c, is approximated as:

$$p_c = (1 - \epsilon_{cs} - \varphi) \cdot p_p \qquad (2\text{-}30)$$

where:

ϵ_{cs} = Porosity of concrete backfill compartment (evolves over time according to Figure 2-10).

φ = Fraction of ballast in the concrete backfill compartment (see Section 2.5.2).

p_p = Solid particle density of the concrete backfill compartment (see Section 2.5.2).

Furthermore, since the concrete porosity evolves continuously, the cement mass in each time step can be approximated with the help of Figure 2-10. The estimated values are plotted in Figure 2-12.

Source of data and justification

Volumes of the BHK backfill compartments are estimated in Section 2.2.2. The porosity of 11 % for the construction concrete is taken from (**Initial state report**, Section 7.3.1). The solid particle density of concrete and cement fractions are calculated from the mixing proportions of the concrete structure (SKB 2014a, Table 7-1), as is given in Section 2.5.2.

Known limitations in data

Since the exact recipe of the concrete that is planned to be used in SFL is not known yet, the relevant information from the SFR repository have been used. There may also be uncertainties in the initial state amounts of concrete. Furthermore, the simplified geometries of the models can result in an underestimated amount of cement in the vaults.

2.7.4 Sorption coefficients of cement in the BHK concrete backfill

Similar sorption coefficient values are used for the cement in the concrete backfill as for the cement in the waste compartment. Therefore, the data and the associated discussion on how to use the data are not reproduced here, but instead, Section 2.5.5 should be consulted.

2.7.5 Sorption coefficients for bentonite in the BHA bentonite backfill

Short description of data

In BHA, radionuclides partition as being dissolved in the pore volume or being sorbed on the bentonite backfill. In the near-field model, a linear sorption is assumed, where the partitioning is governed by the sorption coefficient K_d [m^3/kg]. The partitioning may also be influenced by the complexing agents, which is also included in the model (see Section 2.5.6).

Use in model or evaluation activity

In the near-field model, radionuclides can be retarded by sorption onto the bentonite, and thereby be given more time to decay. The values of the sorption coefficient, K_d, determine the amount of radionuclides that can be sorbed in the BHA backfill. Therefore, each radionuclide is assigned a single-value K_d that is constant in time and space within the backfill compartment. All the C-14 in the BHA vault is assumed to be in organic form.

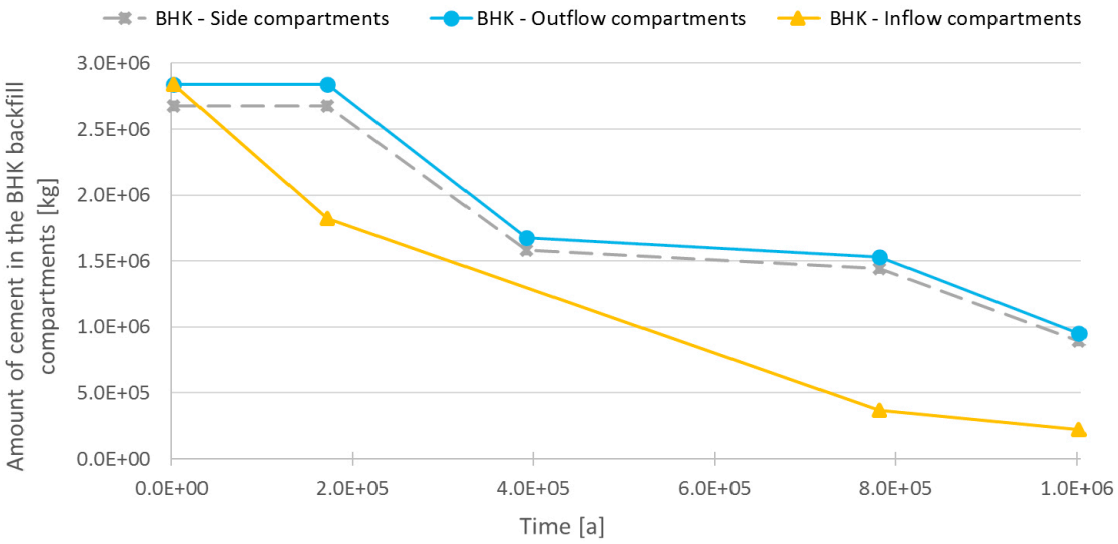

Figure 2-12. *Evolution of the cement mass in the BHK backfill compartments incorporated in the near-field model.*

Input data used in the near-field model

The K_d-values for bentonite in the BHA backfill compartments are tabulated in Table 2-31.

Table 2-31. Sorption coefficients for bentonite in the BHA backfill.

Elements	Ox. State/Analogue	K_d [m^3/kg]	Reference/Note
Ac	Ac(III)	8	(SKB 2014a)
Ag	Ag(I)	0	(SKB 2014a)
Am	Am(III)	61	(SKB 2014a)
Ba	Ba(II)	0.005	(SKB 2014a)
Be	Be(II)/Ba(II)	0.005	Assumed analogue to Ba(II).
C-org	^{14}C, CH_4, organic acids	0	(SKB 2014a)
Ca	Ca(II)	0.005	(SKB 2014a)
Cd	Cd(II)	0.3	(SKB 2014a)
Cl	Cl(-I)	0	(SKB 2014a)
Cm	Cm(III)	61	(SKB 2014a)
Co	Co(II)/Ni(II)	0.3	Assumed analogue to Ni(II).
Cs	Cs(I)	0.11	(SKB 2014a)
Eu	Eu(III)	8	(SKB 2014a)
Gd	Gd(III)/Eu(III)	8	Assumed analogue to Gd(III).
H	–	0	Assumed non-sorbing
Ho	Ho(III)	8	(SKB 2014a)
I	I(-I)	0	(SKB 2014a)
K	K(I)/Cs(I)	0.11	Assumed analogue to Cs(I).
La	La(III)/Eu(III)	8	Assumed analogue to Eu(III).
Mo	Mo(VI)	0	(SKB 2014a)
Nb	Nb(V)	3	(SKB 2014a)
Ni	Ni(II)	0.3	(SKB 2014a)
Np	Np(IV)	63	(SKB 2014a) / Np(V) ruled out.
Pa	Pa(IV,V)	3	(SKB 2014a)
Pb	Pb(II)	74	(SKB 2014a)
Pd	Pd(II)	5	(SKB 2014a)
Po	Po(IV)	0.04	(SKB 2014a)
Pu	Pu(III)	61	(SKB 2014a) / Pu(V) and Pu(VI) ruled out.
Ra	Ra(II)	0.005	(SKB 2014a)
Re	Re(IV)/Tc(IV)	63	Assumed analogue to Tc(IV).
Se	Se(-II)	0	(SKB 2014a) / Pessimistic choice.
Si	S(IV)/U(IV)	63	Assumed analogue to U(IV).
Sm	Sm(III)	8	(SKB 2014a)
Sn	Sn(IV)	63	(SKB 2014a)
Sr	Sr(II)	0.005	(SKB 2014a)
Tb	Tb(III)/Eu(III)	8	Assumed analogue to Eu(III).
Tc	Tc(IV)	63	(SKB 2014a) / Tc(VII) ruled out.
Th	Th(IV)	63	(SKB 2014a)
Ti	Ti(IV)/Zr(IV)	4	Assumed analogue to Zr(IV).
U	U(IV)	63	(SKB 2014a) / U(VI) ruled out.
Zr	Zr(IV)	4	(SKB 2014a)

Source of data and justification

For many of the radionuclides, the K_d-value is taken from SR-PSU (SKB 2014a, Table 7-6) and justified there. However, some of the radionuclides, e.g. radionuclides originating from ESS, have not been evaluated by SKB before. This means that K_d -values have not been assigned for the following nuclides Si, Ti, La, Gd, Tb, Re, K and Be. Therefore, an analogue is sued and the K_d -values are adopted from the chosen analogue. It should be emphasized that ESS-specific radionuclides are not included in the SE-SFL base case calculations.

- H

Hydrogen-3 has no interaction because it is neutral molecule. Therefore, it is assumed to be non-sorbing with $K_d = 0$.

- Si

Si is in group 14 the same group as carbon. However, the sorption behaviour of carbon occurs via non-classical sorption behaviour i.e. crystallisation of calcite (CaCO3) under calcium rich alkaline conditions. No value for Si sorption coefficient is found in the literature. However, Si is part of the cement minerals (C-S-H) and should react with portlandite (CaOH2) to form C-S-H which is insoluble. This justifies setting a high K_d for Si. Sorption coefficient of U(IV) is used as an analogue.

- Ti

Ti is in group 4 in the periodic table of the elements. Ti is assumed to behave similar to Zr(IV).

- La, Gd and Tb (Lanthanides)

La is the first element in the lanthanide row. Sorption coefficient for Lanthanides has been studied extensively and Eu is the lanthanide that has been studied most. In SE-SFL, the K_d for Eu is recommended both for cement and bentonite for all the lanthanides.

- Re

Re, a transition metal, is in group 7 in the periodic table of the elements. Re is found in the same group as Tc. Therefore, Tc is used as an analogue for Re sorption.

- K

K belongs to the alkali elements and the sorption behaviour is characterised by ionic interactions. Cs is one of the elements in this group that its sorption behaviour has been extensively studied. Therefore, Cs is chosen as an analogue for K.

- Be

Be belongs to the alkali earth metals. The sorption behaviour of these species is mainly studied for Ra and Ba. Ba is one of the elements in this group that its sorbing behaviour has been studied extensively. Therefore, Ba is chosen as an analogue for Be.

- Co

The divalent Co(II) form is the only relevant redox state for this radioelement. Co(II) is a close geochemical analogue of Ni(II) and it is therefore recommended that the corresponding K_d range for Ni(II) sorption be used for Co(II).

For a few radionuclides, the likelihood of certain oxidation states has been ruled out as compared to in SKB (2014a, Table 7-6). These are Np(V), Pu(V), Pu(VI), Tc(VII) and U(VI).

Known limitations in data

For radionuclides that are not included in SR-PSU, the supplied K_d-values are estimated from data obtained for one or more analogue species. Uncertainties can, therefore, occur with a lack of suitable analogues.

2.7.6 Sorption reduction factors due to complexing agents

In BHA, Similar sorption reduction factors are used in the bentonite backfill as for the waste compartment. The data and the associated discussion on how to use the data, are not presented here and Section 2.5.6 should be consulted.

2.8 Data for diffusive and advective transport in backfill compartments

2.8.1 Diffusion transport resistance in the BHA backfill compartments

Short description of data

In the near-field model, radionuclides are transported through the BHA backfill compartments by advection and diffusion. The data provided in this section concern the diffusion transport resistances in the BHA backfill compartments.

Use in model or evaluation activity

The procedure adopted in the near-field model to calculate the diffusion transport resistances in the BHA backfill compartments is similar to what is discussed earlier in Section 2.6.1 to determine the diffusion transport resistance in the BHA waste compartment.

Input data used in the near-field model

The diffusion transport resistance in each of the BHA backfill compartment is determined by the dimensions of the compartment, determined in Section 2.2.1, and the effective diffusivity of radionuclides, D_e^{bA}, in bentonite.

$$\boldsymbol{R_{nf}^{bA}} = \frac{\boldsymbol{l^{bA}}}{\boldsymbol{A_{nf}^{bA} D_e^{bA}}} \tag{2-31}$$

$$\boldsymbol{R_{ns}^{bA}} = \frac{\boldsymbol{l^{bA}}}{\boldsymbol{A_{ns}^{bA} D_e^{bA}}} \tag{2-32}$$

Where A_{nf}^{bA} and A_{ns}^{bA} are the cross-section areas of the backfill compartments normal to the diffusive direction along and across the vault, respectively, and l^{bA} is the diffusion length within the compartments. In the near-field model, the diffusion length is set to the backfill thickness D (see Section 2.2.1).

The adopted values for the effective diffusivity in bentonite are also listed in Table 2-32 (Ochs and Talerico 2004, Section 5.4).

Table 2-32. Effective diffusivity in bentonite in the BHA backfill compartment.

Species	Effective diffusivity [m^2/s]
Anions	1.0E-11
Cations/Neutral	1.2E-10
Cs	3.0E-10

The estimated diffusion transport resistances are provided in Table 2-33.

Table 2-33. Diffusion transport resistances in the BHA backfill compartment.

	Diffusion Transport resistance [a/m^3]		
Compartment	Anions	Cations/Neutral	Cs
BHA – Inflow compartment	37.25	3.10	1.24
BHA – Side compartment	0.89	0.07	0.03
BHA – Outflow compartments	37.25	3.10	1.24

In the near-field model, the five sub-compartments that constitute each backfill compartment are assumed to have identical properties. Therefore, each sub-compartment holds one fifth of the backfill compartment's diffusion transport resistance.

Source of data and justification

The cross-section areas of the backfill compartments and the diffusion length are derived in Section 2.2.1. The effective diffusivities in bentonite are adopted from Ochs and Talerico (2004, Section 5.4), which rely on redox condition of radionuclides. Justification of the data can also be found in the reference document. However, for radionuclides that are not included in the reference document, speciation calculations are made to provide proper input data for SE-SFL. The calculations are made for the radionuclide analogue species using the SPANA program[7].

Known limitations in data

As discussed in Section 2.2.1, the geometries of the BHA vault is simplified in the model. For some radionuclides that were not included in Ochs and Talerico (2004, Section 5.4), the assumed analogues are straight forward to apply, while for others, assigning an analogue can be more complex. Furthermore, if a radionuclide is found to be present as neutral as well as anionic species, depending on the PH value in bentonite, the radionuclide is assumed to behave similar to cations, which have larger effective diffusion coefficient, Table 2-32. However, this behaviour is only observed for Tb, Re, Pa and Be which, except for Pa and Be, are not included in the BHA inventory in the base case.

2.8.2 Diffusion transport resistance in the BHK backfill compartments

Short description of data

In the near-field model, radionuclides are transported through the BHK backfill compartments by advection and diffusion. The data provided in this section concern the diffusion transport resistances in the BHK backfill compartments.

Use in model or evaluation activity

The procedure adopted in the near-field model to calculate the diffusion transport resistances in the BHK backfill compartments is similar to what is discussed earlier in Section 2.6.2 to determine the diffusion transport resistance in the BHK waste compartment.

Input data used in the near-field model

The diffusion transport resistance in each of the BHK backfill compartments is determined by the dimensions of the compartment, determined in Section 2.2.2, and the effective diffusivity of radionuclides, D_e^{bK}, in concrete.

$$\boldsymbol{R_{nf}^{bK}} = \frac{\boldsymbol{l^{bK}}}{\boldsymbol{A_{nf}^{bK} D_e^{bK}}} \tag{2-33}$$

$$\boldsymbol{R_{ns}^{bK}} = \frac{\boldsymbol{l^{bK}}}{\boldsymbol{A_{ns}^{bK} D_e^{bK}}} \tag{2-34}$$

Where A_{nf}^{bK} and A_{ns}^{bK} are the cross-section areas of the backfill compartments normal to the vertical and horizontal diffusive direction, respectively, and l^{bK} is the diffusion length within the compartments.

Concrete degradation affects the porosity and radionuclide effective diffusivity in the BHK backfill. Therefore, contrary to BHA, the effective diffusivity, D_e^{bK}, and diffusion length in the BHK backfill compartments, l^{bK}, depend on the degradation state of the concrete.

[7] Källström K, 2016. Speciation calculations for determining diffusion constants in Bentonite within the SE-SFL project. SKBdoc 1559226 ver 0.5, Svensk Kärnbränslehantering AB. Internal document.

In the near-field model, the diffusion length is set to the backfill thickness, *D*, in the Intact Case (IC) and the completely Degraded Case (DC). However, in the Degraded Zone Case (DZC), the diffusion length is set to the half of the backfill thickness.

Furthermore, the effective diffusivity of radionuclides in the BHK concrete backfills is assumed to experience temporal variability due to the concrete degradation, Table 2-34. The data are obtained from the transient simulations of concrete leaching performed in Idiart et al. (2019a). As the data in the table suggest, the concrete degradation is considered to be more prominent where incoming groundwater meets the backfill in the inflow compartment, as compared to degradation where water leaves the backfill from the outflow and side compartments.

The applied effective diffusivities in BHK and their associated timeframes can also be found in the SVN database at:

svn://svn.skb.se/SFL/SFLSAK/Arbetsmaterial/RadionuclideTransport/CalculationCases/CC1/Nearfield/CC_specific_indata/De.xlsx.

svn://svn.skb.se/SFL/SFLSAK/Arbetsmaterial/RadionuclideTransport/CalculationCases/CC1/Nearfield/CC_specific_indata/DeSelectorBHK.xlsx.

Table 2-34. Effective diffusivities in the BHK backfill compartments during the repository evolution.

Compartment	Effective diffusivity [m^2/s]	Timeframe [a]
BHK – Intact concrete backfill	3.50E-12 – 3.71E-12	2.08E+03 – 1.72E+05
BHK – Inflow compartment	3.50E-12 – 1.15E-11	2.08E+03 – 1.72E+05
BHK – Inflow compartment	1.15E-11 – 3.74E-11	1.72E+05 – 7.82E+05
BHK – Inflow compartment	3.74E-11 – 3.86E-11	7.82E+05 – 1.00E+06
BHK – Outflow and side compartments	3.71E-12 – 1.29E-11	1.72E+05 – 3.92E+05
BHK – Outflow and side compartments	1.29E-11 – 1.44E-11	3.92E+05 – 7.82E+05
BHK – Outflow and side compartments	1.44E-11 – 2.27E-11	7.82E+05 – 1.00E+06

To approximate the effective diffusivity in the different BHK compartments and in each time step, a linear interpolation is performed between the data given in Table 2-34. The graphs showing the resulting diffusivities in the BHK backfill compartments are plotted in Figure 2-13.

The resulting diffusion transport resistances for the BHK backfill sub-compartments are shown in Figure 2-14. In the near-field model, the five sub-compartments that constitute each backfill compartment are assumed to have identical properties. Therefore, each sub-compartment holds one fifth of the backfill compartment's diffusion transport resistance.

Source of data and justification

The cross-section areas of the backfill compartments and the diffusion length are derived in Section 2.2.2. The effective diffusivity of the concrete backfill is taken from Idiart and Laviña (2019).

Known limitations in data

As discussed in Section 2.2, the geometries of the vaults are simplified in the model. The diffusion length is not well defined for the partially degraded concrete backfill. Using half of the backfill thickness for the Degraded Zone Case (DZC) implies that the radionuclides only have to diffuse through half of the backfill before being transported, by advection, to the fractures in the host rock. For the degraded concrete the transport is dominated by advection and the diffusion transport resistance becomes negligible.

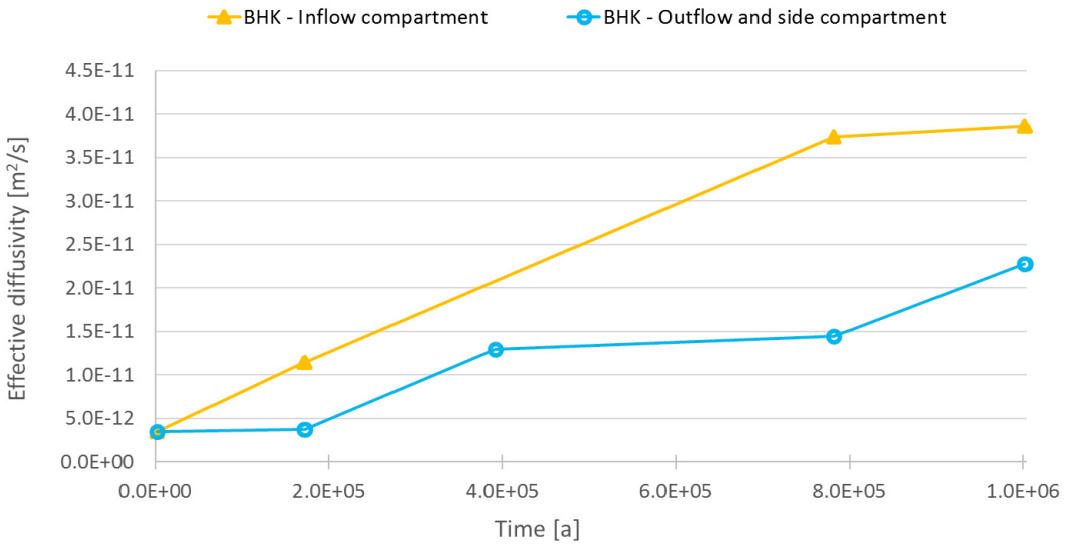

Figure 2-13. *Evolution of the effective diffusivities in the BHK backfill compartments incorporated in the near-field model.*

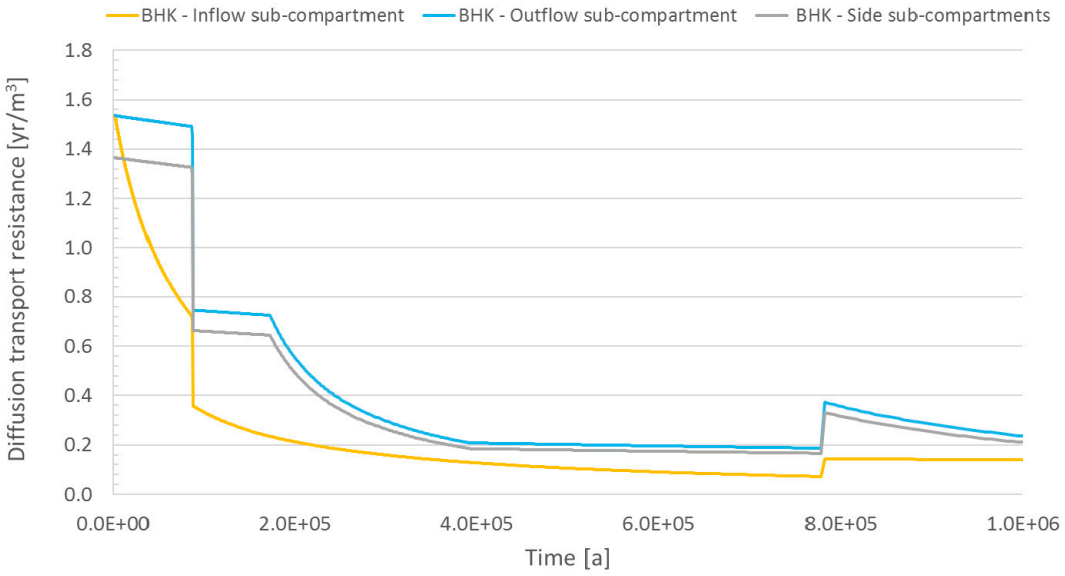

Figure 2-14. *Evolution of the diffusive transport resistance in the BHK backfill sub-compartments.*

2.8.3 Advective flow in the BHA backfill compartments

Short description of data

To calculate the advective release through the BHA backfill compartment, the groundwater flow rates in the BHA vault are needed. The data provided in this section concern the advective flow in the BHA backfill compartments.

Use in model or evaluation activity

In the near-field model, the groundwater flow through the BHA waste compartment is approximated as the sum of the overall flows through the BHA waste control volumes (see Section 2.6.3). Since the groundwater flow in BHA is mostly directed along the vault, the model assumes that no advective transport occurs in the backfill side compartments and the groundwater solely flows through the backfill outflow compartments.

The advective release through the backfill outflow compartment can then be determined by multiplying the activity concentration of dissolved radionuclides times the groundwater flow.

Input data used in near-field model

The groundwater flow through the BHA backfill outflow compartment is estimated in Section 2.6.3, $Q_{out} = 1.55 \times 10^{-3}$ m^3/a (Table 2-24).

Source of data and justification

The groundwater flow information in the BHA backfill outflow compartment is taken from (Table 2-24). It should be noted that in the near-field model, no groundwater flow is assumed in the BHA backfill side compartments. This is justified by the fact that in BHA, the transport by advection is negligible compared to the transport by diffusion.

Known limitations in data

See Section 2.6.3.

Compared to the repository scale model (Abarca et al. 2019), geometries of the BHA waste and backfill compartments are greatly simplified in the near-field model. More specifically, the waste control volumes incorporated in the repository scale model are lumped into the single waste compartment in the near-field model. Therefore, the detailed flow information provided for the control volumes should be reinterpreted before they can be used the near-field model. This is done by summing the total flows through the BHA waste control volumes. This is a simplistic approach. However, because transport in BHA is mostly dominated by molecular diffusion, the estimated flow is believed to be sufficiently accurate for the safety evaluation.

2.8.4 Advective flow in the BHK backfill compartments

Short description of data

In the near-field model, radionuclides are transported through the BHK backfill compartment by advection and diffusion. To calculate the advective component, the groundwater flows through the backfill compartments are needed. Importantly, since the concrete backfill degrades over time, this impacts the local groundwater flow through the vault and the backfill compartments. Therefore, three states of degradation are considered in Abarca et al. (2019) as well as in the near-field model for BHK. These include:

- Intact Case (IC): The concrete backfill is intact and has initial state properties (during the time period 2075–87 083 [a]).
- Degraded Zone Case (DZC): The outer half of the concrete backfill is degraded (during the time period 87 083–782 168 [a]).
- Degraded Case (DC): The entire concrete backfill is degraded (during the time period 782 168–1 002 075 [a]).

Use in model or evaluation activity

In the near-field model, the required information on the groundwater flow through the BHK backfill outflow and side compartments are adopted from the results of the repository scale model (Abarca et al. 2019). The activity concentration of dissolved radionuclides is, then, multiplied by the groundwater flow to calculate the advective release from the BHK backfill compartments. It is worth emphasizing that, the majority of the advective flow in BHK is directed vertically towards the outflow compartment and only a minor part is directed horizontally towards the side compartment.

Input data used in the near-field model

In the near-field model, groundwater flows through the BHK backfill outflow and side compartments are estimated from the groundwater flows leaving the BHK waste compartment (see Section 2.6.4 (Table 2-28)). These values are used in the near-field model to represent the advective flow through the BHK backfill compartments.

Source of data and justification

The magnitudes of the groundwater flow rates towards the BHK backfill are estimated in Section 2.6.4. To calculate the groundwater flow rates through the BHK backfill outflow and side compartments, it is assumed that they can be approximated by the magnitudes of groundwater flow rates leaving the BHK waste control volumes towards the backfill.

This is a fair approximation since in the Intact Case (IC) and Degraded Case (DC), the magnitudes of groundwater flow rates through the BHK waste control volumes are comparable to those in the backfill compartments (Abarca et al. 2019, Figure 6-4). This approximation remains reasonable even in the DZC, where the higher groundwater flow rates in the degraded backfill creates a preferential flow path, allowing the groundwater to bypass the waste compartment. As a result, transport is expected to be mostly driven by diffusion to the groundwater seeping tangentially past the low-permeable backfill interface. In the near-field model, this is reflected in the high value selected for the total equivalent flow in the DZC (see Section 2.9.6).

Known limitations in data

See Section 2.6.4.

2.9 Data for diffusion and advective transport at the vault-rock interfaces

2.9.1 Transport properties of the intersecting fractures at the BHA vault-rock interface

Short description of data

This set of data concern the transport properties of the fractures in the host rock that intersect the BHA vault. An important transport parameter at the vault-rock interface is the equivalent flow rate of the water seeping in a fracture in the host rock. The equivalent flow rate determines the diffusion rate of radionuclide from the vault backfill to the water in the fracture. The chosen data are adopted from the regional scale modelling, which is detailed in Joyce et al. (2019). In the regional scale modelling, it is found that the BHA vault is intersected by 535 fractures. In order to find the particle trajectories, ten particles are injected in each fracture and their transport paths are recorded. It is found that 2 424 particles reach the ground surface. Eventually, the information of the fractures that intersect the BHA vault is recorded for each of the particle trajectories that reaches the surface. The information is used in the near-field model and can be found in the SVN database at:

svn://svn.skb.se/SFL/SFLSAK/Arbetsmaterial/RadionuclideTransport/CalculationCases/CC1/Geosphere/sfl_elaborated_r1_hrd_site_nochem_pline_surfaces_2000.xlsx.

Use in model or evaluation activity

In the near-field model, the transport properties of the intersecting fractures are used to describe the radionuclide transport at the vault-rock interface. More specifically, the data are used to calculate the effective diffusion transport resistances at the fracture openings in the BHA vault (see Section 2.9.2)

Input data used in the near-field model

Out of the information provided for the particle trajectories, the following properties of the intersecting fractures are used as input data in the near-field model.

- Intersection length: Length of the intersection of the fracture and the vault recorded in the column, INTL.
- Fracture aperture: Aperture of the fracture recorded in the column, TRAPP.
- Equivalent flow: Equivalent flow rate in the fracture recorded in the column, QEQ.

Source of data and justification

The chosen data are derived from regional scale model, as described in SE-SFL regional scale hydro-geological modelling with ConnectFlow (Joyce et al. 2019).

Known limitations in data

For discussions on the uncertainties in the modelling and parameterization of terms, the reader may refer to the reference document (Joyce et al. 2019).

2.9.2 Effective diffusion transport resistance to the intersecting fractures at the BHA vault-rock interface

Short description of data

At the BHA vault-rock interface, radionuclides can migrate into the fractures in the surrounding rock by diffusion from the bentonite backfill to the seeping water in a fracture in the host rock. To calculate the diffusive release rate to the fracture in the host rock, the effective diffusion transport resistances at the vault-rock interface are needed. The effective diffusion transport resistance includes the plug resistance, R_{plug}, and the equivalent transport resistance $R_{eq} = \frac{1}{Q_{eq}}$ (Wessely and Shahkarami 2019).

Use in model or evaluation activity

In the near-field model, the effective diffusion resistance against transport to water in a intersecting fracture *i*, i.e. R_{FE}^{i} is used to calculate the effective diffusion transport resistance between the BHA backfill boundary sub-compartments and the fractures in the host rock, R_{E}^{bsc} (see Section 2.9.3).

Input data used in the near-field model

At each fracture opening, the plug resistance can be approximated by: (Neretnieks 1986).

$$R_{plug}^{i} = \frac{\left(1 - 1.35 \cdot \mathrm{Log10}\left(\frac{b_i}{2 \cdot a}\right) + 1.6 \cdot \mathrm{Log10}\left(\frac{D}{a}\right)\right)}{2 \cdot l_i \cdot D_e} \tag{2-35}$$

where:

a = Width of the backfill compartment, 7.7 [m].

b_i = Fracture aperture, [m].

D = Backfill thickness, 2.3 [m].

l_i = Fracture length, [m].

D_e^{bA} = Effective diffusivity of bentonite, [m^2/s] (see Section 2.8.1).

Hence, the effective diffusion resistance at the fracture opening can be determined as

$$R_{FE}^{i} = R_{plug}^{i} + \frac{1}{Q_{eq}^{i}} \tag{2-36}$$

Where Q_{eq}^{i} is the equivalent flow in the fracture *i* provided by the regional hydrogeology model (Joyce et al. 2019).

Source of data and justification

See Section 2.8.1 and Section 2.9.1.

The value used for the backfill compartment width is within the limits for which Equation 2-35 is valid, i.e. 0.03 < d/a <1 and 1E-6 < b/a < 1E-1 (Neretnieks 1986). However, the plug resistance is not very sensitive to the compartment width.

Known limitations in data

See Section 2.9.1.

2.9.3 Effective diffusion transport resistance between the BHA backfill boundary sub-compartments and the host rock

Short description of data

In this section, the estimated effective diffusion resistances to transport from the backfill pore water to water in intersecting fractures, R_{FE}^{i} are used to estimate the effective diffusion transport resistance between a boundary sub-compartment and the host rock in the BHA vault, R_E^{bsc}.

Use in model or evaluation activity

In each time step, the activity concentration of dissolved radionuclides in a compartment is divided by the total effective diffusion transport resistance of all fracture opening and multiplied with the duration of the time step. This is done to obtain the radionuclide specific activity that is transferred between the BHA backfill boundary sub-compartment and the fractures in the rock by diffusion, during the time step.

Input data used in the near-field model

In the near-field model, the total effective diffusion transport resistance from the backfill to the host rock, R_{TE}, is defined as the reciprocal of the harmonic sum of the effective diffusion transport resistances against the release into each individual fracture in the host rock:

$$R_{TE} = \frac{1}{\sum_i \frac{1}{\mathrm{R}_{\boldsymbol{FE}}^{\mathrm{i}}}} \tag{2-37}$$

The model then assumes that the effective diffusion transport resistance at the interface between each boundary sub-compartment and the fractures in the host rock is proportional to the area fraction of the sub-compartment times the total effective diffusion transport resistance:

For sub-compartments that their cross-section areas are normal to the inflow direction:

$$R_E^{bsc} = \frac{A_T}{A_{nf}^{bA}} R_{TE} \tag{2-38}$$

For sub-compartments that their cross-section areas are along the inflow direction,

$$R_E^{bsc} = \frac{A_T}{A_{ns}^{bA}} R_{TE} \tag{2-39}$$

where A_T is the total area of the BHA compartments. The applied input data are summarised in Table 2-35.

Table 2-35. Effective diffusion transport resistance in BHA backfill boundary sub-compartment.

	Effective Diffusion transport resistance, R_E^{bsc} [a/m^3]		
Compartment	**Anions**	**Cations/Neutral**	**Cs**
BHA – Inflow sub-compartment	955.6	320.1	266.2
BHA – Side sub-compartment	25.1	8.4	7.0
BHA – outflow sub-compartments	955.6	320.1	266.2

Source of data and justification

See Section 2.9.2.

Known limitations in data

See Section 2.9.1, simplified geometry.

2.9.4 Transport from the BHA backfill to the water seeping in the host rock

Short description of data

Radionuclides are transported from the BHA boundary sub-compartments to the host rock by diffusion and advection. In this section, the total release rate from the BHA boundary sub-compartments are evaluated.

Use in model or evaluation activity

In each time step, to obtain the radionuclide activity that is released by diffusion from the BHA backfill boundary sub-compartment, the activity concentration of dissolved radionuclides in the outer most backfill sub-compartments are divided by the sum of diffusion resistance in the sub-compartment, R_{ns}^{bA} or R_{nf}^{bA}, and effective diffusion transport resistance of the interface between the backfill boundary sub-compartment and the fractures in the host rock, R_E^{bsc}, and multiplied with the duration of the time step.

Furthermore, to obtain the radionuclide specific activity that is released from the BHA backfill sub-compartment by advection, the activity concentration of dissolved radionuclides in the outflow compartment is multiplied by the total groundwater flow from the outflow compartment, Q_{out}, and by the duration of the time step.

The sum of the advective and diffusive release from BHA constitutes the source term to the geosphere model.

Input data used in near-field model

The effective transport resistance for each backfill sub-compartment is estimated in Section 2.9.3.

The groundwater flow through the BHA backfill outflow compartment, Q_{out}, is 1.55×10^{-3} m^3/a (see Table 2-24), throughout the evaluation time frame. No groundwater flow is assumed in the BHA backfill side compartment.

The total release from the BHA vault can, then, be approximated by:

$$N_T^A = \frac{c_{inflow}}{R_{E,inflow}^{bsc}} + \frac{c_{side}}{R_{E,side}^{bsc}} + \frac{c_{outflow}}{R_{E,outflow}^{bsc}} + c_{out} \cdot Q_{out} \qquad (2\text{-}40)$$

Where:

c = Concentration in a BHA backfill compartment.

R_E^{bsc} = Effective Diffusion transport resistance at the interface between the BHA backfill compartment and the fractures in the host rock.

Q_{out} = Groundwater flow through the BHA backfill outflow compartment is 1.55×10^{-3} m^3/a.

Source of data and justification

See Sections 2.9.3 and 2.8.3.

The groundwater flow in the BHA backfill outflow compartments is taken from Table 2-24.

Known limitations in data

See Sections 2.9.3 and 2.8.3.

2.9.5 Transport properties of the intersecting fractures at the BHK vault-rock interface

Short description of data

This set of data concern the transport properties of fractures in the host rock that intersect the BHK vault. The chosen data are adopted from regional scale modelling, which is detailed in Joyce et al. (2019).

In the regional scale modelling, it is found that the BHK vault is intersected by 424 fractures. In order to find the particle trajectories, ten particles are injected in each fracture and their transport paths are recorded. It is found that 2 035 particles reach the ground surface. Eventually, the information of the fractures that intersect the BHK vault is recorded for each of the particle trajectories that reaches the surface. The information is used in the near-field model and can be found in the SVN database at:

svn://svn.skb.se/SFL/SFLSAK/Arbetsmaterial/RadionuclideTransport/CalculationCases/CC1/Geosphere/sfl_elaborated_r1_hrd_site_nochem_pline_surfaces_2000.xlsx.

Use in model or evaluation activity

In the near-field model, the transport properties of the intersecting fractures are used to describe the radionuclide transport at the vault-rock interface. More specifically, the data are used to calculate the diffusion transport resistances at the fracture openings in the BHK vault (see Section 2.9.6).

Input data used in the near-field model

Out of the information provided for the particle trajectories, the following properties of the fractures that intersect the BHK vault are used as input data in the near-field model.

- Intersection length: Length of the intersection of the fracture and the vault recorded in the column, INTL.
- Flow per meter in the fracture vault intersection recorded in the column, U0.
- Equivalent flow: Equivalent flow rate in the fracture recorded in the column, QEQ.

Source of data and justification

The chosen data are derived from regional scale model, as described in SE-SFL regional scale hydrogeological modelling with ConnectFlow (Joyce et al. 2019).

Known limitations in data

The positions of the fracture intersections are not well defined in the output file from the regional scale hydrogeology model. Therefore, little is known on the number of fractures that intersect a particular backfill compartment. Furthermore, the concrete backfill is assumed to be intact in the ConnectFlow calculation.

It should also be emphasized that the water flow at the vault-rock interface is calculated both by the repository scale model (Abarca et al. 2019) and the regional scale model (Joyce et al. 2019). However, the model predictions of the flow through the BHK vault do not agree in the intact concrete case (IC). Therefore, the predicted flow from the repository scale model is used to calculate the radionuclide release from the vault and the predicted flow from the regional scale model is used to calculate the radionuclide transport along the trajectories in the geosphere (see Chapter 3).

2.9.6 Total equivalent flow rate at the BHK vault-rock interface

Short description of data

Radionuclides are transported from the BHK backfill compartments to the water seeping in fractures in the host rock by diffusion and advection. To calculate the diffusive component, the equivalent flows of water seeping along the backfill host rock interface is required. The total equivalent flow rate at the vault-rock interface is defined as the sum of the equivalent flows of water seeping along the vault-rock interface.

Use in model or evaluation activity

The data is used to calculate the transport rate from the BHK backfill to the water seeping in the fractured rock in Section 2.9.7.

It should be noted that since the concrete has a higher permeability than bentonite, the seeping water can have access to a larger volume within the concrete compared to the limited surface area provided by the fracture aperture. Therefore, the plug resistance R_{plug} is neglected in the BHK concrete backfill. This further discussed in Wessely and Shahkarami (2019).

Input data used in the near-field model

The total equivalent flow rate at the vault-rock interface varies depending on the degradation state of the concrete backfill. In the Intact Case (IC), the total equivalent flow rate is expressed as the sum of the equivalent flow rate in all the intersecting fractures:

$$Q_{eq}^{T} = \sum_{i} Q_{eq}^{i} \qquad (2\text{-}41)$$

In the Degraded Zone Case (DZC), the total equivalent flow rate is viewed as the flow of water in the most degraded part of the backfill. This is estimated as the difference between the flow entering the vault and the flow passing through the waste (Abarca et al. 2019):

$$Q_{eq}^{T} = Q_{vault} - Q_{waste} \qquad (2\text{-}42)$$

with

Q_{vault} = The sum of flows through all backfill volumes = 5.00E+00 m^3/a (Abarca et al. 2019, Table 6.1).

Q_{waste} = The sum of flows through all waste volumes = 4.83E-01 m^3/a (Abarca et al. 2019, Table 6.1).

In the Degraded Case (DC), since the concrete backfill becomes highly permeable, transport is dominated by advection and diffusive transport has marginal effect (Wessely and Shahkarami 2019). Nevertheless, the diffusive component is considered in the in the near-field model by assuming that the total equivalent flow in the Degraded Case (DC) is similar to that in the Intact Case (IC).

Source of data and justification

The equivalent flow rates in the fractures are adopted from Joyce et al. (2019) as discussed in Section 2.9.5. Information on the flow through the vault and the waste are, however, directly taken from the repository scale model (Abarca et al. 2019).

Known limitations in data

See Section 2.9.5.

In the DZC, it is assumed that the contact time of water with the intact concrete backfill is sufficiently long that allows molecular diffusion to effectively even out the concentration across the degraded zone. As a result, water can be fully equilibrated with the waste concentration and the equivalent flow rates in the DZC can be assumed to be equal to the water flow rates in the degraded part of the backfill. This is a pessimistic assumption.

2.9.7 Transport from the BHK backfill to the water seeping in the host rock

Short description of data

Radionuclides are transported from the BHK backfill to the water seeping in the fractures in the host rock mostly by advection and partly by diffusion. To calculate the total release from the BHK vault, the groundwater flows through the backfill compartment and the equivalent flow rates for each boundary sub-compartment are needed.

Use in model or evaluation activity

In each time step, to obtain the radionuclide specific activity that is released from the BHK backfill sub-compartment by advection, the activity concentrations of dissolved radionuclides in the outflow and side compartments are multiplied by the total groundwater flow through the outflow and side compartments and multiplied with the duration of the time step.

Furthermore, to obtain the radionuclide specific activity that is released from the BHK backfill sub-compartment by diffusion, the activity concentration of dissolved radionuclides in the outer most backfill sub compartments are divided by the total diffusion transport resistance of the interface between the backfill and the fractures in the host rock, R_T^{bsc}, and multiplied with the duration of the time step.

Thus, the sum of the advective and diffusive release from BHK constitutes the source term to the geosphere model

Input data used in the near-field model

The total diffusion transport resistance at the interface between the outermost BHK backfill sub compartment, i.e. the boundary sub-compartment *sc*, and the host rock is defined as the sum of the diffusion resistance within the boundary sub-compartment, defined by Equation 2-3, and the inverse of the equivalent flow rate at the interface between the sub-compartment and the host rock:

$$R_T^{bsc} = R_{dif}^{bsc} + \frac{1}{Q_{eq}^{bsc}} \tag{2-43}$$

In the near-field model, the diffusion length in each sub-compartment is set to its half-thickness. Hence, since each backfill compartment consists of five evenly-sized sub-compartments, the diffusion resistance within each boundary sub-compartment can be expressed as:

For sub-compartments that their cross-section areas are normal to the inflow direction:

$$R_{dif}^{bsc} = \frac{R_{nf}^{bK}}{10} \tag{2-44}$$

For sub-compartments that their cross-section area along the inflow direction:

$$R_{dif}^{bsc} = \frac{R_{ns}^{bK}}{10} \tag{2-45}$$

Furthermore, the near-field model assumes that the equivalent flow rate at the interface between each BHK backfill boundary sub-compartment and the fractures in the host rock can be expressed as:

For sub-compartments that their cross-section areas are normal to the inflow direction:

$$Q_{eq}^{bsc} = \frac{A_{nf}^{bK}}{A_T} Q_{eq}^{T} \tag{2-46}$$

For sub-compartments that their cross-section area along the inflow direction:

$$Q_{eq}^{bsc} = \frac{A_{ns}^{bK}}{A_T} Q_{eq}^{T} \tag{2-47}$$

Where Q_{eq}^{T} is the total equivalent flow rate at the vault-rock interface, Equation 2-42, and A_T is the total area of the BHK vault.

Hence, the total release from the BHK vault can, then, be approximated as:

$$N_T^K = \frac{c_{inflow}^{bsc}}{R_{T,inflow}^{bsc}} + \frac{c_{side}^{bsc}}{R_{T,side}^{bsc}} + \frac{c_{outflow}^{bsc}}{R_{T,outflow}^{bsc}} + c_{side}^{bsc} \cdot Q_{side}^{bsc} + c_{outflow}^{bsc} \cdot Q_{outflow}^{bsc} \tag{2-48}$$

where c^{bsc} is the radionuclide concentration in the boundary sub-compartment. The input data used is summarised in Table 2-36.

Table 2-36. Transport measures in the BHK backfill compartment.

Compartment		[m³/a]		
		IC (2075 [a])	DZC (87 578 [a])	DC (782 416 [a])
BHK – Inflow compartment	R_{dif}^{bsc}	1.879	0.438	0.176
	$\frac{1}{R_{T,inflow}^{bsc}}$	0.07	0.91	0.08
	Q_{eq}^{bsc}	0.084	1.507	0.084
BHK – Side compartment	R_{dif}^{bsc}	1.438	0.698	0.344
	$\frac{1}{R_{T,side}^{bsc}}$	0.07	0.73	0.08
	Q_{eq}^{bsc}	0.084	1.507	0.084
	Q_{side}^{bsc}	0.02	0.011	0.24
BHK – Outflow compartment	R_{dif}^{bsc}	1.879	0.912	0.450
	$\frac{1}{R_{T,outflow}^{bsc}}$	0.07	0.63	0.08
	Q_{eq}^{bsc}	0.084	1.507	0.084
	R_{dif}^{bsc}	0.696	0.342	1.452

Source of data and justification

See Section 2.9.6 for the source of the equivalent flow rate data.

See Section 2.2.2 for the BHK geometrical data (Cross section areas of the backfill compartment).

See Section 2.8.2 for information on the diffusion transport resistance in the BHK backfill sub-compartments, R_{dif}^{bsc}.

See Section 2.6.4 for information on the groundwater flow in BHK.

Known limitations in data

The near-field model has a simplified representation of the flow through the BHK waste and backfill compartments. Furthermore, the near-field model assumes the compartments in the concrete backfill can be treated as fully mixed compartments.

Other limitations are described in, Sections 2.2.2, 2.6.4, 2.8.2 and Section 2.9.6.

2.10 Distribution of radionuclide release on host rock trajectories

2.10.1 Source term distribution factors in BHA

Short description of data

The groundwater carrying a released radionuclide from the BHA vault flows into a number of trajectories in the host rock. The total release from the BHA vault is distributed over the host rock trajectories by assigning a source term distribution factor to each such trajectory and multiplying this distribution factor by the total release rate, N_T^A (see Section 2.9.4).

Use in model or evaluation activity

In the near-field model, the distribution factors of trajectories that do not reach the ground surface are assumed to be zero. However, trajectories that start from the BHA vault and reach the ground surface are assigned a distribution factor, DF^{i}_{BHA}, based on the effective diffusion transport resistances at the fracture openings where the trajectories originate. That is:

$$DF^{j}_{BHA} = \frac{\frac{1}{R^{j}_{\boldsymbol{FE}}}}{\sum_{j}\frac{1}{R^{j}_{\boldsymbol{FE}}}} = \frac{\frac{1}{R^{j}_{\boldsymbol{FE}}}}{\frac{1}{R_{TE}}} \qquad (2\text{-}49)$$

Where R^{j}_{FE} is the effective diffusion transport resistance at the fracture opening where trajectory *j* originates (see Section 2.9.2). The sum of the distribution factors of trajectories emanating from a vault is one.

To determine the release rate from each trajectory, the total release rate from the vault is multiplied by the trajectory source term distribution factor. It should be emphasized that in BHA, the distribution factors are mainly controlled by the diffusion transport resistances of solutes in bentonite and that the effective diffusivities of anions, cations and Cs differ (see Section 2.8.1).

Input data used in the near-field model

Given the information provided for the particle trajectories, the effective diffusion transport resistances are calculated in Section 2.9.2. Hence, the source term distribution factors in BHA are calculated via Equation 2-49. They can be found in the SVN database at:

svn://svn.skb.se/SFL/SFLSAK/Arbetsmaterial/RadionuclideTransport/CalculationCases/CC1/Geosphere/sfl_elaborated_r1_hrd_site_nochem_pline_surfaces_2000.xlsx.

Source of data and justification

See Sections 2.9.2 and 2.9.3. It should be emphasized that no activity is allocated to trajectories that do not reach the ground surface. This is a pessimistic approach.

Known limitations in data

See Section 2.9.4.

The advective flow is not considered when distributing the radionuclide release. This is believed to be an acceptable approach because diffusion is assumed to be the dominating transport mechanism in the BHA backfill.

2.10.2 Source term distribution factors in BHK

Short description of data

The groundwater carrying a released radionuclide from the BHK vault flows into a number of trajectories in the host rock. If a trajectory emanates from the near-field and reaches the biosphere, it is allocated part of the activity source term. This is done by assigning a source term distribution factor to each such trajectory and multiplying this factor by the BHK release term (see Section 2.9.7).

Use in model or evaluation activity

In the near-field model, each trajectory that starts from the BHK vault and reaches the ground surface is allocated a specific source term distribution factor, based on the transport properties of the trajectory. However, the source term distribution factor of trajectories that do not reach the ground surface are assumed to be zero.

In the near-field model, the distribution factor for trajectory *j* is expressed as:

$$DF_{BHK}^{j} = \frac{U_j \cdot L_{f,j}}{\sum_j U_j \cdot L_{f,j}} \quad (2\text{-}50)$$

where

U_j = Flow per meter in the intersecting fracture where trajectory *j* originates (see Section 2.9.5).

$L_{f,j}$ = Intersection Length of the fracture and the vault (see Section 2.9.5).

The sum of all source term distribution factors of trajectories emanating from a vault is one. To determine the release rate from each trajectory, the total release rate from the vault is multiplied by the trajectory source term distribution factor.

Input data used in the near-field model

Given the information provided for the particle trajectories in Section 2.9.5, the source term distribution factors in BHK are calculated. They can be found in the SVN database at:

svn://svn.skb.se/SFL/SFLSAK/Arbetsmaterial/RadionuclideTransport/CalculationCases/CC1/Geosphere/sfl_elaborated_r1_hrd_site_nochem_pline_surfaces_2000.xlsx.

Source of data and justification

See Section 2.9.5.

Similar to BHA, no activity is allocated to trajectories that do not reach the ground surface. This is a pessimistic approach.

Known limitations in data

See Section 2.9.5. The distribution factor only considers the advective flow and diffusion is not considered when distributing the radionuclide release. This is believed to be an acceptable approach since advection is assumed to be the dominating transport mechanism.

A stationary flow field is assumed throughout the evaluation time period in the *present-day evaluation case*. Furthermore, although the concrete degradation results in an increased release flow from the near-field, the possible impact of the barrier degradation on the distribution factor is neglected and the distribution factor is assumed to have no temporal variability.

3 Data used in the geosphere model

Modelling of radionuclide transport in the geosphere has been performed in several previous safety assessments (SKB 2010b, 2015b). In SE-SFL, radionuclide transport in the geosphere, i.e. the host rock surrounding the SFL repository near-field, is modelled using the computational tool, FARFCOMP. The geosphere model used in SE-SFL is different from those used in previous safety assessments. It is described in **Radionuclide transport report**, Section 4.4 and Appendix B.

This chapter aims to identify and present the data used in the geosphere model for the base case. The data are also verified against the reference documents. It should be noted that, compared to the base case, some particular features, events, and processes are handled differently in the sensitivity evaluation cases. These cases are discussed in Chapter 4.

3.1 Identification of parameters used in the geosphere model

After escaping from the near-field, the dissolved radionuclides may further migrate in the geosphere, where different mechanisms control their transport behaviour. In a fractured host rock, radionuclides can be carried by underground water through conductive parts of fractures. The water flow rates differ between the fractures and the velocity may also vary across individual fractures. These mechanisms give rise to advection and dispersion in the individual fractures. Moreover, the rock matrix is porous, and the dissolved radionuclides can enter into the stagnant water in pores of the rock matrix by molecular diffusion and be withdrawn from the flowing water. Many radionuclides are also retarded by sorption onto the matrix internal surface and that of the fracture, and thereby are given more time to decay.

In the regional hydrogeology model, groundwater carrying radionuclides flows through discrete fractures (Joyce et al. 2019). The paths of radionuclides are determined by particle tracking, where ten particles are injected in each fracture that intersects the near-field vaults. Each individual particle is then followed tracing out its transport path, i.e. trajectory, which is built up of a series of fracture segments.

In SE-SFL, radionuclide release to the biosphere is evaluated using the geosphere model and its computational code FARFCOMP. The geosphere model and FARFCOMP are described in detail in **Radionuclide transport report**, Appendix B. However, a brief overview of the model is presented here.

Essentially, the geosphere model is established on the dual porosity concept, where the dissolved radionuclides are transported through discrete parallel fractures situated in a porous rock matrix. See Figure 3-1 for an illustration of the conceptual parallel Fracture-Matrix system, where a constant ground-water velocity (v, m a^{-1}), fracture aperture ($2b$, m), and maximum penetration depth ($2d_{max}$, m), i.e. average distance between fractures, is applied.

The transport processes in the system of Figure 3-1 can be described by the following two coupled, one-dimensional equations, one for the fracture and one for the porous matrix. The coupling is provided by the continuity of concentrations along the interface.

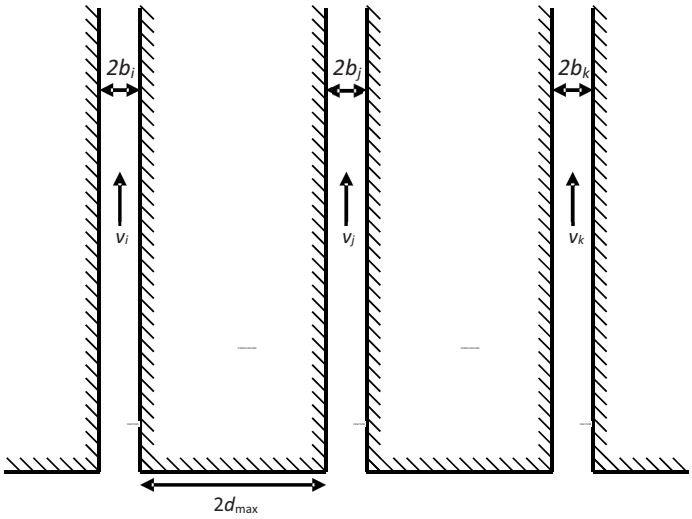

Figure 3-1. *Conceptual parallel Fracture–Matrix system used in the geosphere model, after Tang et al. (1981).*

$$\frac{\partial C_f^n}{\partial t} = -v\frac{\partial C_f^n}{\partial z} + D_L\frac{\partial^2 C_f^n}{\partial z^2} - \lambda^n C_f^n + \sum_{p\in P_n}\lambda^n C_f^p Br_p^n + \frac{D_e^n}{b}\frac{\partial C_m^n}{\partial x}\bigg|_{x=0} \tag{3-1}$$

$$R_m^n\frac{\partial C_m^n}{\partial t} = D_e^n\frac{\partial^2 C_m^n}{\partial x^2} - R_m^n\lambda^n C_m^n + \sum_{p\in P_n} R_m^p\lambda^n C_m^p Br_p^n \tag{3-2}$$

In the above equation:

C_f^n = Concentration of radionuclide n in the flowing water of the fracture [Bq m^{-3}].

C_m^n = Pore water concentration of radionuclide n in rock matrix adjacent to the fracture [Bq m^{-3}].

t = Time [a].

v = Mean water velocity in water bearing fracture [m a^{-1}].

z = Distance in the flow direction [m].

D_L = Longitudinal dispersion coefficient [m^2 a^{-1}].

b = Half-aperture of the fracture [m].

D_e^n = Effective diffusivity of radionuclide n in the rock matrix [m^2 a^{-1}].

x = Distance into the rock matrix [m].

λ^n = Decay rate for radionuclide n [a^{-1}].

P_n = Set of indices of parents of radionuclide n [–].

Br_p^n = Branching ratio from parent radionuclide p to radionuclide n [–].

R_m^n = Capacity factor for radionuclide n in rock matrix [–], defined as:

$$R_m^n = \varepsilon_m + Kd_m^n\rho_m \tag{3-3}$$

with

ε_m = Porosity of the rock matrix [–].

Kd_m^n = Sorption coefficient in rock matrix for radionuclide n [kg m^{-3}].

ρ_m = Bulk density of the rock matrix [kg m^{-3}].

The initial and boundary conditions of the equations are given in **Radionuclide transport report**, Section 4.4.

In the geosphere model, the rock matrix and transport paths, i.e. trajectories, are divided into one-dimensional smaller compartments to approximate the solution to the dual-porosity problem (Norman and Kjellbert 1990). Figure 3-2 shows a schematic view of the Fracture-Matrix system implemented in the geosphere model.

The trajectories are partitioned into fracture compartments of equal length that have constant properties. However, because a higher numerical resolution is required near the interface between the fracture and the rock matrix, due to the high concentration gradient at the interface, the thickness of rock matrix compartments is chosen to increase exponentially from the fracture-matrix interface into the matrix. This is illustrated in Figure 3-3. The level of discretisation along the trajectories, thickness of the first matrix compartment, maximum penetration depth and the level of discretisation in the porous matrix are then input parameters to the geosphere model.

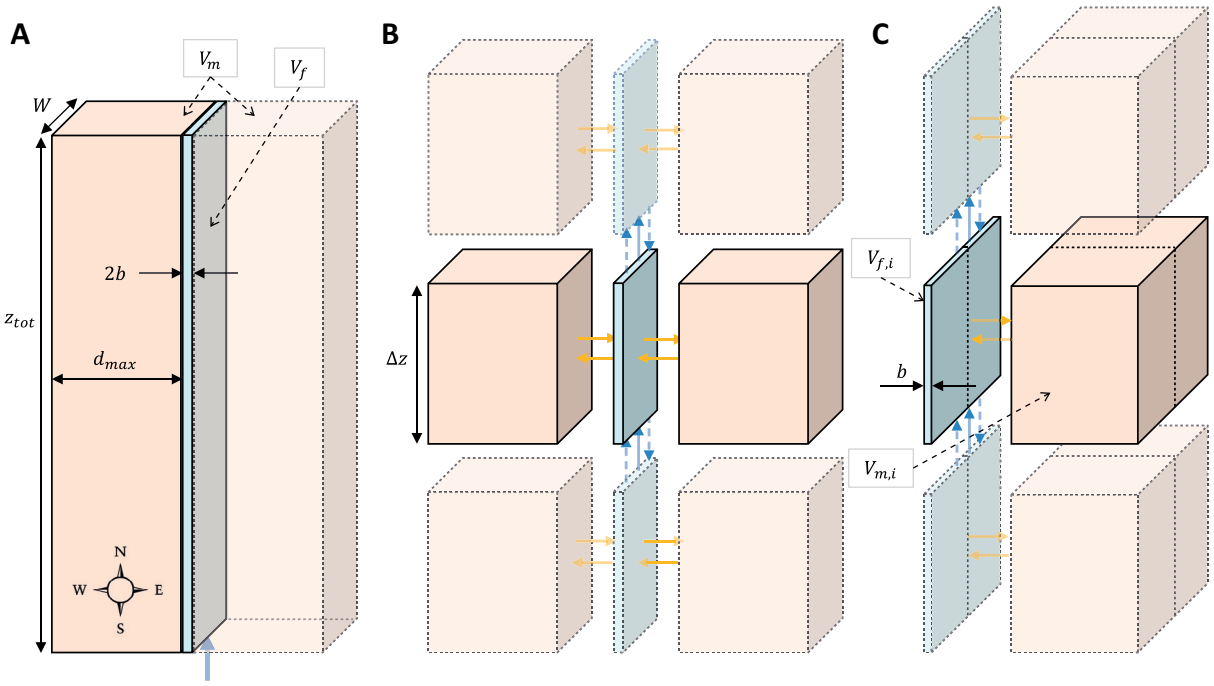

Figure 3-2. *Schematic view of the fracture–matrix system implemented in the geosphere model (A). Discretising the simple volumes in (A) in sections along the fracture (B). Rearranging the volumes so that only one rock matrix volume needs to be considered per discretised fracture volume (C). V_f and V_m are the volumes of the modelled fracture and porous rock matrix, respectively. z_{tot} is the total length of the fracture and Δz is the length of fracture compartment i. Blue arrows represent advective (solid) and dispersive (dashed) transport along the fracture and yellow arrows represent diffusive transport with the rock matrix.*

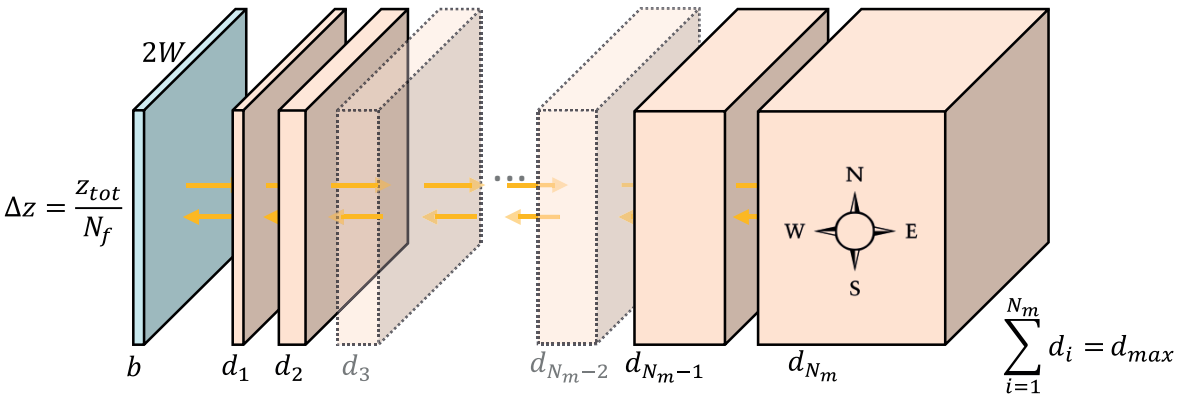

Figure 3-3. *Schematic view of the rock matrix discretisation. d_1 is depth of the first matrix compartment adjacent to the fracture compartment (m) and Nm is number of rock-matrix compartments (–).*

Transport properties of the individual trajectories are taken from the regional hydrogeology model and are directly imported to FARFCOMP. The FARFCOMP then calculates the radionuclide transport rate in each fracture compartment. It should be noted that in the *present-day evaluation case*, the trajectory properties have no temporal variation, due to the stationary flow field in the host rock. The main mechanisms included are:

1. Distribution of the radionuclide release from the near-field over various trajectories at the vault-rock interface.
2. Advective transport of radionuclides along the fracture compartments.
3. Diffusive transport from the fracture compartments into the adjacent rock matrix compartments.
4. Partitioning of radionuclides as mobile or immobile species in the rock matrix compartments, i.e. linear sorption.
5. Radioactive decay and ingrowth.
6. Dispersion in fracture compartments.

Distribution of the radionuclide release from the near-field over the host rock trajectories is done by assigning a source term distribution factor to each trajectory and multiplying this distribution factor by the near-field total release rate (see Section 2.10). In BHK, each trajectory is allocated a weighted part of the BHK source term, which is proportional to the Darcy flux in the trajectory at the vault-rock interface (see Section 2.10.2). In BHA, however, the effective diffusion transport resistances in the bentonite backfill control the source term distribution factor. This is detailed in Section 2.10.1.

Because a stationary flow field is assumed in the *present-day evaluation case*, each trajectory is allocated a temporally constant portion of the source term, though in BHK, the activity source term increases due to the concrete degradation.

In the host rock, retardation of radionuclides occurs as they diffuse into the porous rock matrix surrounding the fracture compartments. In the rock matrix, linear equilibrium sorption is also assumed for radionuclides that sorb onto mineral surfaces (see Section 3.3.5).

Radionuclides can also be stored in micropores in the rock matrix. Fickian diffusion is assumed when modelling the solute exchange between the flowing water in the fracture compartments and the stagnant water in the micropores in the rock matrix. The effective diffusivity and maximum penetration depth in the rock matrix compartments are provided in Sections 3.3.3 and 3.3.4, respectively. In the modelling, each radionuclide is viewed as a unique species, as opposed to being distributed on numerous species having different retention properties. The rock matrix surrounding the trajectories is assumed homogenous. It should also be noted that possible complexation of radionuclides with, e.g. , ISA, impact of colloidal transport, and possible effect of sorption one the fracture surface are neglected in the base case (see Section 3.3.7).

As radionuclides migrate, they decay and produce decay products according to the simplified decay chains (see Section 2.4.2). The fate of the decay products are accounted for in FARFCOMP. In the geosphere model, releases from all trajectories that emanate from a given vault are lumped together at the ground surface. This gives separate activity release curves tied to the BHA and BHK vaults, which are then used as input data in the biosphere model.

3.2 Transport properties in geosphere

3.2.1 Trajectory data

Short description of data

In the hydrogeology model, groundwater carrying radionuclides flows through multitude of trajectories within the host rock. However, only the trajectories that reach the ground surface are of interest for the SFL safety evaluation. In the file delivered by the hydrogeological modelling, the following parameters are provided for each trajectory:

- The flow-related transport resistances, F-factor [a/m].
- The total advective travel time, t_w [a].
- The trajectory start- and end-point coordinates.

Use in model or evaluation activity

FARFCOMP is based on a compartmental conceptualization of the trajectories and rock matrix, where the radionuclide transport and retention take place. The trajectory data are directly imported into FARFCOMP, where the transport equations are solved. In each fracture compartment, the flow wetted area, *aw*, is used as a parameter. In the simplified case of a uniform fracture of width *W,* length *L* and aperture *b*, $a_w = 2WL/(WLb)$, the flow related transport resistance, *F*, is used to calculate flow-wetted surface area, a_w, by dividing it by the travel time, t_w ($a_w = F/t_w$).

It should be noted that only the trajectories that reach the ground surface, i.e. those that have the OK flag = 0 in the hydrogeological modelling, are allocated part of the source term. In other words, no radionuclides are allocated to trajectories that do not reach the ground surface.

Input data used in the geosphere model

The properties of trajectories that reach the ground surface are store in the SVN database at:

svn://svn.skb.se/SFL/SFLSAK/Arbetsmaterial/RadionuclideTransport/CalculationCases/CC1/Geosphere/sfl_elaborated_r1_hrd_site_nochem_pline_surfaces_2000.xlsx.

The file covers 2 424 trajectories in BHA and 2 035 trajectories in BHK.

In the geosphere model, each advective path through fractures in the rock is divided into 20 fracture compartments of equal length. The choice of the level of discretisation is verified through comparison between the model predicted results and results from FARF31 and analytical solutions (**Radionuclide transport report**, Appendix B).

Source of data and justification

The trajectory data are taken from SE-SFL regional scale hydrogeological modelling with ConnectFlow. The data are obtained with regard to the first realization made in Joyce et al. (2019) based upon a snap-shot of the regional scale simulation in 2000 [a]. It should be noted that the effect of chemical reactions in the geosphere is neglected when calculating the groundwater flows. The prerequisite for the hydrogeological modelling and the justification of the results are provided in the reference document.

Known limitations in data

Limitations in the data are described in Joyce et al. (2019). It is worth mentioning that a static flow field is assumed, attempting to capture the actual flow field at the Laxemar site in the year 2000, whereas the true flow field will evolve over the safety evaluation timeframe.

3.2.2 Dispersion (Peclet number)

Short description of data

Hydrodynamic dispersion in geosphere can rise from molecular random movements, i.e. molecular diffusion as well as non-uniformities in the water velocity within the pore-structure of the host rock, i.e. mechanical dispersion. Hydrodynamic dispersion is often characterized by a dispersion coefficient, similar to a Fickian-diffusion process. The importance of the hydrodynamic dispersion for solute transport in crystalline rock is discussed in detail in SKB (2010d).

Use in model or evaluation activity

FARFCOMP uses a constant Peclet number to describe hydrodynamic dispersion in the fracture compartments. This means that the dispersion coefficient increases with the length of the fracture compartments. This agrees with what is often observed in field experiments. Furthermore, no temporal variability of the Peclet number is accounted for.

Input data used in the geosphere model

The Peclet number used in the base case is given in Table 3-1. The Peclet number is also stored in the SVN database at:

svn://svn.skb.se/SFL/SFLSAK/Arbetsmaterial/RadionuclideTransport/CalculationCases/CC1/Geosphere/MatlabSpecific.xlsx.

Table 3-1. Peclet number used in the geosphere model.

Parameter	Value [–]	Model	Reference
Peclet number	10	FARFCOMP	(SKB 2010a, Table 6-85)

Source of data and justification

The constant Peclet number, Pe = 10, is a typical value found in field tracer tests in fractured rocks (Gelhar et al. 1992). Furthermore, Pe = 10 is applied in the previous safety assessment studied for both the Forsmark and Laxemar sites (SKB 2010a, Table 6-85, SKB 2010c, Table A7-6).

Known limitations in data

There are some practical uncertainties affecting the Peclet values obtained from tracer experiments. There are also some conceptual uncertainties in how to interpret the hydrodynamic dispersion data obtained for a discrete fracture network in the host rock. Furthermore, dispersion data that are derived from in-situ experiments often fail to correctly describe spread in radionuclide breakthrough curves at larger scales. This is mainly because radionuclides often experience different spatial heterogeneities at large scales, e.g. variable aperture (Moreno et al. 1990) that cannot be captured in in-situ experiments.

The conceptual understanding of hydrodynamic dispersion and associated uncertainties are discussed in SKB (2010d, Sections 5.2 and 6.1).

3.2.3 Groundwater flow scaling factors

Short description of data

The hydrogeological modelling in SE-SFL is performed assuming a stationary flow field. Therefore, groundwater flow scaling factors are introduced in the geosphere model to reflect the changes in the flow field during a glacial cycle. This is further described in Section 4.2.2 (SKB 2010b, Section 2.1.2).

Use in model or evaluation activity

In the *present-day evaluation case*, it is assumed that the flow field does not vary during the safety evaluation time period. Therefore, the scaling factor does not deviate from 1.

Input data used in the geosphere model

In the *present-day evaluation case*, the scaling factor equals 1.

Table 3-2 Groundwater flow scaling factor used in the present-day evaluation case.

Parameter	Value [–]	Evaluation period
Groundwater flow scaling factor	1	2075 years to end of evaluation.

Source of data and justification

Assuming a stationary flow field is a modelling decision.

Known limitations in data

As a response to shoreline displacement and climate changes, the flow field will change over time. This case is explored in the sensitivity evaluation case in Section 4.2.2.

3.3 Retention properties in geosphere

3.3.1 Radionuclide speciation in geosphere

Short description of data

Depending on their speciation, the dissolved radionuclides will attain different retention properties in the geosphere, i.e. effective diffusivity, sorption coefficient, and sorption reduction factor (see Sections 3.3.3, 3.3.5 and 3.3.7).

The charge of species, i.e. whether the species are anionic, cationic, or Neutral, will also impact their effective diffusivities. Furthermore, the charge and redox state of the species will impact their sorption coefficient.

Use in model or evaluation activity

In the FARFCOMP, an individual radionuclide is not distributed over different species having different retardation properties. Instead, each radionuclide is assigned unique retardation properties that do not change over time and space. The only exception is C-14, which is grouped into three separate pseudo-variants, namely, organic carbon, inorganic carbon, and induced carbon. It is assumed that these separate types do not chemically interact with each other, That is, organic C-14 does not react to become inorganic C-14, and vice versa. All C-14 released from BHA is assumed to be organic while all C-14 released from BHK is assumed to be inorganic or induced.

Input data used in the geosphere model

Table 3-3 gives the assumed redox state of radionuclides in the geosphere model, which will impact their sorption coefficient. The table also gives the dominant species and the assumed charge category.

Source of data and justification

For most of the radionuclides, the speciation data are adopted from the SR-Site geosphere radionuclide transport report (SKB 2010b, Table 2-3). These data correspond to an anoxic groundwater at repository depth (~500 m) at Forsmark, with the salinity of 5 190 mg/l, bicarbonate concentration of 22 mg/l and the pH of 8. The speciation based on this groundwater is believed to be adequate also for the Laxemar site in SE-SFL. In the geosphere model, Uranium is assumed to be in the U(IV) state. Regarding H(I), the proton is pessimistically assumed to be part of anionic species, although it is likely that the majority of hydrogen is part of H_2O.

Table 3-3. Chemical states of radionuclides in the geosphere model.

Elements	Oxidation state	Assumed charge	Dominant or important species	References
Ac	Ac(III)	Cation	$AcCO_3^+$	(SKB 2010b)*
Ag	Ag(I)	Anion	$AgCl_2^-$, $AgCl_4^{3-}$, $AgCl_3^{2-}$	(SKB 2010b)
Am	Am(III)	Cation	$AmCO_3^+$	(SKB 2010b)
Ba	Ba(II)	Cation	Ba^{2+}	(Crawford 2013)**, (Widestrand et al. 2010)***
Be	Be(II)	Cation	Be^{2+}	Group 2 in periodic table.
Ca	Ca(II)	Cation	Ca^{2+}	(Crawford 2013)
				Group 2 in periodic table.
Cd	Cd(II)	Cation	$CdCl^+$, Cd^{2+}, $CdCl_2$	(SKB 2010b)
C-inorg	C(IV)	Anion	HCO_3^-	(SKB 2010b)
C-ind	C(IV)	Anion	–	Pessimistic assumption.
C-org	C(-IV)	Neutral	CH_4, CO_2H (organic acid)	(SKB 2010b)
Cl	Cl(-I)	Anion	Cl^-	(SKB 2010b)
Cm	Cm(III)	Cation	$CmCO_3^+$	(SKB 2010b)
Co	Co(II)	Anion	$HCoO_2^-$	(Widestrand et al. 2010)
Cs	Cs(I)	Cation	Cs^+	(SKB 2010b)
Eu	Eu(III)	Cation	$EuCO_3^+$	(SKB 2010b)
Gd	Gd(III)	Cation	$GdCO_3^+$, Gd^{3+}, GdF^{2+}	(Widestrand et al. 2010)
H	H(I)	Anion	H_2O	Pessimistic assumption.
Ho	Ho(III)	Cation	$HoCO_3^+$	(SKB 2010b)
I	I(-I)	Anion	I^-	(SKB 2010b)
K	K(I)	Cation	K^+	Group 1 in periodic table.
La	–	Anion	–	Pessimistic assumption.
Mo	Mo(VI)	Anion	MoO_4^{2-}	(SKB 2010b)
Nb	Nb(V)	Anion	NbO_3^-, $Nb(OH)_5$	(SKB 2010b)
Ni	Ni(II)	Cation	Ni^{2+}, $NiCl^+$	(SKB 2010b)
Np	Np(IV)	Neutral	$Np(OH)_4$	(SKB 2010b)
Pa	Pa(V)	Neutral	$PaO_2(OH)$	(SKB 2010b)
Pb	Pb(II)	Cation	$PbCO_3$, $PbCl^+$, $PbOH^+$, Pb^{2+}	(SKB 2010b)
Pd	Pd(II)	Neutral	$Pd(OH)_2$	(SKB 2010b)
Po	Po(IV)	Anion	PoO_3^{2-}	(Crawford 2013, Table 6−2)
Pu	Pu(III)	Cation	$PuOH^{2+}$, Pu^{3+}	(SKB 2010b)
Ra	Ra(II)	Cation	Ra^{2+}	(SKB 2010b)
Re	–	Anion		Pessimistic assumption.
Se	Se(-II)	Anion	HSe^-	(SKB 2010b)
Si		Anion		Pessimistic assumption.
Sm	Sm(III)	Cation	$SmCO_3^+$	(SKB 2010b)
Sr	Sr(II)	Cation	Sr^{2+}	(SKB 2010b)
Tb		Anion		Pessimistic assumption.
Tc	Tc(IV)	Anion	$TcO(OH)_2$, TcO_4^-	(SKB 2010b)
Th	Th(IV)	Anion	$Th(OH)_3CO_3^-$	(SKB 2010b)
Ti		Anion		Pessimistic assumption.
U	U(IV)	Neutral	$U(OH)_4$	(SKB 2010b)
Zr	Zr(IV)	Anion	$Zr(OH)_5^-$	(SKB 2010b)

* Tables 2-3 and 2-4.

** Table 6-1.

*** Table 3-3.

It should also be noted that a few radionuclides, i.e. Ba, Ca, Co, and Po were not included in SR-Site, but were in SR-PSU. Although the redox state of these elements are provided in Crawford (2013, Table 6-1), the dominating species are not given. The only exception is Po(IV) (Crawford 2013, Table 6-2). The speciation data used for Ba and Co correspond to the groundwater composition at the Äspö Hard Rock Laboratory (Widestrand et al. 2010). Regarding Ca, it is assumed that Ca is divalent cationic in analogy to other elements in Group 2 of the periodic table of elements.

The following radionuclides were not included neither in SR-Site or SR-PSU. However, in the geosphere model:

- K is assumed to be monovalent cationic in analogy to other elements in Group 1 of the periodic table.
- Be is assumed to be divalent cationic, in analogy to other elements in Group 2 of the periodic table.
- Gd is assumed to be cationic based on the speciation data provided in Widestrand et al. (2010).

Furthermore, no speciation considerations have been made for La, Re, Si, Tb, and Ti. Therefore, ignoring their actual speciation, they are pessimistically assumed to be anionic and non-sorbing (Section 3.3.5).

Known limitations in data

This is a known limitation that each radionuclide is assigned a single set of retardation parameters in the models. Therefore, this approach may not represent the radionuclides' complex speciation distribution. Furthermore, the adopted speciation data correspond to groundwater types that may not exactly represent those encountered in the Laxemar site. This is particularly true for pH that changes by the cementitious material in the repository.

It should also be noted that speciation calculations are often difficult to perform and may not always include the functional groups of the mineral surfaces that surround the fractures or rock matrix pore water. Therefore, discrepancies have often been observed in speciation calculations in the aqueous phase and in the rock matrix (Widestrand et al. 2010, Nilsson et al. 2010). Furthermore, some inconsistencies have been observed in the assumed charge of some nuclides in relation to anion exclusion. In these situations, the data are pessimistically chosen so that the geosphere model results in a higher release**.** This is exemplified below by the choice of retention properties for Co and Tc.

In Widestrand et al. (2010), it has been suggested that there are anionic cobalt species in relevant aqueous solutions. However, in Nilsson et al. (2010), it has been shown experimentally that when the aqueous solution comes in contact with rock, Co will sorb in cationic form. Therefore, Co is considered as anionic in terms of its effective diffusivity. However, it is assumed to behave like a cation when it sorbs, analogous to Ni(II) (Crawford 2013).

Regarding Tc, it is indicated in SKB (2010c, Table A8-4) that $TcO(OH)_2$ and not TcO_4^- dominates the speciation. This is considered when choosing the K_d-value in Section 3.3.5, for Tc(IV). Yet, in Table 3-3, Tc is assumed to be anionic, and this assumption is incorporated in the adopted effective diffusivity.

3.3.2 Rock matrix porosity

Short description of data

The data concern the porosity of the rock matrix used in the geosphere model. A single value is suggested for the porosity, which is used for all locations within the bedrock.

Use in model or evaluation activity

The rock matrix porosity is used in FARFCOMP to account for the storage capacity of the rock matrix for dissolved radionuclides. In the geosphere model, the rock matrices along all the flow paths are represented by compartments with a constant porosity. Thus, the porosity is assumed to have no temporal or spatial variability. Moreover, the possible effect of anion exclusion is assumed to be insignificant in the rock matrix. Therefore, the given porosity is used regardless of radionuclide speciation.

Input data used in the geosphere model

Table 3-4 provides the porosity value used in FARFCOMP in the base case. They can also be found in SVN database at:

svn://svn.skb.se/SFL/SFLSAK/Arbetsmaterial/RadionuclideTransport/CalculationCases/CC1/Geosphere/CC1_Physical%20and%20chemical%20data.xlsx. (Worksheet = Diffusivities and porosities)

Table 3-4 Rock matrix porosity used in the geosphere model in the Base case.

Parameter	Value [%]	Reference
Rock matrix porosity, cations and Neutral species	0.19	(SKB 2010c, Table A8-5)
Rock matrix porosity, anions	0.19	(SKB 2010c, Table A8-5)

Source of data and justification

The porosity data are taken from SR-Site (SKB 2010c, Table A8-5) and are site specific. The data are assumed to be valid for the host rock at large depth as well as for shallower rock. The data are justified in SKB (2010c, Section A8).

Known limitations in data

Using a single-value is a pessimistic approach because undisturbed rock matrices have generally a lower porosity than rock matrices adjacent to fractures, which may be chemically altered, thus, featuring a higher degree of micro-fracturing. It should also be noted that the additional pore space of fractures, whether hydraulically conductive or non-conductive, is not included in this porosity. Furthermore, the effect of anion exclusion is not accounted for. However, this can be seen as an evaluation choice rather than a limitation because the anion exclusion effect is observed to be small at the site.

3.3.3 Rock matrix diffusivity

Short description of data

The data concern the radionuclide effective diffusivities in the host rock. Different diffusivities are used for anions as well as Neutral solutes and cations. The suggested data are used for all locations within the Laxemar host rock.

Use in model or evaluation activity

The effective diffusivity is used in FARFCOMP to account for transport of dissolved radionuclides in the stagnant pore spaces of the rock matrix.

In the geosphere model, the rock matrix is represented by compartments with a constant effective diffusivity along all the flow paths within the host rock. Thus, the effective diffusivity is assumed to have no temporal or spatial variability. The effect of anion exclusion is accounted for by assigning different effective diffusivities for anions as well as Neutral nuclides and cations.

Input data used in the geosphere model

Table 3-5 provides the effective diffusivity used in FARFCOMP in the base case. They can also be found in SVN database at:

svn://svn.skb.se/SFL/SFLSAK/Arbetsmaterial/RadionuclideTransport/CalculationCases/CC1/Geosphere/CC1_Physical%20and%20chemical%20data.xlsx. (Worksheet = Diffusivities and porosities)

Table 3-5 Rock matrix effective diffusivity used in the geosphere model in the Base case.

Speciation category	Value [m^2/s]	Reference
Cations and Neutral species	2.7E-14	(SKB 2010c, Table A8-6)
Anions	8.5E-15	(SKB 2010c, Table A8-6)

Source of data and justification

The effective diffusivities are taken from SR-Site (SKB 2010c, Table A8-6) and are site specific. They are valid for the host rock at large depth. The data are justified in SKB (2010c, Section A8).

Known limitations in data

The reader may refer to the reference document (SKB 2010c) for discussions on the uncertainties in the data. The proposed data are based on measurements in non-fractured and undisturbed rock matrix at the Laxemar site. Therefore, this is a pessimistic approach because undisturbed rocks generally have lower effective diffusivities than rock matrices adjacent to fractures, which may be chemically altered, thus, featuring a higher degree of micro-fracturing. Furthermore, the additional capacity for diffusion in fractures, whether hydraulically conductive or non-conductive, is not included in this effective diffusivity.

3.3.4 Maximum penetration depth

Short description of data

The data concern the maximum penetration depth, and level of discretisation in the rock matrix. The microporous network in the rock matrix is assumed to be connected at large scales (SKB 2010a, Section 6.8, SKB 2010c, Section A8).

The maximum penetration depth is represented by the average half spacing between conductive fractures within the Laxemar bedrock. A single-value is suggested for all flow paths in the entire bedrock. It should be noted that, increasing the parameter to large values (beyond a few decimetres) will have marginal effect on the model predicted results (Crawford and Löfgren 2019).

Use in model or evaluation activity

In the geosphere model, the rock matrices along the flow paths are represented by compartments to which solutes can diffuse. Due to the necessity of a higher numerical resolution at the interface between the fracture and the rock matrix, due to the high concentration gradient, the thickness of matrix compartments is set to increase exponentially from the fracture-matrix interface away into the matrix so that the sum of the compartment thicknesses equals the maximum penetration depth. In the geosphere model, the depth of the first rock matrix compartment is assumed to be 0.1 mm. Furthermore, the maximum penetration depth is assumed to have no temporal or spatial variability and is used for all dissolved radionuclides and for all trajectories.

Input data used in the geosphere model

Table 3-6 provides the maximum penetration depth and rock matrix discretisation data used in FARFCOMP in the base case. They can also be found in SVN database at:

svn://svn.skb.se/SFL/SFLSAK/Arbetsmaterial/RadionuclideTransport/CalculationCases/CC1/Geosphere/CC1_Physical%20and%20chemical%20data.xlsx. (Worksheet = Rocktypes misc. parameters)

svn://svn.skb.se/SFL/SFLSAK/Arbetsmaterial/RadionuclideTransport/CalculationCases/CC1/Geosphere/MatlabSpecific.xlsx.

Table 3-6 Maximum penetration depth used in the geosphere model in the Base case.

Parameter	Value [m]	Reference
maximum penetration depth	4.5	(SKB 2010c, Section A7-9)
Number of matrix compartments	20	
Thickness of the first rock matrix compartment	0.0001	

Source of data and justification

The maximum penetration depth is taken from SR-Site (SKB 2010c, Sections A8 and A7-9) and is site specific. It is assumed to be valid for the host rock at large depth as well as for shallower rock. The data are justified in SKB (2010c, Sections A7 and A8).

The choices of thickness of the first matrix compartment and number of compartments have been conducted by comparison of the solution of the compartmental model with solutions of the semi-analytical code FARF31.

Known limitations in data

The maximum penetration depth is derived from the average half spacing between conductive fractures at the Laxemar site. This fracture spacing is generally larger at large depth and smaller in shallow rock. Therefore, the value may overestimate the thickness of rock matrix to which solutes can diffuse in shallow rock. However, the maximum penetration depth only becomes a significant modelling parameter at small values, i.e. smaller than the typical fracture spacing in shallow rock. Therefore, this is not seen as a significant limitation. Moreover, the underlying assumption of the large-scale connectivity of the microporous network is supported in SKB (2010d, Section 5.3).

3.3.5 Rock matrix sorption coefficients

Short description of data

The data concern linear sorption coefficients of the modelled radionuclides in the rock matrix. The data are obtained from laboratory measurement and in-situ tracer tests. When no data is available for a radionuclide, the K_d is derived using sorption data for an analogue element. Otherwise, the radionuclide is assumed to be non-sorbing.

The data, generally, represent the undisturbed rock matrix and are used for all locations within the host rock. Therefore, the additional sorption capacity of fracture coatings, fault gauge, etc. is neglected.

For elements sorbing by cation exchange, considerations have been made concerning the Laxemar groundwater composition. Generally, the general groundwater composition, i.e. redox conditions and pH, is considered when deciding on the element speciation in Section 3.3.1.

Use in model or evaluation activity

The sorption coefficient is used in FARFCOMP to account for the storage of sorbing radionuclides in the rock matrix.

In the geosphere model, the rock matrices along all the flow paths are represented by compartments with constant sorption coefficient. Thus, the sorption coefficient is assumed to have no temporal or spatial variability.

Input data used in the geosphere model

Table 3-7 provides the sorption coefficient data used in FARFCOMP in the base case. They can also be found in SVN database at:

svn://svn.skb.se/SFL/SFLSAK/Arbetsmaterial/RadionuclideTransport/CalculationCases/CC1/Geosphere/CC1_Physical%20and%20chemical%20data.xlsx. (Worksheet = Sorption Coefficients)

Table 3-7. Sorption coefficient used in the geosphere model in the Base case.

Element	K_d [m^3/kg]	Reference
Ac	1.48E-02	(SKB 2010c)*
Ag	6.54E-04	(SKB 2010c)
Am	1.48E-02	(SKB 2010c)
Ba	1.0E-03	(Crawford 2013)**
Be	0	Pessimistic assumption.
Ca	0	(Crawford 2013)
Cd	2.07E-03	(SKB 2010c)
C-inorg/ C-ind	0	(SKB 2010c), HCO_3^-.
C-org	0	(SKB 2010c), CH_4, $-CO_2H$.
Cl	0	(SKB 2010c)
Cm	1.48E-02	(SKB 2010c)
Co	7.40E-04	(Crawford 2013)
Cs	6.54E-04	(SKB 2010c)
Eu	1.48E-02	(SKB 2010c)
Gd	0	Pessimistic assumption.
H	0	(SKB 2010c)
Ho	1.48E-02	(SKB 2010c)
I	0	(SKB 2010c)
K	0	Pessimistic assumption.
La	0	Pessimistic assumption.
Mo	0	(SKB 2010c)
Nb	1.98E-02	(SKB 2010c)
Ni	2.07E-03	(SKB 2010c)
Np	9.92E-02	(SKB 2010c), Np(IV).
Pa	5.92E-02	(SKB 2010c), Pa(V).
Pb	2.52E-02	(SKB 2010c)
Pd	5.20E-02	(SKB 2010c)
Po	2.52E-02	(Crawford 2013), Po(-II, II, VI).
Pu	2.78E-02	(SKB 2010c), PU(III).
Ra	4.53E-04	(SKB 2010c)
Re	0	Pessimistic assumption.
Se	2.95E-04	(SKB 2010c), Se(-II).
Si	0	Pessimistic assumption.
Sm	1.48E-02	(SKB 2010c)
Sr	6.42E-06	(SKB 2010c)
Tb	0	Pessimistic assumption.
Tc	9.92E-02	(SKB 2010c), Tc(IV)
Th	5.29E-02	(SKB 2010c)
Ti	0	Pessimistic assumption.
U	9.92E-02	(Crawford 2010), U(IV).
Zr	2.13E-02	(SKB 2010c)

* Table A8-4, Best estimate.

** Tables 6-1 and 6-2, Best estimate.

Source of data and justification

The data are mostly taken from SR-Site (SKB 2010c, Table A8-4). For nuclides that were not included in SR-Site, the data are taken from the safety assessment SR-PSU (Crawford 2013). Moreover, when no reliable data is found for a radionuclide, it is pessimistically assumed to be non-sorbing.

The K_d-values are reasonably valid for the host rock at large depth as well as for shallower rock. When a reference data indicate that a K_d-value varies along a flow path (with depth in the host rock or with distance from the engineered barrier), the lowest reported K_d-value is pessimistically assumed along the entire flow path. The data are further justified in Crawford (2010, 2013) and SKB (2010c, Section A8).

Known limitations in data

The uncertainty in K_d-values is known to be significant for many of the radionuclides (Crawford 2010, 2013). Therefore, the general approach is to assign a rather pessimistic data. In some cases, the radionuclides are assumed to be non-sorbing, even though general understanding would dispute this. This can be exemplified by Gd, which has been experimentally observed to sorb quite strongly to the rock matrix in in-situ tracer tests (Nilsson et al. 2010). In Crawford (2013) and SKB (2010c, Section A8) the data are sometimes accompanied by large uncertainty ranges. A significant part of these ranges is due to limitations in empirical data or knowledge. The ranges are only partly due to spatial and temporal variability that may be handled by flow path averaging. The use of best estimate single values in the base case is, therefore, a limitation.

3.3.6 Rock matrix density

Short description of data

The data concern the density of the rock matrix in the geosphere model. A single-value is suggested for the density, which is used for all locations within the Laxemar bedrock.

Use in model or evaluation activity

The density of the dry rock matrix is used in FARFCOMP to account for the storage capacity of the rock matrix for dissolved radionuclides. A single value is suggested for the rock matrix density that does not vary by time and space.

Input data used in the geosphere model

Table 3-8 provides the rock matrix density used in the geosphere model in the base case. It can also be found in SVN database at:

svn://svn.skb.se/SFL/SFLSAK/Arbetsmaterial/RadionuclideTransport/CalculationCases/CC1/Geosphere/CC1_Physical%20and%20chemical%20data.xlsx. (Worksheet = Rocktypes misc. parameters)

Table 3-8 Rock matrix density used in the geosphere model in the Base case.

Parameter	Value [kg/m^3]	Reference
Rock matrix density	2700	(SKB 2010c, Table A4-11)

Source of data and justification

The density data are taken from SKB (2010c, Table A4-11) and are site specific. The justification is also given in the reference document.

Known limitations in data

There are no known limitations in the data point that would significantly impact the safety evaluation.

3.3.7 Sorption reduction factors, surface sorption and colloids in geosphere

Short description of data

Sorption reduction factors: Complexing agents in the groundwater, such as Isosaccharinic Acid (ISA), may form complexes with radionuclides. These complexes can be dissolved in the groundwater and diffuse into the pores of the rock matrix. The complexation can, therefore, reduce the tendency of radionuclides to sorb to the mineral surfaces in the rock. In the geosphere model, this process is formulated by introducing the sorption reduction factor (see Section 2.5.6).

Colloid sorption: A radionuclide may also sorb on colloids that are too large to enter the micropores of the rock matrix. Therefore, when the radionuclide is sorbed on the colloid, it cannot further diffuse into the rock matrix and sorb on its mineral surfaces (SKB 2010d, Sections 5.9 and 6.1). This phenomenon is not included in SE-SFL It should, however, be noted that if sorption on colloids is accounted for, the value of colloidal mass density r [kg/m^3] is required as input parameter.

Surface sorption coefficient: Dissolved species in the flowing fracture water may also sorb on the fracture surface. However, this process is neglected in SE-SFL, and the surface sorption coefficient is set to zero.

Use in model or evaluation activity

In the geosphere model, sorption reduction factors are incorporated in the FARFCOMP by reducing the radionuclide K_d-values. However, the effect of complexing agents in the geosphere is not modelled in the base case. Furthermore, surface sorption is assumed to be negligible in geosphere, compared to the matrix diffusion and subsequent sorption in the rock matrix.

Input data used in the geosphere model

Table 3-9 provides the data used in the geosphere model that impact the sorption coefficient in the host rock in the base case.

Table 3-9 Parameters impacting the sorption coefficients in the host rock in the Base case.

Parameter	Data	Radionuclides	Parts of flow path
Sorption reduction factor [–]	1	All	All
Colloid sorption coefficient [m^3/kg]	0	All	All
Colloidal mass density [kg/m^3]	0	All	All
Surface sorption coefficient [m^{-1}]	0	All	All

Source of data and justification

The decisions to neglect the colloidal sorption and the sorption reduction factors in the base case are made in the **Radionuclide transport report**, Section 4.4. In addition, in SKB (2010d, Section 5.9), it is argued that the colloidal mass density is insignificant.

Known limitations in data

The data in Table 3-9 suggest that the concerned processes are not accounted for in the base case. This is due to the decisions made when setting up the base case. As such, possible limitations rather reflect on the decisions than on the actual data. The background discussion can be found in the geosphere process report for SR-Site (SKB 2010d, Section 6.1), and in the **Radionuclide transport report**.

4 Sensitivity evaluation cases

This chapter describes input data used in the sensitivity evaluation cases selected in order to provide further input to the site selection process and development of the repository design for SFL. The sensitivity evaluation cases inherit a great majority of prerequisites and input data from the *present-day evaluation case*, while a limited set of data is modified. Only input data that differs from the *present-day evaluation case* are described.

4.1 Sensitivity of the safety evaluation to conditions in the repository

This section presents the input data used in the evaluation cases that are carried out to assess the sensitivity of the safety evaluation to different properties and conditions in the repository.

The sub-categories within this chapter explain how the near-field and geosphere models applied in each sensitivity evaluation case differ from the approach in the *present-day evaluation case.* When an aspect of the model is not discussed for a given analysis, the approach, parameters and assumptions are the same as in the *present-day evaluation case*.

4.1.1 No effect of complexing agents in BHA

Short description of data

As discussed in Section 2.5.6, dissolved and mobile complexing agents can react with radionuclides and, thus, cause them to have a lesser tendency to sorb to immobile minerals of the cement and bentonite in the BHA backfill. The data that concern the sorption reduction factors in the base case are given in Section 2.5.6. The evaluation case presented here, however, studies a scenario in which no complexing agents are assumed to be present in the BHA vault and, therefore, no reduction in the radionuclide K_d-values is assumed.

Use in model or evaluation activity

In the absence of complexing agents, the sorption reduction factors for all the radionuclides are set to 1 in this evaluation case. Please see Section 2.5.6.

Input data used in evaluation case

In this evaluation case, the sorption reduction factors for all the radionuclides are set to 1.

Source of data and justification

Please see the **Radionuclide transport report**, Section 6.2.

Known limitations in data

The amount of complexing agent, especially cellulose that is a precursor to ISA, is not well-known in the BHA waste (**Initial state report**, Section 3.7.1). It should be noted that the amount of complexing agents allowed for disposal will be regulated by the means of waste acceptance criteria (WAC).

4.1.2 Lower steel corrosion rate in BHK

Short description of data

The near-field model assumes that the metallic components corrode at a constant rate during the time of interest for SE-SFL. In the base case, the corrosion rate is set to 10 nm/a, which is representative

of Stainless-steel under anoxic alkaline conditions. In the evaluation case presented here, an alternative scenario is studied where the metal corrosion rate is scaled down. The aim is to illustrate the effect of uncertainty in the metal corrosion rate on the radionuclide release.

Use in model or evaluation activity

Similar to the base case, the metallic components in BHK are assumed to corrode at a constant rate throughout the evaluation time period. In the other words, the corrosion rate of a metallic component remains constant until the component is completely corroded. Thereafter, no corrosion will occur and, therefore, no induced activity will be released (see Section 2.5.4). In the evaluation case presented here, an alternative lower corrosion rate is considered instead.

Input data used in evaluation case

Information that concerns the release of induced activity from metallic components are given in Sections 2.5.3 and 2.5.4. Table 4-1 provides the corrosion rate used in the near-field model in this sensitivity evaluation case. The corrosion rate is assumed to be constant throughout the assessment period until the component has corroded completely and all the induced activity has been released.

Table 4-1. Alternative corrosion rate of metallic components in BHK.

Parameter	Value [nm/a]
Corrosion rate	1

Source of data and justification

The experimental data for long-term corrosion rates generally falls in the range 1–100 [nm/a] (Diomidis 2014, Swanton et al. 2015). The qualified corrosion rate data together with their distribution functions are provided in SKB (2014a). The applied corrosion rate is selected from the proposed range to represent a slower corrosion release from the metallic components, compared to the base case.

Known limitations in data

The reader may refer to the reference documents (Diomidis 2014, Swanton et al. 2015) for discussions on the uncertainties in the corrosion rate data.

4.1.3 Alternative concrete backfill in BHK

Short description of data

Radionuclide transport in the BHK concrete backfill is controlled by diffusion and advection. However, due to the gradual degradation of concrete, the flow rate increases over time and advection becomes the dominant transport mechanism (Wessely and Shahkarami 2019). The *alternative concrete backfill in BHK evaluation case* studies a scenario in which the BHK concrete backfill in the base case is replaced by a new concrete backfill, which exhibits enhanced resistance against groundwater flow (Idiart et al. 2019b). The purpose of this study is, therefore, to assess the impacts of lower groundwater flow rates in the BHK waste and backfill compartments on the radionuclide releases and the subsequent delivered dose.

Use in model or evaluation activity

In the near-field model, the sum of the advective release (via groundwater flow) and diffusive release (via the equivalent flow rate) constitutes the release term form the BHK vault. In this evaluation case, the groundwater flow scaling factor G is introduced to incorporate the flow changes in BHK waste and backfill. The groundwater flow rate is downscaled by the scale factor G. However, since

the radionuclide transport in BHK is advection controlled, the effect of changes in the diffusive release is neglected, thus the equivalent flow rates are not altered.

Input data used in evaluation case

The groundwater flow rates in the BHK vault are given in Section 2.6.4, for the base case. The groundwater flow rates considered in the *alternative concrete backfill in BHK evaluation case* are 10 times lower than those in the base case. Furthermore, the concrete porosity and effective diffusivity is scaled by a factor of 0.5 provided that the concrete is intact or partly degraded. Nevertheless, when the concrete is completely degraded, the water flow porosity and effective diffusivity are assumed to be the similar to those in the base case.

Table 4-2 provides the scaling factor used in the near-field model in the *alternative concrete backfill in BHK evaluation case*. See also the **Radionuclide transport report**, Section 6.4.

Table 4-2. Scaling factor used in the near-field model in the "Alternative concrete backfill in BHK" evaluation case.

Parameter	Value [–]
Scaling Factor (G)	10

It should be noted that in the near-field model, the inverses of the scaling factor (G) is used.

Source of data and justification

See Section 2.6.4.

Known limitations in data

The choice of the groundwater flow scaling factor is arbitrary.

4.1.4 Placement of ESS-specific radionuclides

Short description of data

The evaluation case presented in this section studies a scenario in which the radionuclide inventory of the ESS-specific radionuclides in BHA and BHK are set to 1 Bq. The goal is to study the proposed repository concept considering the impacts of the ESS-specific radionuclides on the radionuclide release. All the radionuclides included in the base case are also included in the calculations with a unit initial activity inventory of 1 Bq. However, the induced activity of the metal parts is neglected in the BHK waste. It should be emphasized that the ESS-specific radionuclides are not included in the base case.

Use in model or evaluation activity

See Sections 2.3.1 and 2.3.2.

Input data used in evaluation case

The radionuclide inventories in BHA and BHK, except for the induced activity in metals, are set to 1 Bq. These include the ESS-specific radionuclides.

Information of the radionuclides originating from the ESS inventory is given in Section 2.4.1.

In this evaluation case, the radionuclide inventories in both BHA and BHK are modelled as being instantly released from the waste matrix after the repository closure in the year 2075.

Five variants of this evaluation case are studied for SE-SFL, as follows:

- **Variant A:** The effective diffusivity and porosity data are similar to those in the base case.
- **Variant B:** All the ESS-specific radionuclides are viewed as anions, while the K_d values are similar to those used in the base case.
- **Variant C:** All the ESS-specific radionuclides are viewed as cations, while the K_d values are similar to those used in the base case.
- **Variant D:** All the ESS-specific radionuclides are viewed as anions and sorption reduction factor = 1.
- **Variant E:** All the ESS-specific radionuclides are viewed as cations and sorption reduction factor = 1.

Source of data and justification

See Sections 2.3.1 and 2.3.2.

Known limitations in data

See Sections 2.3.1 and 2.3.2.

The amounts of radionuclides in the ESS inventory are not well known. However, the ESS-specific radionuclides are included in the analysis to compare the repository concepts with regards to these radionuclides as well.

4.2 Sensitivity of the safety evaluation to site-specific conditions

This section presents the input data used in the evaluation cases that are carried out to investigate the sensitivity of the safety evaluation to the site-specific conditions that may influence the performance of the repository. When an aspect of the model is not discussed for a given analysis, the approach, parameters and assumptions are assumed similar to the base case.

4.2.1 Lower groundwater flow

Short description of data

The hydrogeological modelling in SE-SFL is performed assuming a stationary flow field at the Laxemar site. The *lower groundwater flow evaluation case* aims to assess the impacts of lower groundwater flow rates in the SFL repository and surrounding bedrock.

This is motivated by the fact that the bedrock at Laxemar exhibits a wide hydraulic conductivity distribution, which may make it possible to identify a body of rock for the repository that has favourable hydraulic characteristics.

For this purpose, the groundwater flow scaling factors are incorporated in the near-field model to account for possible changes in the flow field magnitude. The approach, however, uses the same flow paths used in the *present-day evaluation case* (Joyce et al. 2019, Abarca et al. 2019) and, thus, ignores the changes in flow direction. The approach is further described in SKB (2010b, Section 2.1.2).

Use in model or evaluation activity

In the near-field model, the sum of the advective release (via groundwater flow) and diffusive release (via the equivalent flow rate) from the BHA and BHK vaults constitutes the source term to the geosphere model. In the near-field model, the groundwater flow scaling factor G is introduced to incorporate the changes in the flow magnitude. Hence, the groundwater flow rate is downscaled by the scale factor G and the equivalent flow rate is downscaled by the square root of G. All the other parameters and assumptions of the model remain unchanged.

It should be noted that in the degraded zone case (DZC) in the BHK backfill, the total equivalent flow rate is viewed as the flow of water in the most degraded part of the backfill, which is also downscaled with a factor G (see Section 2.6.4).

In the geosphere model, the advective travel times (t_w, a), F-factors, and equivalent Darcy flux at the release point from the vault into a single fracture (U) are scaled by the given factor.

Input data used in evaluation case

The groundwater flow rates in the *present-day evaluation case* are provided in Section 2.6.3, 2.6.4. The equivalent flow rates in the fractures are taken from SE-SFL regional scale hydrogeological modelling (Joyce et al. 2019).

The groundwater flow rates considered in the *lower groundwater flow evaluation case* are 10 (variant A), 100 (variant B) and 1 000 (variant C) times lower than those in the *present-day evaluation case*. Table 4-3 provides the scaling factors used in the near-field model. The data are also stored in the SVN database at:

svn://svn.skb.se/SFL/SFLSAK/Arbetsmaterial/RadionuclideTransport/CalculationCases/CC2A/Geosphere/HydrologicalScaleFactor.txt.

svn://svn.skb.se/SFL/SFLSAK/Arbetsmaterial/RadionuclideTransport/CalculationCases/CC2B/Geosphere/HydrologicalScaleFactor.txt.

svn://svn.skb.se/SFL/SFLSAK/Arbetsmaterial/RadionuclideTransport/CalculationCases/CC2C/Geosphere/HydrologicalScaleFactor.txt.

Table 4-3. Scaling factor used in the models in the "low groundwater flow" evaluation case.

Scaling factor	Value [–]
Variant A	10
Variant B	100
Variant C	1 000

It should be noted that in the near-field model, the inverses of the scaling factors are used.

Source of data and justification

See Sections 2.6.3, 2.6.4. 2.9.4 and 2.9.7. See also the **Radionuclide transport report**, Section 7.2.

Known limitations in data

The assumption that the flow rates in the bedrock, bentonite and concrete backfill are reduced by the same factor is a simplification. A reduction in the groundwater flow rate in the rock may not necessarily result in an equal reduction in all parts of the near-field.

In general, groundwater flow is affected by pressure gradients and the hydraulic properties of the bedrock. However, the cause of the reduction in groundwater flow rate is not specified in this evaluation case.

See Sections 2.6.3, 2.6.4. 2.9.4 and 2.9.7. See also the **Radionuclide transport report**, Section 7.2.

4.2.2 Initially submerged conditions

Short description of data

In the *present-day evaluation case*, the SFL repository is located on land. The *initially submerged conditions evaluation case* analyses the effect of placing SFL in a location below the sea, where lower groundwater flow rates are expected. However, the spatial location of the shoreline varies

in time due to changes in the relative sea-level. Therefore, the direction and magnitude of hydraulic gradient will change over time leading to a transition from the lower groundwater flow rates to the present rate.

As an alternative to representing the full details of transient groundwater flow fields in the transport simulations, a pessimistic bounding abstraction is adopted based on the groundwater flow scaling factors. The approach includes the changes in flow magnitude but uses the same flow paths as in the *present-day evaluation case* (Joyce et al. 2019). In other words, the approach ignores the changes in flow direction. This abstraction is pessimistic because it greatly overestimates the vertical component of the flow velocity compared with detailed simulations (Vidstrand et al. 2010).

Use in model or evaluation activity

In the near-field model, the sum of the advective release (via groundwater flow) and diffusive release (via the equivalent flow) from the BHA and BHK vaults constitutes the source term to the geosphere model. In the near-field model, the groundwater flow rate is assumed to be 100 times lower than that in the *present-day evaluation case* until the coastal influence starts, i.e. a designated time point during the evaluation period. This is modelled by introducing the groundwater flow scaling factor G =100, and linearly increasing the groundwater flow up to the corresponding flow rate in the *present-day evaluation case*. Similar approach is adopted in the near-field model to reflect the initially submerged conditions on the equivalent flow rate. However, the equivalent flow rate is assumed to be 10 times lower than that in the *present-day evaluation case* until the coastal influence starts.

As in the *lower groundwater flow evaluation cases,* the advective travel times (t_w), F-factors, and equivalent Darcy flux at the release point from the vault into a single fracture (U) are scaled by the given factor.

All other near-field and geosphere parameters are the same as in the *present-day evaluation case*.

It should be noted that the inverse of the scaling factor is used in the models.

Input data used in evaluation case

The groundwater flow rates in the near-field vaults are provided in Sections 2.6.3, 2.6.4. The equivalent flow rates in the fractures are taken from SE-SFL regional scale hydrogeological modelling with ConnectFlow (Joyce et al. 2019).

Table 4-4 and Figure 4-1 present three variants of the evaluation case included to represent the different time points, after the repository closure, when the groundwater flux starts to be influenced by the surface environment; 10 000 years (variant A), 5 000 years (variant B) and 0 years (variant C). Time for repository closure (and the start of the simulation) is 2075 [a] in all three variants. The linear interpolation occurs over a time period of 4 300 years, see figure 4-1. The scale factors can also be found in SVN database at:

svn://svn.skb.se/SFL/SFLSAK/Arbetsmaterial/RadionuclideTransport/CalculationCases/CC4A/Geosphere/HydrologicalScaleFactor.txt.

svn://svn.skb.se/SFL/SFLSAK/Arbetsmaterial/RadionuclideTransport/CalculationCases/CC4B/Geosphere/HydrologicalScaleFactor.txt.

svn://svn.skb.se/SFL/SFLSAK/Arbetsmaterial/RadionuclideTransport/CalculationCases/CC4C/Geosphere/HydrologicalScaleFactor.txt.

Table 4-4. Instances at which the coastal influence starts (Radionuclide transport report, Section 7.3).

Time	Value [a]
Variant A	12075
Variant B	7075
Variant C	2075 (no downscaling)

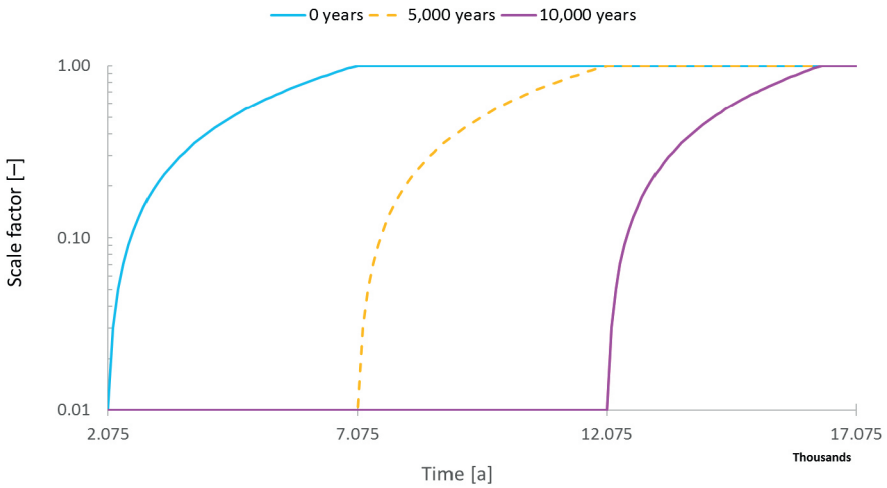

Figure 4-1. *Groundwater flow rate the in near-field and geosphere models, relative to the corresponding flow rate in the present-day evaluation case, in variants A, B and C of the initially submerged evaluation case.*

It should be noted that for the degraded zone case (DZC) in the BHK backfill, the total equivalent flow rate is viewed as the flow of water in the most degraded part of the backfill, which is also downscaled with a factor G =10.

Source of data and justification

See Sections 2.6.3, 2.6.4, 2.9.4 and 2.9.7. See also the **Radionuclide transport report**, Section 7.3.

Known limitations in data

See Sections 2.6.3, 2.6.4, 2.9.4 and 2.9.7.

4.2.3 Alternative geosphere retention properties

Short description of data

The evaluation case presented in this section aims to investigate how the differences in the bedrock retention properties influence the geosphere model prediction results. For this purpose, two variants are calculated using geosphere retention parameters that have been applied in previous safety assessments of radioactive waste repositories in Forsmark (Variant A) and Olkiluoto (Variant B) sites. The differences between the two data sets are mainly attributed to site-specific conditions.

The parameters adopted from the Olkiluoto site include K_d-values, rock matrix porosity, rock matrix density, diffusivity and maximum penetration depth. Whereas, in variant A, only the K_d-values and rock porosity are adopted from the Forsmark site and all other parameters are retained as in the base case, i.e. Laxemar site.

The data are used in FARFCOMP to account for the storage capacity of the rock matrix for dissolved radionuclides.

Use in model or evaluation activity

The data are handled in a similar manner as described for the SE-SFL base case (see Section 3.3).

Input data used in evaluation case

Table 4-5 to Table 4-7 provide the retention properties used in the geosphere model for the sensitivity evaluation case, Variant A (Forsmark site). They can also be found in SVN database at:

svn://svn.skb.se/SFL/SFLSAK/Arbetsmaterial/RadionuclideTransport/CalculationCases/CC7A/Geosphere/CC7A_Physical and chemical data.xlsx. (Worksheet = Sorption Coefficients)

svn://svn.skb.se/SFL/SFLSAK/Arbetsmaterial/RadionuclideTransport/CalculationCases/CC7A/Geosphere/CC7A_Physical and chemical data.xlsx. (Worksheet = Diffusivities and porosities)

Table 4-5. Sorption coefficient used in the geosphere model (Forsmark Site).

Element	K_d [m³/kg]	Reference/Note
Ac	1.48E-02	(SKB 2010a)*
Ag	3.49E-04	(SKB 2010a)
Am	1.48E-02	(SKB 2010a)
Ba	1.00E-03	(SKB 2014a)**
Be	0.00	No reference is found.
Ca	0.00	(SKB 2014a)
Cd	1.10E-03	(SKB 2010a)
C-ind	0.00	(SKB 2010a)
C-inorg	0.00	(SKB 2010a)
Cl	0.00	(SKB 2010a)
Cm	1.48E-02	(SKB 2010a)
Co	7.40E-04	(SKB 2014a)
C-org	0.00	(SKB 2010a)
Cs	3.49E-04	(SKB 2010a)
Eu	1.48E-02	(SKB 2010a)
Gd	0.00	ESS radionuclide.
H	0.00	(SKB 2010a)
Ho	1.48E-02	(SKB 2010a)
I	0.00	(SKB 2010a)
K	0.00	No reference is found.
La	0.00	ESS radionuclide.
Mo	0.00	(SKB 2010a)
Nb	1.98E-02	(SKB 2010a)
Ni	1.10E-03	(SKB 2010a)
Np	5.29E-02	(SKB 2010a)
Pa	5.92E-02	(SKB 2010a)
Pb	2.52E-02	(SKB 2010a)
Pd	5.20E-02	(SKB 2010a)
Po	2.52E-02	Assumed analogue to Pb
Pu	1.48E-02	(SKB 2010a)
Ra	2.42E-04	(SKB 2010a)
Re	0.00	ESS radionuclide.
Se	2.95E-04	(SKB 2010a)
Si	0.00	ESS radionuclide.
Sm	1.48E-02	(SKB 2010a)
Sr	3.42E-06	(SKB 2010a)
Tb	0.00	ESS radionuclide.
Tc	5.29E-02	(SKB 2010a)
Th	5.29E-02	(SKB 2010a)
Ti	0.00	ESS radionuclide.
U	5.29E-02	(SKB 2010a) / Assumed analogue to U(IV).
Zr	2.13E-02	(SKB 2010a)

* Table 6-89 Column 2.

** Data taken for temperate domain conditions (brackish/saline) at pH < 10, Table 8-6.

Table 4-6. Rock matrix porosity used in the geosphere model (Variant A).

Parameter	Value [%]	Reference/Note
Rock matrix porosity, cations and Neutral species	0.18	(SKB 2010a) / Table 6-90
Rock matrix porosity, anions	0.18	(SKB 2010a) / Table 6-90

Table 4-7. Rock matrix effective diffusivity used in the geosphere model (Variant A).

Speciation category	Value [m^2/s]	Reference
Cations and Neutral species	2.7E-14	(SKB 2010c) / Table A8-6
Anions	8.5E-15	(SKB 2010c) / Table A8-6

All the other parameters and assumptions of the model including the maximum penetration depth, 4.5 m, and rock matrix density, 2 700 kg/m^3, remain unchanged in the *alternative geosphere retention properties evaluation case*. Table 4-8 to Table 4-11 provide the retention properties of the bedrock in the Olkiluoto site used in the geosphere model (Variant B). They can also be found in SVN database at:

svn://svn.skb.se/SFL/SFLSAK/Arbetsmaterial/RadionuclideTransport/CalculationCases/CC7B/Geosphere/CC7B_Physical and chemical data.xlsx. (Worksheet = Sorption Coefficients)

svn://svn.skb.se/SFL/SFLSAK/Arbetsmaterial/RadionuclideTransport/CalculationCases/CC7B/Geosphere/CC7B_Physical and chemical data.xlsx. (Worksheet = Diffusivities and porosities)

It can be seen that compared to the K_d-values in the Olkiluoto site, the K_d-values in the Forsmark site deviate less from the corresponding values used in the Laxemar site, i.e. (the base case). The K_d-values in the Forsmark site (Variant A) is about half of the corresponding values in the Laxemar site for Ag, Ni, Tc, U and some of its decay products, while in the Olkiluoto site (Variant B), the K_d-values are higher than those in the Laxemar site for Ni, Mo, Ra and Tc. Furthermore, the K_d-values in the Olkiluoto site are lower than the corresponding values in the Laxemar site for Ag and U.

Table 4-8. Sorption coefficient used in the geosphere model (Olkiluoto Site).

Element	K_d [m^3/kg]	Reference/Note
Ac	1.48E-02	(SKB 2010a)*
Ag	0.00	(Posiva 2013)***
Am	1.50E-01	(Posiva 2013)
Ba	1.00E-03	(SKB 2014a)**
Be	5.50E-03	(Posiva 2013)
Ca	0.00	(SKB 2014a)**
Cd	1.10E-03	(SKB 2010a)
C-ind	0.00	(Posiva 2013)
C-inorg	0.00	(Posiva 2013)
Cl	0.00	(Posiva 2013)
Cm	1.50E-01	(Posiva 2013)
Co	7.40E-04	(SKB 2014a)[b]
C-org	0.00	(Posiva 2013)
Cs	5.40E-02	(Posiva 2013)
Eu	1.48E-02	(SKB 2010a)
H	0.00	(SKB 2010a)
Ho	1.48E-02	(SKB 2010a)
I	0.00	(Posiva 2013)
K	0.00	No reference is found.
Mo	3.00E-04	(Posiva 2013)
Nb	4.20E-01	(Posiva 2013)
Ni	5.50E-03	(Posiva 2013)
Np	4.00E-01	(Posiva 2013)
Pa	2.20E-02	(Posiva 2013)
Pb	2.52E-02	(SKB 2010a)
Pd	5.50E-03	(Posiva 2013)
Po	2.52E-02	Assumed similar to Pb.
Pu	1.50E-01	(Posiva 2013)
Ra	3.30E-03	(Posiva 2013)
Se	0.00	(Posiva 2013)
Sm	1.50E-01	(Posiva 2013)
Sr	3.00E-05	(Posiva 2013)
Tc	4.00E-01	(Posiva 2013)
Th	4.00E-01	(Posiva 2013)
U	1.60E-02	(Posiva 2013)
Zr	4.00E-01	(Posiva 2013)

* Table 6-89 Column 2.

** Data taken for temperate domain conditions (brackish/saline) at pH < 10, Table 8-6.

*** Table 7-16, Column “Unaltered Rock”.

Table 4-9. Rock matrix porosity used in the geosphere model (Variant B).

Parameter	Value [%]	Reference/Note
Rock matrix porosity, cations and Neutral species	0.5	(Posiva 2013) / Table 7-16
Rock matrix porosity, anions	0.5	(Posiva 2013) / Table 7-16

Table 4-10. Rock matrix effective diffusivity used in the geosphere model (Variant B).

Speciation category	Value [m^2/s]	Reference
Cations and Neutral species	6.02E-14	(Posiva 2013) / Table 7-16
Anions	6.02E-14	(Posiva 2013) / Table 7-16

Table 4-11. Maximum penetration depth used in the geosphere model (Variant B).

Parameter	Value [m]	Reference
Maximum penetration depth	3	(Posiva 2013) / Table 7-16

All the other parameters and assumptions of the model including the rock matrix density, 2 700 kg/m^3 (Posiva 2013, Table 7-16) remain unchanged in the *alternative geosphere retention properties evaluation case*.

Source of data and justification

In Variant A, the K_d-values and rock porosity in Forsmark site are directly taken from the data report for the safety assessment SR-Site (SKB 2010a). For Variant B, the retention properties of the Olkiluoto site are taken from the report for safety case for the disposal of spent nuclear fuel at Olkiluoto (Posiva 2013). Nevertheless, no value is reported in SKB (2010a) and Posiva (2013) for sorption coefficient of Po in the geosphere. Therefore, the K_d-value of Po is assigned based on its analogue element, Pb (Crawford 2013, Appendix C). Similarly, no K_d-value is found for K in the geosphere. The K is, therefore, pessimistically assumed to be non-sorbing. In Forsmark site, no K_d-value is reported for Be (SKB 2010a). Its K_d-value is, therefore, assumed to be zero. It should also be noted that the K_d-value of Uranium in Forsmark is pessimistically selected based on U(IV). This approach is also adopted in both the SR-Site and SR-PSU main scenarios.

Known limitations in data

The reader may refer to the reference documents (SKB 2010a and Posiva 2013) for discussions on the uncertainties in the data.

4.2.4 Alternative realisations of stochastic bedrock fractures

Short description of data

The groundwater flow through the geosphere is modelled using a stochastic discrete fracture network (DFN) approach (Joyce et al. 2019). The DFN simulation results provide the transport performance measures in each particle trajectory in the host bedrock (see Section 3.2.1).

In the *bedrock fracture network evaluation case*, a set of five DFN realisations are made to analyse the impact of the spatially varying properties of the host rock on the performance of the BHA vault. The different realizations offer different degrees of intersection between the vaults and flowing fractures as well as different transport performance measures in trajectories. It also yields to changes in the distribution of discharge points in the biosphere.

Use in model or evaluation activity

The groundwater flow and trajectory data are calculated for five different discrete fracture network realisations. The trajectory transport performance measures are then used as input data in the near-field and geosphere models for radionuclide transport calculations (see Sections 2.9.1, 2.9.2, 2.9.5, 2.9.6, and 3.2.1).

In the *bedrock fracture network evaluation case*, this hypothetical situation is also investigated, where the BHA vault is placed at the location of BHK, provided that the geometry of the BHK vault is maintained. Therefore, in total, 10 distinct variants of this evaluation case are studied.

The groundwater flow in the near-field model is controlled by the groundwater flow field in the geosphere. It can, therefore, be inferred that both the advective and diffusive components of the near-field release will be influenced by changes in the geosphere flow field. Nevertheless, in BHA, diffusion dominates the radionuclide transport. Therefore, the advective components of the near-field release (in different realisations) can be assumed equal to that in the first realisation, which is used in the base case.

The diffusive component of the near-field release is calculated by introducing the equivalent flow rate, $Q_{eq,}$ which is a measure for the capacity of the groundwater to carry away radionuclides. The equivalent flow rate can largely be affected by changes in the groundwater flows in the intersecting fractures surrounding the vault. Therefore, the equivalent flow rates are calculated for each fracture network realisation.

Input data used in evaluation case

The files that contain information and data related to transport properties of intersecting fractures with the BHA vault, are compiled in the SVN database at:

svn://svn.skb.se/SFL/SFL-SAK/Arbetsmaterial/RadionuclideTransport/CalculationCases/CC1_rX. (X = 1:5)

svn://svn.skb.se/SFL/SFLSAK/Arbetsmaterial/RadionuclideTransport/CalculationCases/CC1_rX_BHK. (X = 1:5)

Source of data and justification

The data are adopted from the regional scale modelling, which is detailed in Joyce et al. (2019).

Known limitations in data

See Sections 2.9.1, 2.9.2, 2.9.5, 2.9.6, and 3.2.1.

4.2.5 Drilled well

Short description of data

The *drilled drinking water well evaluation case* evaluates the dose from five hypothetical wells drilled north and northeast of the SFL repository, close enough to be affected by the potential releases from the SFL repository.

Due to pumping in the water supply wells, the groundwater flow field in the vicinity of the wells will be locally affected, which allows the wells to potentially attract a certain amount of water carrying the escaped radionuclides from the repository. Therefore, depending on the pumping rate and well positions, the contaminant plume from SFL can enter the wells, resulting in separate discharge areas for the contaminants. This will enhance the contaminant distribution over the biosphere.

The data provided in this section are used in the geosphere model to describe the effect of individual hypothetical water supply wells on radionuclide release to the biosphere.

Use in model or evaluation activity

To calculate the transport parameters in the host rock and find the particle trajectories, five separate hydrogeological simulations are made with ConnectFlow, each containing a single well at a specific location in the landscape (Joyce et al. 2019). Thereafter, trajectories that either reach the ground surface or the wells are identified, and the following parameters are recorded for them:

- The flow-related transport resistances, F-factor [a/m].
- The total advective travel time, t_w [a].
- The trajectory start- and end-point coordinates.

A simple strategy is adopted in the *drilled drinking water well evaluation case* to calculate the dose release to the wells. Instead of running separate transport calculations in the geosphere model, a scaling factor is introduced based on the fraction of the injected particles that reach the specific drilled well. The approach then multiplies this factor by the radionuclide releases obtained in the *present-day evaluation case* to give the release from the given well. The scaling factor, thus, reflects the fraction of the escaped radionuclides that reach the specific drilled well.

Input data used in evaluation case

To calculate the scaling factor, the particle tracking information from the five separate hydrogeological simulations is analysed. It is found that only in one well location, w3, a small proportion of particles enter the well (Joyce et al. 2019). The data suggest that out of particles escaped from the BHA vault, 2 298 particles reach either the ground surface or the well location w3. This number is 2012 for the BHK vault. However, only 73 and 43 particles that escaped from BHA and BHK enter the well w3, respectively. Hence, for the *drilled drinking water well evaluation case*, an estimation is made such that the water-supply well w3 can attract 3.1 % and 2.1 % of a radionuclide release from the BHA and BHK, respectively.

As a result, the dose releases from the well w3, from BHA and BHK, are calculated by multiplying the above fractions times the radionuclide releases obtained in the *present-day evaluation case.*

Source of data and justification

The trajectory data are taken from SE-SFL regional scale hydrogeological modelling with ConnectFlow (Joyce et al. 2019). The prerequisite for the hydrogeological modelling and the justification of the positions of the wells and the results are also provided in the reference document.

Normally, the geosphere model should have been run to calculate the release from each well. However, an approximation is made in this evaluation case, based on the number of particles that reach the given well, such that a release from a well is viewed as the fraction of total release in the *present-day evaluation case*. This is acceptable because individual water supply wells are not likely to have a significant effect on contaminant transport pathways or discharge locations. The results are therefore expected to be very similar to those in the *present-day evaluation case*. However, the particle tracking approach is quite sensitive to even small changes in the groundwater flow field. Therefore, even a small perturbation in a particle path can cause the particle to enter a different branch through the fracture network and hence arrive at a quite different exit location.

Known limitations in data

Limitations in the data are described in Joyce et al. (2019).

4.3 Sensitivity of the safety evaluation to uncertainties relating to the future climate evolution

4.3.1 Simplified glacial cycle evaluation case

Short description of data

The *simplified glacial cycle evaluation case* is designed in order to evaluate the post-closure safety of the proposed repository concept for the glaciation variant of the reference evolution that covers the colder end of the range, within which future climate may vary (**Radionuclide transport report**, Section 5.4). This evaluation case also facilitates evaluation of the effects of periglacial, glacial, and submerged conditions on the features, events and processes (FEPs) undertaken for the analysis of the post-closure safety of the SFL repository (**Main report**, Section 2.5.3).

Use in model or evaluation activity

The properties of the engineered barriers in SFL are assumed to develop in the same way as in the *present-day evaluation case*. Furthermore, the changes in the external conditions in *simplified glacial cycle evaluation case* are assumed to have no effect on the pattern of the flow field and thus the length of the flow pathways. Nevertheless, the changes in the external conditions are shown to influence the rate of groundwater flow in the repository and the host bedrock. Previous studies performed for the reconstructed glacial period for the Spent Fuel Repository in Laxemar (Vidstrand et al. 2010) and Forsmark (Vidstrand et al. 2013, 2014) and for the extended SFR in Forsmark (Odén et al. 2014) are used to estimate the groundwater flow for various parts of the glacial period. The relative effects of shoreline development, and ice sheet advance and retreat, on groundwater flow rate are reflected in a scale factor (**Main report**, Section 6.4).

Similar approach is adopted in this evaluation case to define the groundwater flow rate relative to the *present-day evaluation case*. Thus, in the near-field model, the groundwater flow rates in BHA and BHK (all cases) are multiplied by the scale factor. The equivalent flow rates in BHA and in the intact case (IC) for BHK are multiplied by the square-root of the same factor. It should, however, be noted that in the degraded zone case (DZC), the equivalent flow rate is viewed as the flow of water in the most degraded part of the backfill, which is also multiplied by the scaling factor.

In the geosphere model, the total advective travel time (t_w, a) for a water particle, and the sum of the flow-related transport resistances (F, a m^{-1}), are also scaled by the given factor. The derivation of the scale factors for the different climate periods are discussed in the **Radionuclide transport report**, Appendix C.

Input data used in evaluation case

The evolution of groundwater flow in the bedrock and repository during the different stages of the glaciation cycle are illustrated in Figure 4-2. The y-axis denotes the groundwater scale factors as compared to the *present-day evaluation case*.

Periglacial climate domain

In the simulations performed for periglacial conditions in Forsmark and Laxemar, the magnitude of the median groundwater flow in the unfrozen parts of the bedrock varies between 0.4 to 3 times the magnitude of the estimated median groundwater flow for present-day conditions (see **Radionuclide transport report**, Appendix C). In SE-SFL, the magnitude of the groundwater flow is assumed to be the same as during present-day conditions during periods of periglacial conditions, i.e. scale factor = 1.

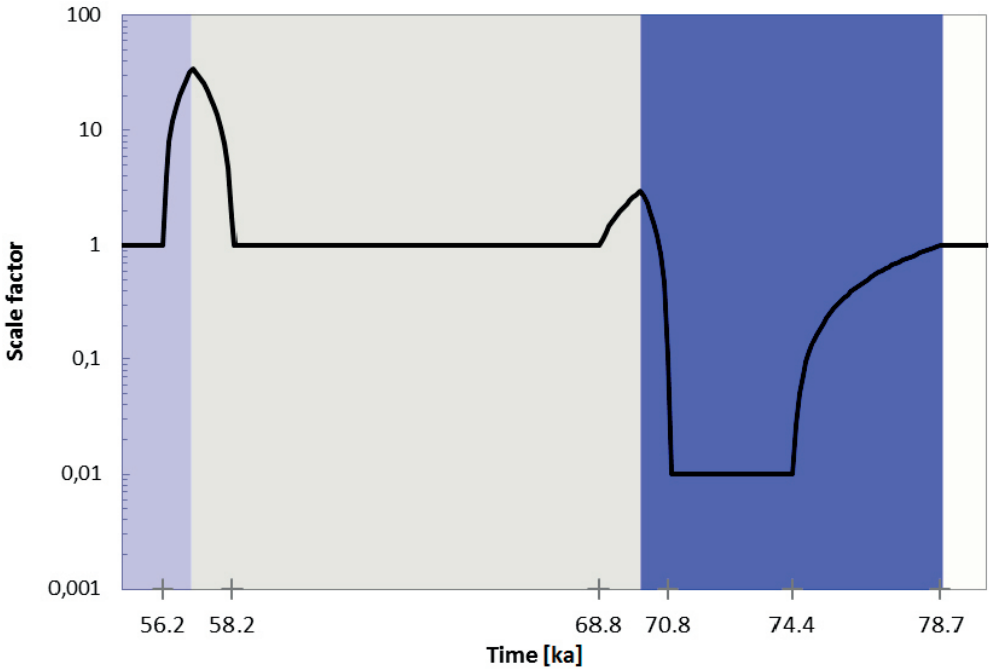

Figure 4-2. *Scale factor representing groundwater flow in bedrock and repository as compared to present-day temperate terrestrial conditions in the simplified glacial cycle evaluation case. The evolution is shown for the period from 52 000 to 82 000 years, during which the scale factor deviates from 1. Background colour represents climate domains/surface conditions; white = temperate, grey=periglacial, light grey=glacial and blue=submerged.*

Ice sheet advance

During the periods of glacial conditions, the gradient of the ice sheet surface determines the groundwater flow. In the ground flow simulations (Vidstrand et al. 2010, 2013, 2014), a steep ice sheet profile resulting in an associated large increase in groundwater flow, was assumed during ice sheet advance over a region with permafrost. The assumption is in accordance with the Weichselian ice sheet reconstruction (**Climate report**, Sections 2.2 and 4.3, SKB 2010e, Appendix 2).

The evolution assumed in the *simplified glacial cycle evaluation case* is based on the general evolution simulated for Forsmark (Vidstrand et al. 2013, Figure 7) and for Laxemar (Vidstrand et al. 2010, Figure 6-6). As a relevant example, the maximum groundwater flow increase during ice-sheet advance is taken to be 35 (**Radionuclide transport report**, Appendix C). The maximum occurs 50 years after the ice sheet margin has passed the repository location, in agreement with the simulations.

Glaciation period

During peak glaciation, the ice-sheet surface gradients are low, similar to the regional topographical gradients in the Laxemar area during temperate terrestrial conditions. During the period between ice-sheet advance and retreat the groundwater flow rate is therefore assumed to be the same as during present-day conditions.

Ice sheet retreat

Contrary to the ice sheet advance, a flatter profile was assumed during the ice sheet retreat (Vidstrand et al. 2013, Figure 7). This results in a smaller increase in the groundwater flow. The assumption is in accordance with the Weichselian ice sheet reconstruction (**Climate report**, Sections 2.2 and 4.3, SKB 2010e, Appendix 2).

Since no such simulations have been performed for Laxemar, the evolution assumed for ice-sheet retreat is based on the general evolution simulated for Forsmark (Vidstrand et al. 2013, Figure 7). In the simulations, the maximum groundwater flow increase during ice-sheet retreat varies between 3 to 20 times the magnitude simulated for the present-day conditions. To avoid overestimating the amounts of radionuclides that are flushed out in the submerged period (when dose consequences are expected to be marginal) the maximum groundwater flow increase during ice-sheet retreat is taken to be 3. The maximum occurs when the ice-sheet margin passes the repository location, in agreement with the simulations.

Transition from submerged to terrestrial temperate conditions

The scaling of the groundwater flow during the transition from submerged to terrestrial temperate conditions is determined based on previous modelling studies of groundwater flow in Laxemar and Forsmark. Simulations of bedrock hydrology in Laxemar suggest that the groundwater flow rate at repository depth was approximately 100 times lower than today during the submerged period prior to the emergence of land in Laxemar (Vidstrand et al 2010). In accordance with these results the groundwater flow rate is assumed to be 100 times lower than in the *present-day evaluation case* until the coastal influence starts, i.e. at 74 400 [a].

Simulations of bedrock hydrology in Forsmark suggest that the groundwater flow at repository depth increases approximately linearly from present sea covered conditions until times when the landscape has emerged out of the sea (Oden et al. 2014). In accordance with the patterns in Forsmark, it is assumed that the groundwater flow rate increases linearly until biosphere object 206 has reached the stage of an isolated lake, i.e. at 78 700 [a].

Source of data and justification

See Section 5.4 in the **Radionuclide transport report**.

Known limitations in data

See Vidstrand et al. (2010, 2013, 2014).

References

SKB's (Svensk Kärnbränslehantering AB) publications can be found at www.skb.com/publications. SKBdoc documents will be submitted upon request to document@skb.se.

References with abbreviated names

Main report, 2019. Post-closure safety for a proposed repository concept for SFL. Main report for the safety evaluation SE-SFL. SKB TR-19-01, Svensk Kärnbränslehantering AB.

Biosphere synthesis report, 2019. Biosphere synthesis for the safety evaluation SE-SFL. SKB TR-19-05, Svensk Kärnbränslehantering AB.

Climate report, 2019. Climate and climate-related issues for the safety evaluation SE-SFL. SKB TR-19-04, Svensk Kärnbränslehantering AB.

FEP report, 2019. Features, events and processes for the safety evaluation SE-SFL. SKB TR-19-02, Svensk Kärnbränslehantering AB.

Initial state report, 2019. Initial state for the repository for the safety evaluation SE-SFL. SKB TR-19-03, Svensk Kärnbränslehantering AB.

Radionuclide transport report, 2019. Radionuclide transport and dose calculations for the safety evaluation SE-SFL. SKB TR-19-06, Svensk Kärnbränslehantering AB.

Other references

Abarca E, Sampietro D, Molinero J, von Schenck H, 2019. Modelling of the near-field hydrogeology – temperate climate conditions. Report for the safety evaluation SE-SFL. SKB R-19-03, Svensk Kärnbränslehantering AB.

Bodin L, Delay F, de Marsily G, 2003. Solute transport in a single fracture with negligible matrix permeability: 2. Mathematical formalism. Hydrogeology Journal 11, 434–454.

Crawford J, 2010. Bedrock K_d data and uncertainty assessment for application in SR-Site geosphere transport calculations. SKB R-10-48, Svensk Kärnbränslehantering AB.

Crawford J, 2013. Quantification of rock matrix K_d data and uncertainties for SR-PSU. SKB R-13-38, Svensk Kärnbränslehantering AB.

Crawford J, 2018. Screening of radionuclides for radionuclide and dose calculations. Report for the safety evaluation SE-SFL. SKB P-16-09, Svensk Kärnbränslehantering AB.

Crawford J, Löfgren M, 2019. Modelling of radionuclide retention by matrix diffusion in a layered rock model. SKB R-17-22, Svensk Kärnbränslehantering AB.

Diomidis N, 2014. Scientific basis for the production of gas due to corrosion in a deep geological repository- Nagra Arbeitsbericht NAB 14-21, Nagra, Switzerland.

Elfwing M, Evins L Z, Gontier M, Grahm P, Mårtensson P, Tunbrant S, 2013. SFL concept study. Main report. SKB TR-13-14, Svensk Kärnbränslehantering AB.

Firestone R B, Baglin C M (ed), Chu S Y F (ed), 1998. Table of isotopes: 1998 update. 8th ed. New York: Wiley.

Gelhar L W, Welty C, Rehfeldt K R, 1992. A critical review of data on field-scale dispersion in aquifers. Water Resources Research 28, 1955–1974.

Grolander S, Jaeschke B, 2019. Biosphere parameters used in radionuclide transport modelling and dose calculations in SE-SFL. SKB R-19-18, Svensk Kärnbränslehantering AB.

Herschend B, 2014. Long-lived intermediate level waste from Swedish nuclear power plants. Reference Inventory. SKB R-13-17, Svensk Kärnbränslehantering AB.

ICRP, 2008. Nuclear decay data for dosimetric calculations. Oxford: Elsevier. (ICRP Publication 107; Annals of the ICRP 38).

Idiart A, Laviña M, 2019. Modelling of concrete degradation in a one-million-year perspective – Hydro-chemical processes. Report for the safety evaluation SE-SFL.SKB R-19-13, Svensk Kärnbränslehantering AB.

Idiart A, Laviña M, Coene E, 2019a. Modelling of concrete degradation – Hydro-chemo-mechanical processes. Report for the safety evaluation SE-SFL. SKB R-19-12, Svensk Kärnbränslehantering AB.

Idiart A, Olmeda J, Laviña M, 2019b. Modelling of concrete degradation – Influence of concrete mix design. Report for the safety evaluation SE-SFL. SKB R-19-14, Svensk Kärnbränslehantering AB.

Joyce S, Appleyard P, Hartley L, Tsitsopoulos V, Woollard H, Marsic N, Sidborn M, Crawford J, 2019. Groundwater flow and reactive transport modelling of temperate conditions. Report for the safety evaluation SE-SFL. SKB R-19-02, Svensk Kärnbränslehantering AB.

Jörg G, Bühnemann R, Hollas S, Kivel N, Kossert K, Van Winckel S, Gostomski C L, 2010. Preparation of radiochemically pure ^{79}Se and highly precise determination of its half-life. Applied Radiation and Isotopes 68, 2339–2351.

Moreno L, Tsang C-F, Tsang Y, Neretnieks I, 1990. Some anomalous features of flow and solute transport arising from fracture aperture variability. Water Resources Research 26, 2377–2391.

Neretnieks I, 1986. Stationary transport of dissolved species in the backfill surrounding a waste canister in fissured rock: some simple analytical solutions. Nuclear Technology 72, 194–200.

Neretnieks I, Liu L, Moreno L, 2010. Mass transfer between waste canister and water seeping in rock fractures. Revisiting the Q-equivalent model. SKB TR-10-42, Svensk Kärnbränslehantering AB.

Nilsson K, Byegård J, Selnert E, Widestrand H, HöglundS, Gustafsson E, 2010. Äspö Hard Rock Laboratory. Long Term Sorption Diffusion Experiment (LTDE-SD). Results from rock sample analyses and modelling. SKB R-10-68, Svensk Kärnbränslehantering AB.

Norman S, Kjellbert N, 1990. FARF31 – A far field radionuclide migration code for use with the PROPER package. SKB TR 90-01, Svensk Kärnbränslehantering AB.

Ochs M, Talerico C, 2004. SR-Can. Data and uncertainty assessment. Migration parameters for the bentonite buffer in the KBS-3 concept. SKB TR-04-18, Svensk Kärnbränslehantering AB.

Odén M, Follin S, Öhman J, Vidstrand P, 2014. SR-PSU Bedrock hydrogeology. Groundwater flow modelling methodology, setup and results. SKB R-13-25, Svensk Kärnbränslehantering AB.

Posiva, 2013. Safety Case for the disposal of spent nuclear fuel at Olkiluoto – Models and data for the repository system 2012. Posiva 2013-01, Posiva Oy, Finland.

Schrader H, 2004. Half-life measurements with ionization chambers – A study of systematic effects and results. Applied Radiation and Isotopes 60, 317–323.

SKB, 1993. Plan 93. Costs for management of the radioactive waste from nuclear power production. SKB TR 93-28, Svensk Kärnbränslehantering AB.

SKB, 1999. Deep repository for long-lived low- and intermediate-level waste. Preliminary safety assessment. SKB TR-99-28, Svensk Kärnbränslehantering AB.

SKB, 2010a. Data report for the safety assessment SR-Site. SKB TR-10-52, Svensk Kärnbränslehantering AB.

SKB, 2010b. Radionuclide transport report for the safety assessment SR-Site. SKB TR-10-50, Svensk Kärnbränslehantering AB.

SKB, 2010c. Comparative analysis of safety related site characteristics. SKB TR-10-54, Svensk Kärnbränslehantering AB.

SKB, 2010d. Geosphere process report for the safety assessment SR-Site. SKB TR-10-48, Svensk Kärnbränslehantering AB.

SKB, 2010e. Climate and climate-related issues for the safety assessment SR-Site. SKB TR-10-49, Svensk Kärnbränslehantering AB.

SKB, 2010f. Design, production and initial state of the backfill and plug in deposition tunnels. SKB TR-10-16, Svensk Kärnbränslehantering AB.

SKB, 2011a. Long-term safety for the final repository for spent nuclear fuel at Forsmark. Main report of the SR-Site project. SKB TR-11-01, Svensk Kärnbränslehantering AB.

SKB, 2011b. Site selection – siting of the final repository for spent nuclear fuel. SKB R-11-07, Svensk Kärnbränslehantering AB.

SKB, 2014a. Data report for the safety assessment SR-PSU. SKB TR-14-10, Svensk Kärnbränslehantering AB.

SKB, 2014b. Model summary report for the safety assessment SR-PSU. SKB TR-14-11, Svensk Kärnbränslehantering AB.

SKB, 2014c. Waste form and packaging process report for the safety assessment SR-PSU. SKB TR-14-03, Svensk Kärnbränslehantering AB.

SKB, 2014d. Engineered barrier process report for the safety assessment SR-PSU. SKB TR-14-04, Svensk Kärnbränslehantering AB.

SKB, 2015a. Safety analysis for SFR Long-term safety. Main report for the safety assessment SR-PSU. Revised edition. SKB TR-14-01, Svensk Kärnbränslehantering AB.

SKB, 2015b. Radionuclide transport and dose calculations for the safety assessment SR-PSU. Revised edition. SKB TR-14-09, Svensk Kärnbränslehantering AB.

SKI/SSI, 2001. SKI:s och SSI:s gemensamma granskning av SKB:s preliminära säkerhetsanalys för slutförvar för långlivat låg- och medelaktivt avfall. Granskningsrapport. SKI rapport 01:14, Statens kärnkraftinspektion, SSI-rapport 2001:10, Statens strålskyddsinstitut. (In Swedish.)

Swanton S W, Baston G M N, Smart N R, 2015. Rates of steel corrosion and carbon-14 release from irradiated steels – state of the art review (D2.1). European Commission.

Tang D H, Frind E O, Sudicky E A, 1981. Contaminant transport in fractured porous media: Analytical solution for a single fracture. Water Resources Research 17, 555–564.

Vidstrand P, Rhén I, Zugec N, 2010. Groundwater flow modelling of periods with periglacial and glacial climate conditions – Laxemar. SKB R-09-25, Svensk Kärnbränslehantering AB.

Vidstrand P, Follin S, Selroos J-O, Näslund J-O, Rhén I, 2013. Modeling of groundwater flow at depth in crystalline rock beneath a moving ice-sheet margin, exemplified by the Fennoscandian Shield, Sweden. Hydrogeology Journal 21, 239–255.

Vidstrand P, Follin S, Selroos J-O, Näslund J-O, 2014. Groundwater flow modeling of periods with periglacial and glacial climate conditions for the safety assessment of the proposed high level nuclear waste repository site at Forsmark, Sweden. Hydrogeology Journal 22, 1251–1267.

Wessely O, Shahkarami P, 2019. Development of radionuclide transport models for the near-field. Report for the safety evaluation SE-SFL. SKB R-19-05, Svensk Kärnbränslehantering AB.

Wiborgh M (ed), 1995. Prestudy of final disposal of long-lived low and intermediate level waste. SKB TR 95-03, Svensk Kärnbränslehantering AB.

Widestrand H, Byegård J, Nilsson K, Höglund S, Gustafsson E, Kronberg M, 2010. Long Term Sorption Diffusion Experiment (LTDE-SD). Performance of main in situ experiment and results from water phase measurements. SKB R-10-67, Svensk Kärnbränslehantering AB.

Arkitektkopia AB, Bromma, 2019

SKB is responsible for managing spent nuclear fuel and radioactive waste produced by the Swedish nuclear power plants such that man and the environment are protected in the near and distant future.

skb.se